An Investigation of the Fundamental Period of Vibration of Irregular Steel Structures

THESIS

Presented in Partial Fulfillment of the Requirements for the Degree Master of Science in the Graduate School of The Ohio State University

By

Kelly Christine Young

Graduate Program in Civil Engineering

The Ohio State University

2011

Master's Examination Committee:

Dr. Hojjat Adeli, Advisor

Dr. Shive Chaturvedi

Dr. K.V. Balasubramanyam

ABSTRACT

The determination of the fundamental period of vibration of a structure is essential to earthquake design. Current code equations (ASCE, 2010) provide formulas for the approximate period of earthquake-resistant building systems, which are dependent only on the height of the structure or number of stories. Such a formulation is overly conservative and unable to account for structures with geometric irregularities. This study investigated the fundamental periods of three different types of steel earthquake-resistant building structures: moment resisting frames (MRF), concentrically braced frames (CBF), and eccentrically braced frames (EBF) with varying geometric irregularities. A total of 24 MRFs, 12 CBFs, and 12 EBFs are designed and analyzed with ETABS v.9.7.2. The fundamental periods based on vibration theory for each example were compared with empirical equations, including current code equations as well as equations proposed in recent literature. Based on the results obtained from vibration theory (Rayleigh equation), equations for the approximate fundamental periods are put forth for MRFs, CBFs, and EBFs which take into account vertical and horizontal irregularities. Through statistical comparison, it was found that a 3-variable power model which is able to account for irregularities resulted in a better fit to the Rayleigh data than equations which were dependent on height only. The proposed equations were validated through a comparison of available measured period data. For braced frames, the

proposed equations were also compared with a database of examples from literature. These proposed equations will allow design engineers to quickly and accurately estimate the fundamental period of MRF, CBF, and EBF structures by taking into account irregularities.

DEDICATION

This document is dedicated to my loving family.

ACKNOWLEDGMENTS

I wish to express my sincere appreciation to my advisor, Dr. Hojjat Adeli, for all of his support and encouragement throughout my career at Ohio State. It has been a great privilege to work under his guidance. I would like to thank him for his understanding and support throughout this project. I would also like to thank Dr. Shive Chaturvedi and Dr. K.V. Balasubramanyam for serving on my advisory committee.

I would like to acknowledge gratefully the AISC/U.S. Steel Fellowship and the financial support of the First-Year Engineering program, College of Engineering, The Ohio State University. I would also like to thank Computers & Structures, Inc. for providing an ETABS license which made this research possible, and Dr. Oh-Sung Kwon and Dr. Robert Tremblay for sharing their data with me.

Finally, I wish to express my sincerest gratitude to my family and friends for their love and support throughout my academic career. I would have not been able to succeed without their kind words of encouragement, advice, love, and never-ending support.

VITA

May 1, 1987 .....Born – Findlay, Ohio

June 2009 .....B.S. Civil Engineering, The Ohio State University

2010 to present .....Graduate Teaching Associate, First-year Engineering Program, The Ohio State University

Fields of Study

Major Field: Civil Engineering

TABLE OF CONTENTS

LIST OF TABLES

LIST OF FIGURES

CHAPTER 1: INTRODUCTION AND REVIEW OF THEORY

1.1 Introduction

A large portion of modern urban infrastructure is made up of buildings with structural irregularities. While often desired by owners for their unique attributes, these irregular structures have architectural and aesthetic considerations which often require irregularities in mass, strength, stiffness, or structural form. Through the study of these structures' performance during earthquakes, it has also been found that irregular structures exhibit significantly different behavior than their regular counterparts during seismic activity.

The determination of the fundamental period of vibration of structures is essential to earthquake design and assessment. A reasonably accurate estimation of the fundamental period in such irregular structures is necessary in both response-spectrum and static earthquake analysis of structures. An accurate estimation would allow for an improved estimation of the global seismic demands on an irregular structure.

As such, the goal of this research is to investigate the accuracy of existing code-based equations for estimation of the fundamental period of irregular building structures and provide suggestions to improve their accuracy. More specifically, the objectives of this research are:

1. To perform a parametric study of the fundamental period of three different types of steel structures: moment resisting frames (MRF), concentrically braced frames (CBF), and eccentrically braced frames (EBF) in terms of number of stories, number of bays, configuration, and types of irregularity. Three types of irregular structures are examined in this study: a) structures with varying setbacks (vertical irregularity), b) structures with reentrant corner irregularity (horizontal irregularity), and c) structures with a combination of vertical and horizontal irregularity. Also examined is the regular counterpart of each irregular structure. Each structure is designed and analyzed using the program ETABS v.9.7.2 nonlinear analysis and design software.
2. To compare the fundamental periods of each structure obtained from a) Rayleigh method b) Adeli method c) ASCE 7-10 equations, and d) ETABS generated fundamental period based on a normal mode analysis. For CBFs and EBFs, the fundamental periods obtained from the equation proposed by Tremblay (2005) will also be included in the comparison. All calculations are carried out using MATLAB R2009 and Excel 2010.
3. Develop improved equations to estimate the fundamental period of steel MRF, CBF, and EBF structures by nonlinear regression analysis taking into account plan and elevation irregularities.

1.2 Literature Review

The estimation of the fundamental period of a building structure is essential for determination of the design base shear and lateral design forces. A number of studies have been performed on the fundamental period of building structures. As more buildings are instrumented and recorded seismic response data have become available, a number of recent studies have compared results obtained from empirical code equations for the fundamental period with actual measured data of structures during seismic events.

1.2.1 Empirical Equations for Fundamental Period of Structures

Seismic design codes specify empirical formulas to estimate the fundamental period which are based on data from instrumented buildings subjected to ambient vibrations or small to moderate earthquakes. Up until 2002, the fundamental period estimated by ASCE 7-02 (ASCE, 2002) code for all structures was in the form:

$$T = \mathrm{C_t} H^{3/4} \tag{1}$$

where H is the height of the structure in feet and C_t is a parameter based on structure type. This equation was present in design codes for nearly 30 years. Equation (1) is still in use in the building codes of many countries, including Eurocode 8, which limits its use to buildings less than 40m (131 feet) (CEN, 2004). Also present in certain design codes for many years, the fundamental period of braced steel frames and concrete shear walls was estimated as:

$$T = 0.05 \frac{H}{\sqrt{D}} \tag{2}$$

Parameter D corresponds to the dimension of the braced frame in a direction parallel to the applied force, called the depth of the structure in this paper. In Eq. (2) H and D are in feet. This equation was first introduced in California building codes for reinforced concrete shear wall structures, and was more recently present in the 1995 National Building Code of Canada (Tremblay R. , 2005).

ASCE 7-10 (ASCE, 2010) defines two equations for the approximate fundamental period in seconds:

$$T_a = C_t H^x \tag{3}$$

$$T_a = 0.01N \tag{4}$$

where the values of the parameters C_t and x in Eq. (3) for steel structures are given in Table 1, and N in Eq. (4) is the total number of stories.

Table 1: ASCE 7-10 values of approximate period parameters

Structure Type	**C_t**	**X**
Steel moment-resisting frame	0.028	0.8
Eccentrically braced steel frame	0.03	0.75
Concentrically braced steel frame	0.02	0.75

The parameters of Eq. (3) for moment resisting structures is based on a study by Goel and Chopra (1997) in which they performed regression analysis on the fundamental periods of 42 steel buildings located in southern California measured during eight California earthquakes occurring between 1971 and 1994 including the 1971 San Fernando earthquake (M=6.6) and 1994 Northridge earthquake (M=6.7). The buildings ranged

from 3 stories to up to 60 stories. Equation (3) has not been calibrated for CBFs or EBFs since the late 1980s when the equation was first introduced in UBC-88 (Kwon & Kim, 2010). The same old C_t and x values are used in ASCE 7-10. Equation (4) has been present in the code since the 1970s. ASCE 7-10 limits its use for buildings of 12 stories or fewer, with story heights of at least 10 feet.

Despite more buildings being equipped with instrumentation, there is still a gap in data collection for certain types of structures, such as braced steel frames. Recognizing this, Tremblay (2005) performed analytical modeling on an array of braced steel frame configurations published in the literature. Included in the database were 220 braced steel frames: 195 CBFs and 25 EBFs. Of these, only three structures of each type represented frames that had actually been built; the remaining cases were textbook examples or hypothetical frames. The database did not include structures with mass or geometric irregularities. Tremblay found that Eq. (3) results in more conservative period estimates than Eq. (2) for all CBF and EBF examples. When the ratio of analytically computed period to code predicted period (Eq. 2 and Eq. 3) was evaluated for each example, it was found that Eq. (3) resulted in a smaller scatter of the data compared with Eq. (2), leading to the conclusion that expressing the period as a function of both height and depth does not yield a benefit when compared to a function of height only. Based on this information, Tremblay proposed the following equation as an alternative to the estimation of the fundamental period of concentrically braced frames, with period varying linearly with building height in feet:

$$T = 0.0076\mathrm{H} \tag{5}$$

Tremblay suggests that Eq. (5) can provide a uniform lower-bound prediction for most buildings assigned a normal importance category. Tremblay's conclusion, however, will be revisited in this research.

The code formulations have been calibrated and revised over the past 30 years. Kwon and Kim (2010) present an extensive review of the evolution of the code equations from the 1970s to the present. In addition, the authors conducted a quantitative comparison of measured fundamental period and estimated fundamental periods calculated from the code equations. Included in their database are 65 steel MRF buildings, 17 CBF buildings, and 8 EBF buildings located in California, with a few exhibiting geometric irregularities. All buildings were instrumented by the California Strong Motion Instrumentation Program (CSMIP.) The authors identified the apparent periods of the buildings by the transfer function method. As expected, the authors determined that the current code formula generally provides a conservative prediction for fundamental period for MRF buildings of all heights ranging from single story buildings up to buildings of 700 feet. However, it was found that when looking at buildings between 6 and 8 stories, the difference between the code approximation and the measured period is relatively large . This leads the authors to conclude that further refinement to these equations is needed depending on building heights without actually suggesting any improvement. When considering concentrically braced frames, the authors compare measured periods with the estimated period from ASCE 7-10 (Eq. 3), as well as the equation proposed by Tremblay (Eq. 5.) For structures over 250 feet, ASCE Eq. (3)

yielded a large underestimate whereas for low to medium rise structures, the equation generally followed the lower bound of the measured data. The equation proposed by Tremblay provided a better fit to the measured data than Eq. (3). The 8 measured fundamental periods of EBFs were also compared with the code equation. However, the measured data only reflected structures under 100 feet and over 250 feet, making a conclusion regarding the relationship between measured data and the code equation difficult. For the given number of data points, it appeared that Eq. (3) yields accurate results for structures under 100 feet, and generally underestimates the period for structures over 250 feet.

Gong et al. (2011) present an empirical formula for evaluating the fundamental period of MRFs by analyzing a total of 36 such structures located in California. All structures had recorded seismic response data from at least one seismic event. The buildings ranged from 3 stories to 18 stories with all buildings having a total height less than 80m (262 feet.) Chopra and Goel (2000) suggest that the most significant data should be taken from structures that are strongly shaken but not damaged to the point of entering the inelastic range. Based on this conclusion, Gong et al. (2011) report the fundamental period for each structure 'before damage' and 'after damage' by dividing up response time-history into segments. The first segment is considered to reflect the undamaged structure that has not yet undergone significant deformation. Based on a regression analysis of this initial fundamental period, the authors propose the following equation for the fundamental period of steel moment resisting frames with H in meters:

$$T = 1.2\mathrm{H}^{0.6} \tag{6}$$

This formula yields results almost identical to ASCE Eq. (3) for buildings less than 20m, but more conservative results for buildings taller than 20m.

To date, no research was found that took into account structural dimensions aside from the maximum height and depth of the lateral force resisting system, with the exception of Adeli (1985), which will be further discussed in the next section.

1.2.2 Fundamental Period Based on Vibration Theory

The code specifies that the fundamental period may be determined through an alternative substantiated analysis such as normal mode analysis or Rayleigh's method, both of which require the use of a computer program, making these theory-based methods of determining the fundamental period cumbersome for most practicing engineers. More commonly, the fundamental period is determined through empirical equations provided in design codes, such as ASCE 7-10.

The Rayleigh equation is based on structural properties and deformational characteristics. The fundamental period in seconds is computed through the following formula:

$$T = 2\pi \sqrt{\sum_{i=1}^{N} w_i \delta_i^2 \Big/ g \sum_{i=1}^{N} f_i \delta_i} \tag{7}$$

where w_i is the portion of the total weight of the structure assigned to level i, f_i is the lateral force at level i, δ_i is the deflection at level i relative to the base due to lateral forces, g is acceleration due to gravity, and N is the total number of stories in the

building. The computation of the deflection at each level for multi-story structures necessitates the need for a computer-aided analysis.

For two dimensional 1, 2, or 3-story MRFs with up to 3 bays Hsiao (2009) proposed a hand-calculation approach to make Eq. (7) more practical without the necessity of structural analysis software. A general stiffness matrix of a three-story, three-bay moment resisting frame is introduced which simplifies the computation of horizontal displacements for moment frames with flexural beams. The stiffness matrix is based on slope-deflection equations. This proposed method was shown to produce results similar to those obtained from a normal mode analysis. But, it is limited to a very small sub-class of MRFs.

Recognizing the short-comings of empirical equations which depend only on a structure's height and sometimes depth, Adeli (1985) proposed approximate explicit formulae for the estimation of the fundamental period of several building systems including moment-resisting frames, braced frames, and frames with shear walls based on vibration theory, which take into account many structural parameters. The formulae were derived from the differential equations of free vibrations of a cantilever column, taking into account both bending and shear deformation while making a number of simplifying assumptions. The equation for the fundamental period of shear mode of vibration in seconds for MRFs is represented by:

$$T_S = 1.15H\sqrt{\frac{W\left((N_C-1)k_g + N_C k_C\right)}{N_s N_C (N_C-1) g E k_g k_c}} \tag{8}$$

Where H = height of structure in feet, W = total weight, N_C = number of columns, k_g = average stiffness of girders, k_c = average stiffness of columns, N = number of stories , g = acceleration due to gravity, and E = modulus of elasticity of steel. The column stiffness is defined as the column moment of inertia divided by column height, and the girder stiffness is defined as girder moment of inertia divided by girder length. Similarly the equation for the fundamental period of shear mode of vibrations of X-braced frames is:

$$T_S = \frac{2.83}{\cos \alpha_b} \sqrt{\frac{W\mathrm{H}}{\mathrm{gEA_b} \sin \alpha_b}} \tag{9}$$

where A_b denotes the cross-sectional area of bracing, and α_b is the horizontal angle of inclination of the bracing. Equation (9) is also valid for K-braced frames, including eccentric K-bracing examined in this research. This point has been verified in Appendix E.

The equation for the fundamental period of bending mode of vibration in seconds is:

$$T_B = 6.2 \frac{H}{D} \sqrt{\frac{WH(N_C - 1)}{gEA_C N_C (N_C + 1)}} \tag{10}$$

where D = dimension of the structure in feet in the direction parallel to the applied forces and A_C = the average cross sectional area of columns. Equation (10) is based on the assumption that lateral deflection is produced by elongation or shortening of columns applies for MRFs, as well as CBFs and EBFs.

The fundamental periods for shear and bending modes of vibration are then combined using Dunkerley's equation:

$$T = \sqrt{T_S^2 + T_B^2} \tag{11}$$

Several examples showed that these expressions produced more accurate results than the code equations when compared with the results of Rayleigh's equation.

ETABS, the software used for simulation in this research, calculates the fundamental period of the structure based on a vibration modal analysis using the stiffness and mass properties of the structure. The fundamental period is taken as the period of the mode calculated to have the largest participation factor in the direction the lateral earthquake loads are applied.

1.3 Structural Irregularities

Along with studies into the fundamental period of structures, another topic which has attracted attention of researchers is the seismic performance of buildings with irregularities in mass, stiffness, strength, and structural form. Modern design codes lay out guidelines for each type of vertical and horizontal irregularity. ASCE 7-10 provides the following definitions for the two types of irregularities studied in this paper:

1. Vertical geometric irregularity: Exists when the horizontal dimension of the seismic force resisting system in any story is more than 130% of any adjacent story. Referring to Figure 1, a vertical geometric irregularity exists if $1.3D_1 < D$.
2. Reentrant corner irregularity: Exists when both plan projections of the structure beyond a reentrant corner are greater than 15% of the plan dimension of the structure in the given direction. With reference to Figure 1, this type of irregularity exists when $a > 0.15D$ and $b > 0.15D$.

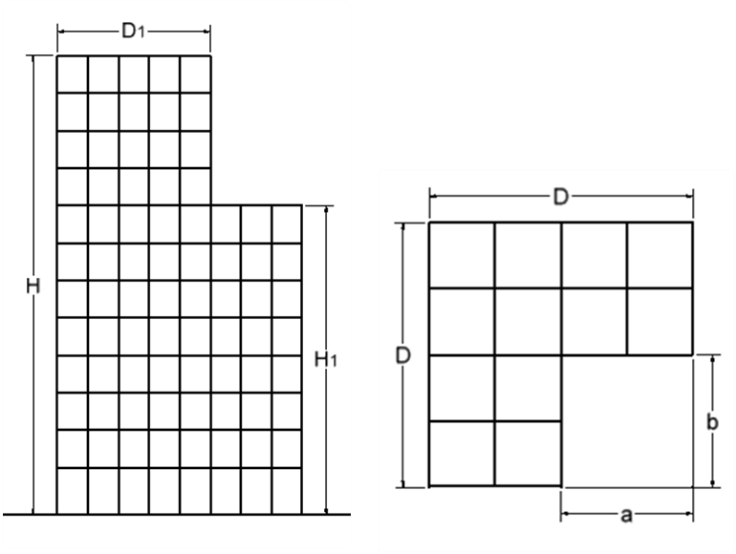

Figure 1: Vertical and horizontal irregularity definitions

CHAPTER 2: METHODOLOGY

The first step of this research is the design of each structure according to the prevalent design codes: The American Institute of Steel Construction (AISC) Load and Resistance Factor Design (LRFD), and ASCE 7-10. The steel frame design parameters are given in Table 2.

Table 2: Steel frame design parameters

	Moment Resisting Frames	Concentrically Braced Frames	Eccentrically Braced Frames
Frame Type =	OMF	OCBF	EBF
Seismic Design Category =	B	B	B
Importance Factor =	1	1	1
ρ=	1	1	1
S_{DS} =	0.3	0.3	0.3
R =	3.5	3.25	3.25
ω_0 =	3	2	2
C_d =	3	3.25	4
φ(Bending) =	0.9	0.9	0.9
φ (Compression) =	0.9	0.9	0.9
φ (Shear) =	0.9	0.9	0.9
Consider Deflection =	Yes	Yes	Yes
DL Limit, L / =	120	120	120
Live Load Limit, L / =	360	360	360
Total Load Limit, L / =	240	240	240
Stress Ratio Limit =	1	1	1

Seismic design is based on the equivalent lateral force procedure of ASCE 7-10. All other loads and load combinations are in accordance with ASCE 7-10. The location of the structures corresponds with a short period spectral response acceleration (S_S) of 0.28g at a period of 0.2 seconds and a long period spectral response acceleration (S_1) of 0.087g at a 1.0 second period. Site class D is assumed. Following Chapter 11 of ASCE 7-10 a seismic design category B results.

The static loads considered for the design of each structure include dead, live, earthquake, and wind loading. The load combinations considered for steel frame design are followed in accordance with the guidelines in ASCE 7-10. Uniform live and dead loads are assigned to each floor. A 50 psf live load is assigned at each level. The uniform dead load consists of the self-weight of the building structure, plus an additional 15 psf to account for partitions, ceilings, ductwork, and any additional structural items. Included in the self-weight are all steel members and a 9 inch thick concrete slab. A 250 plf additional dead load is assigned to all perimeter beams to account for cladding. The direction of the earthquake is one of the principal axes of the plan. An occupancy factor of 1.0 is used. ASCE 7-10 wind loading is also applied to the structure. The following wind coefficients are defined: a basic design wind speed is 85 mph, with an assumed exposure category C for open terrain and scattered obstructions. The gust factor and directionality factor are both set to 0.85.

Steel members are designed with a minimum specified yield stress of 50 kips per square inch (ksi) and a minimum tensile strength of 65 ksi. For design of beam and column sections, a wide flange (W) shape is selected from the AISC *Steel Construction*

Manual (AISC, 2005). It is assumed that there are no architectural restrictions on member geometry. For each group of beams and columns, the lightest W shape is used. ETABS starts by selecting the median W shape from the AISC database for each group of members. An analysis is run with this initial selection, and then new sections are assigned to each member. This cycle of analysis and design is repeated until all members pass the stress/capacity check and all deflection criteria are satisfied.

A rigid diaphragm is assumed for each floor. Additionally, design groups are defined for every three, four, or five stories, depending on the height of the structure: five story structures have similar stories 1-3 and 4-5; ten story structures have similar stories 1-4, 5-7, and 8-10, twenty story structures have similar stories every four stories, and thirty story structures have similar stories every 5 stories. Beams in each floor are clustered in two groups, interior and perimeter beams, and the same section is used in each group. Similarly, columns and bracings in each group are given the same section.

The process for the parametric study is outlined in Figure 2.

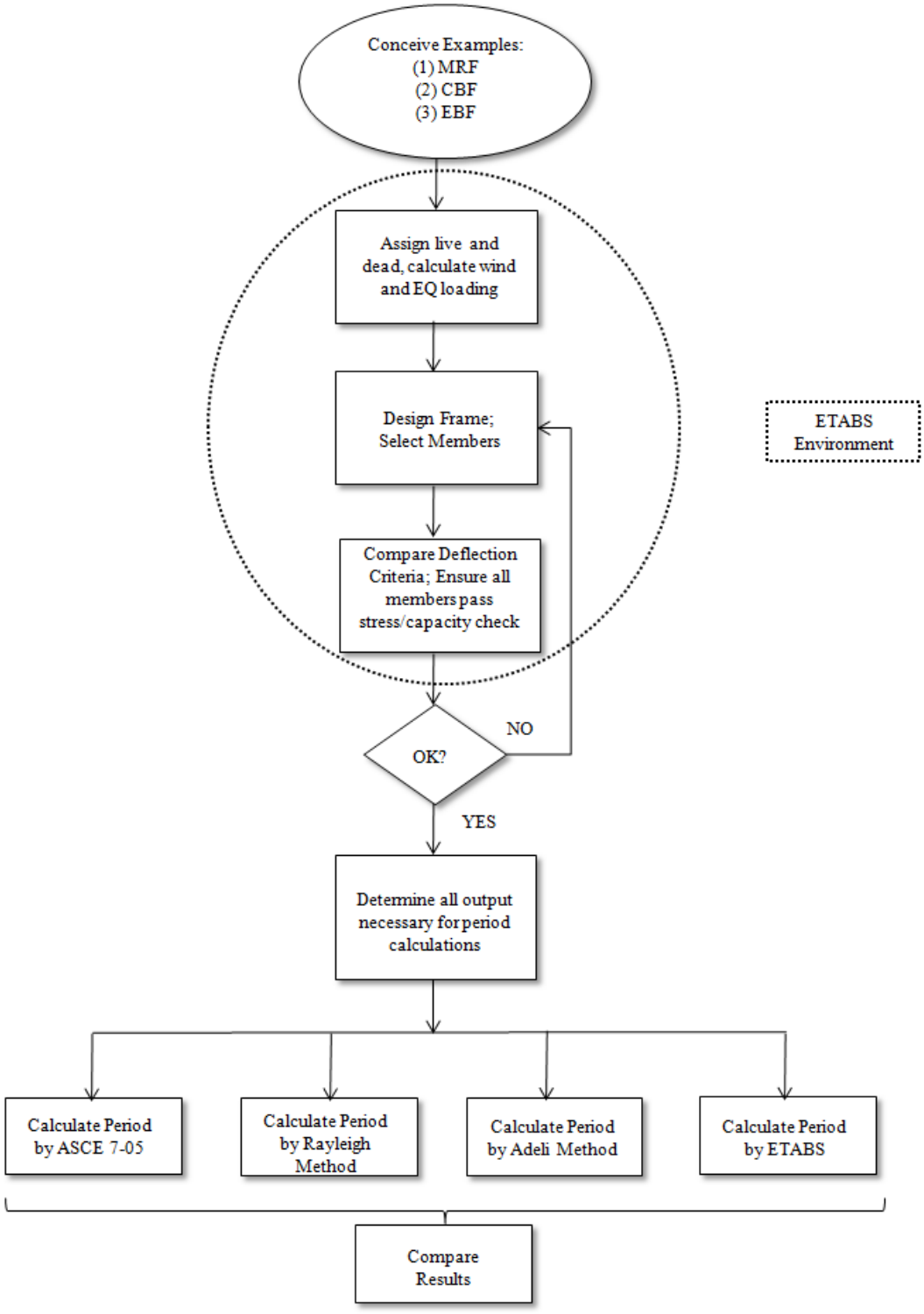

Figure 2: Process for parametric study

CHAPTER 3: MOMENT RESISTING FRAMES

3.1 Building Design Model

All MRF structures are modeled with either 20 stories, 10 stories, or 5 stories (N) and 5 or 8 bays (N_b). All structures with 5 bays have a uniform story height of 10 feet, with the exception of the first story, which is 12 feet. The bays have a uniform spacing of 15 feet. Eight-bay structures have a uniform story height of 12 feet and a uniform bay spacing of 25 feet.

A total of 24 MRF structures are evaluated: 6 vertically irregular structures, 6 horizontally irregular structures, 6 vertically and horizontally irregular structures, and 6 regular reference structures. Three-dimensional models of 5-bay MRFs are shown in Figure 3 (for 5-story structures), Figure 4 (for 10-story structures), and Figure 5 (for 20-story structures). A model of each 8-bay MRFs is shown in Figure 6 (for 5-story structures), Figure 7 (for 10-story structures), and Figure 8 (for 20-story structures.)

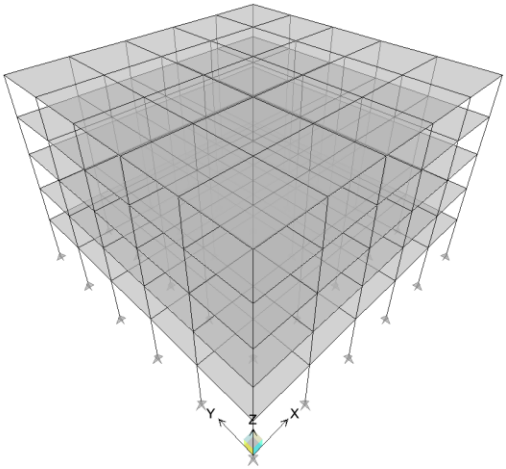

MRF-R-5-5

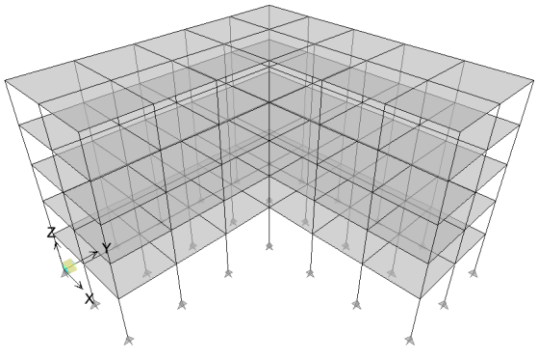

MRF-H-5-5

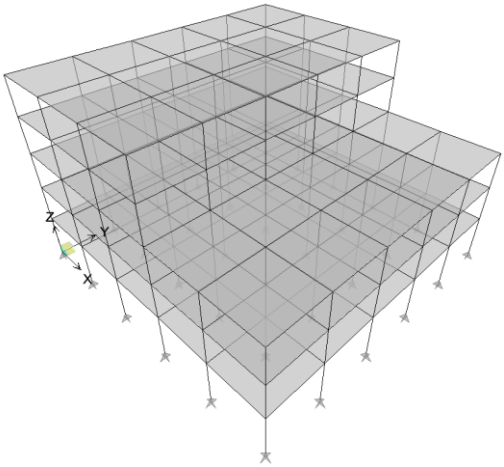

MRF-V-5-5

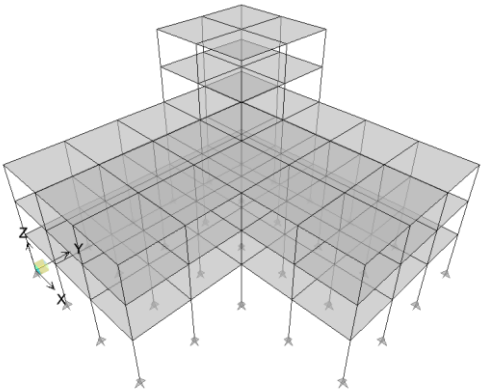

MRF-C-5-5

Figure 3: 5 story, 5 bay MRF views

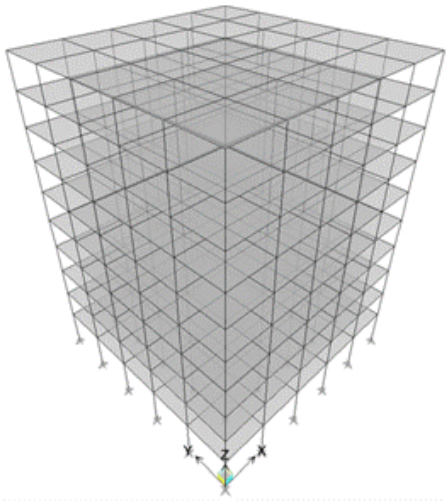

MRF-R-10-5

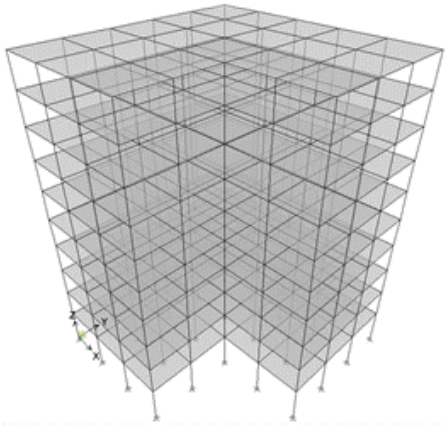

MRF-H-10-5

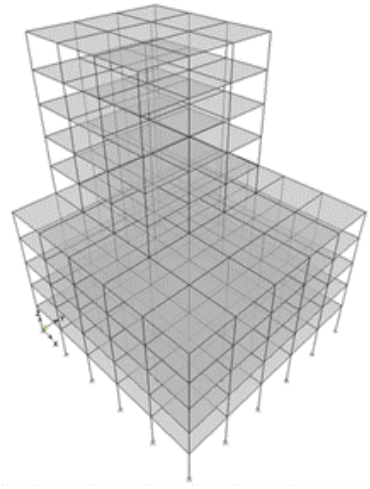

MRF-V-10-5

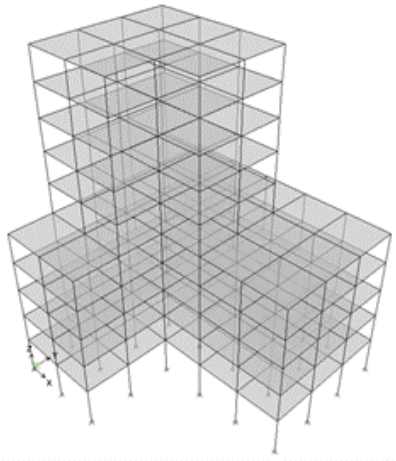

MRF-C-10-5

Figure 4: 10 story, 5 bay MRF views

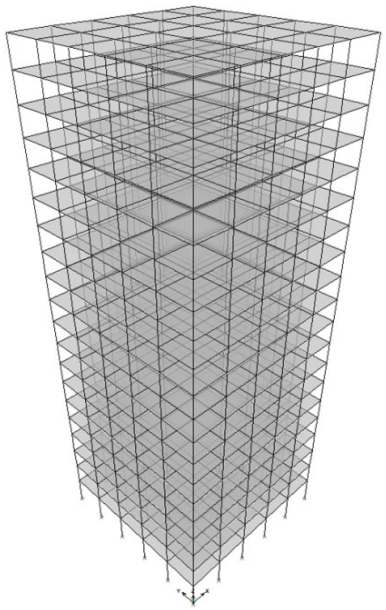

MRF-R-20-5

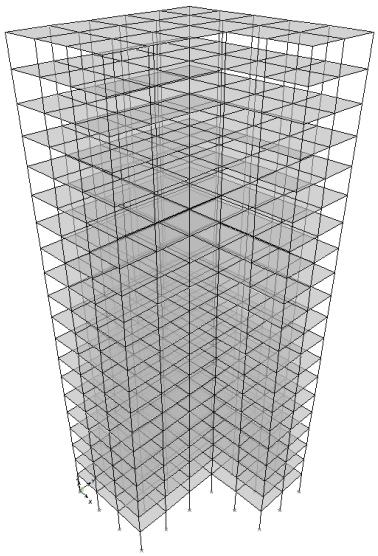

MRF-H-20-5

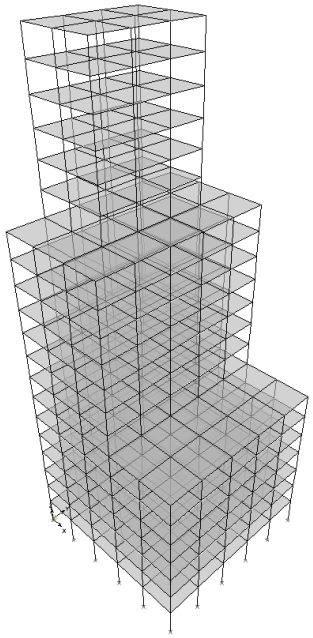

MRF-V-20-5

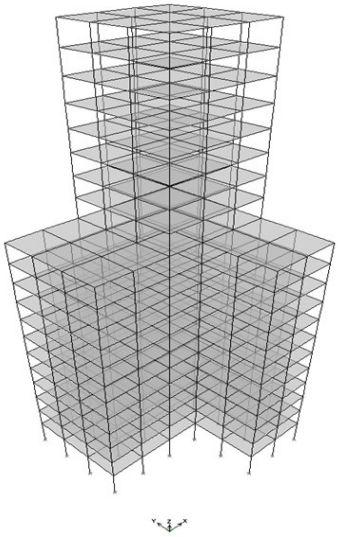

MRF-C-20-5

Figure 5: 20 story, 5 bay MRF views

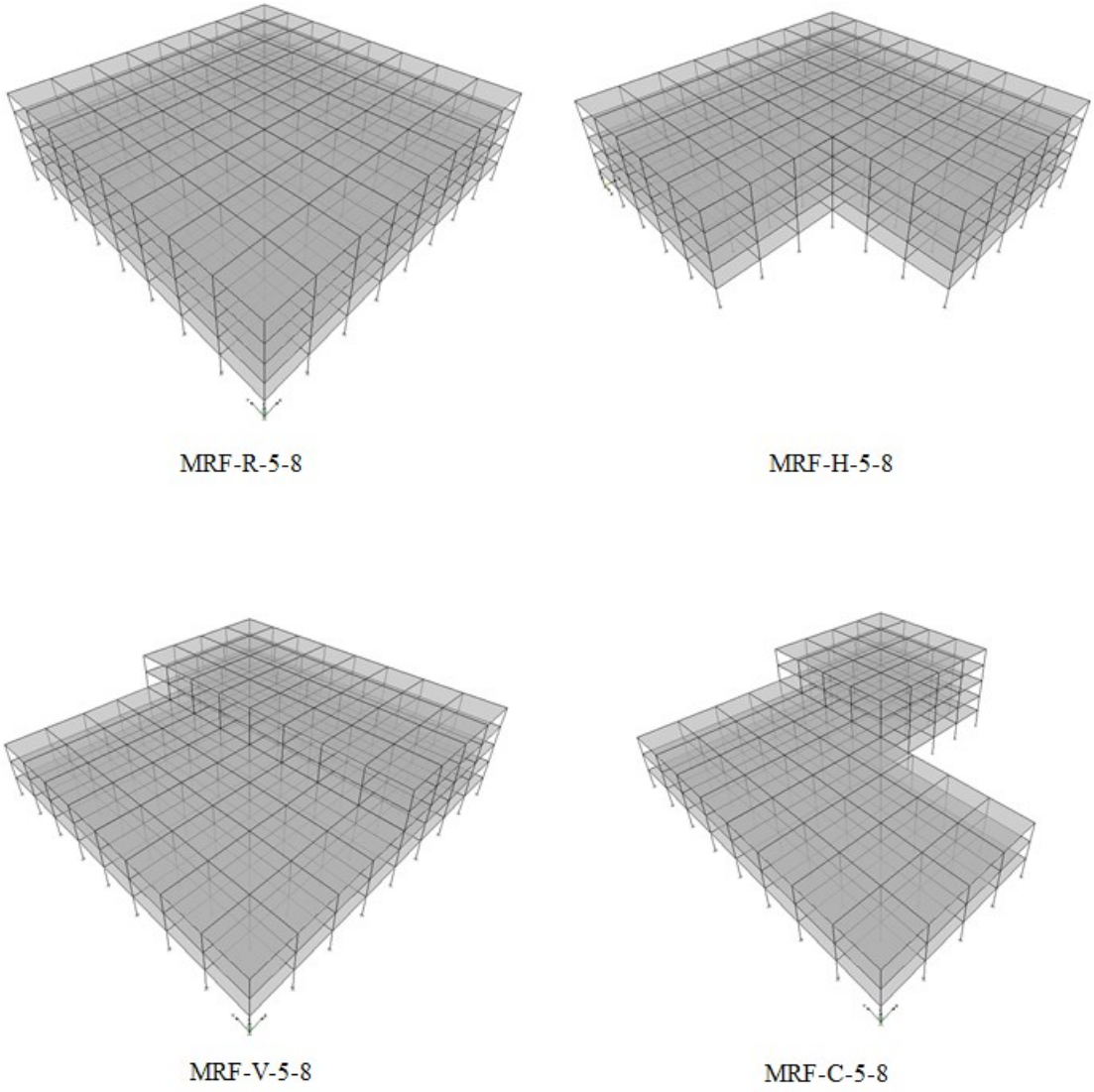

Figure 6: 5 story, 8 bay MRF views

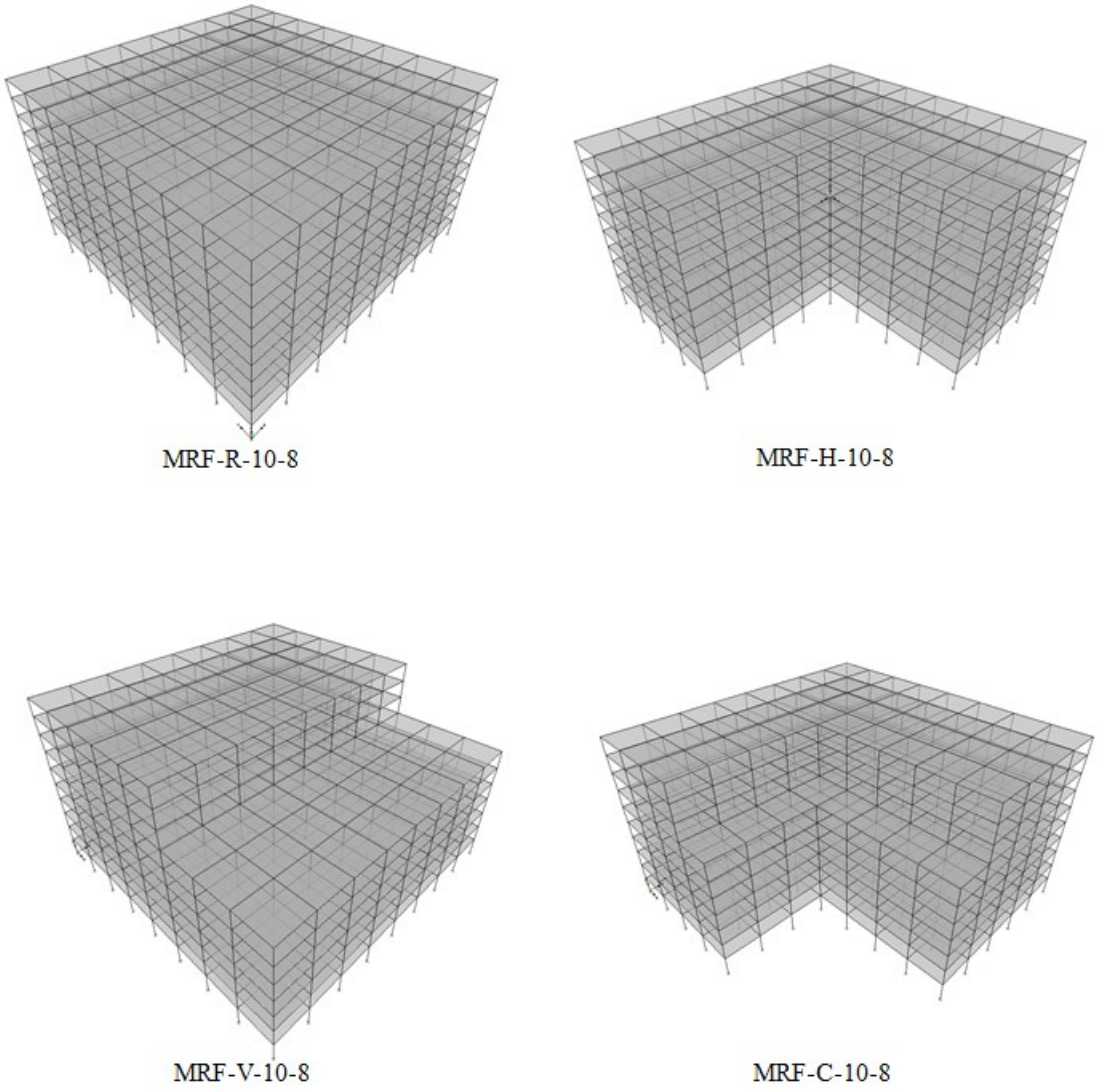

Figure 7: 10 story, 8 bay MRF views

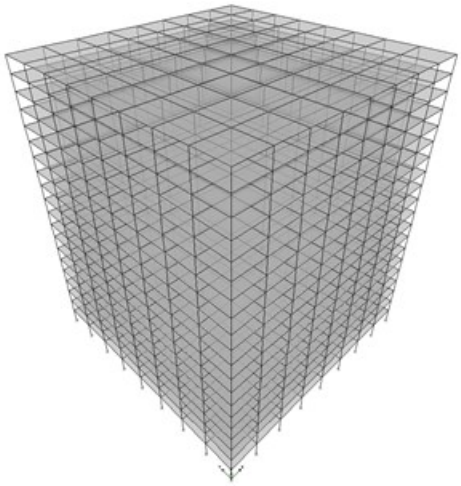

MRF-R-20-8

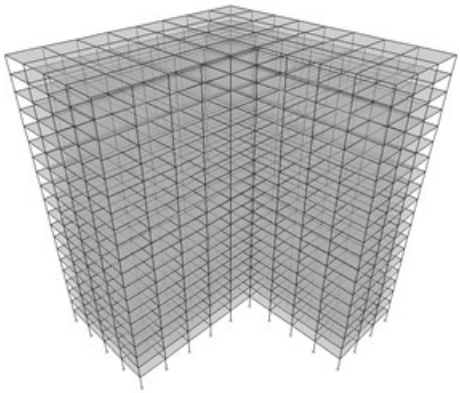

MRF-H-20-8

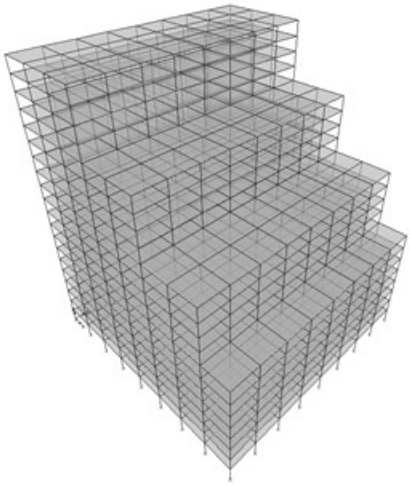

MRF-V-20-8

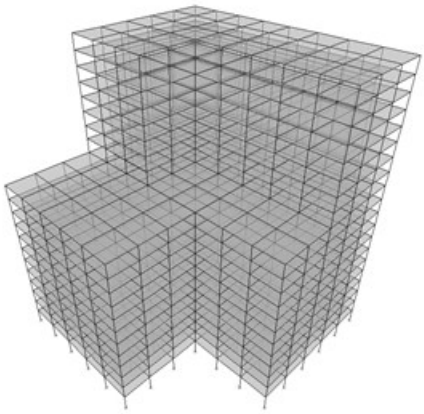

MRF-C-20-8

Figure 8: 20 story, 8 bay MRF views

Each structure has a designation beginning with MRF followed by V, H, C, or R representing vertical, horizontal, combination irregularity, respectively, or their regular counterpart. Following is a numerical designation indicating the number of stories and the number of bays. For example, MRF-V-20-8 represents a 20 story, 8 bay moment resisting frame with a vertical irregularity. Likewise, the designation MRF-R-5-8 represents a 5 story, 8 bay MRFs with no structural irregularity. The setbacks and reentrant corner irregularities are defined in terms of the depth and height, respectively, of the irregularity. For each structure, the criterion for irregularity is checked to ensure that an irregularity is present as defined by the code as described in Section 1.3, and none falls under the classification of extreme irregularity.

As defined by ASCE 7-10, the coefficients used in Eq. (3) for steel moment resisting frames are $C_t = 0.028$ and $x = 0.8$. The deflection, lateral force, and weight per story used in the Rayleigh Eq. (7) come directly from the structural models developed in ETABS. The period calculated from ETABS comes directly from the mode of vibration which has the largest modal participation mass ratio in the direction under consideration. The geometric and property data used in the Adeli equation are all based off of weighted averages for the earthquake resisting frames in the direction under consideration.

3.2 Results

Design and property data and loading and deflection data for 5- bay and 8- bay moment frame structures are given in Appendix A (Table 16 to Table 39.) For each story the column section, beam section, lateral deflection of each story, assigned weight, and seismic force assigned to each story are given. This data is used in the Rayleigh and Adeli equations.

The fundamental periods for all MRFs sorted by height of the structure using ASCE Eq. (3), Rayleigh equation (Eq. 7), ETABS generated period, and Adeli equation are summarized in Table 3 and graphically in Figure 9. The fundamental periods of 5 and 10 story MRFs are plotted versus number of stories using ASCE Eq. (2), Rayleigh equation, ETABS generated period and Adeli equation are shown in Figure 10.

.

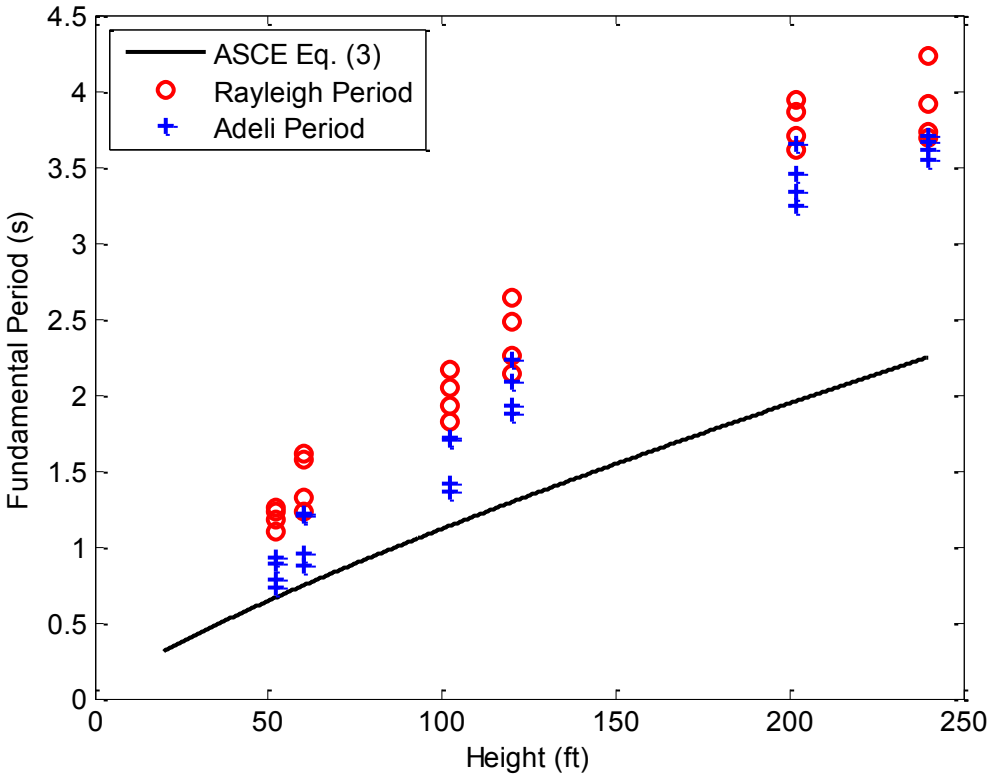

Figure 9: Fundamental periods of MRFs as a function of height

Table 3: Fundamental periods of MRFs sorted by height

Building Designation	H	H_{av}/H	D_{av}/D	T_{ASCE} Eq. (3)	T_{ASCE} Eq. (4)	$T_{Rayleigh}$	T_{ADELI}	T_{ETABS}
MRF-R-5-5	52	1.00	1.00	0.66	0.50	1.17	0.79	1.18
MRF-V-5-5	52	0.87	0.84	0.66	0.50	1.25	0.89	1.26
MRF-H-5-5	52	1.00	0.70	0.66	0.50	1.10	0.74	1.10
MRF-C-5-5	52	0.69	0.75	0.66	0.50	1.22	0.93	1.17
MRF-R-5-8	60	1.00	1.00	0.74	0.50	1.61	1.22	1.62
MRF-V-5-8	60	0.71	0.87	0.74	0.50	1.23	0.96	1.23
MRF-H-5-8	60	1.00	0.88	0.74	0.50	1.57	1.20	1.57
MRF-C-5-8	60	0.74	0.70	0.74	0.50	1.32	0.88	1.33
MRF-R-10-5	102	1.00	1.00	1.13	1.00	2.05	1.72	2.05
MRF-V-10-5	102	0.64	0.72	1.13	1.00	1.92	1.42	1.93
MRF-H-10-5	102	1.00	0.88	1.13	1.00	2.16	1.71	2.17
MRF-C-10-5	102	0.79	0.72	1.13	1.00	1.83	1.36	1.86
MRF-R-10-8	120	1.00	1.00	1.29	1.00	2.64	2.22	2.64
MRF-V-10-8	120	0.82	0.80	1.29	1.00	2.13	1.87	2.14
MRF-H-10-8	120	1.00	0.78	1.29	1.00	2.47	2.08	2.48
MRF-C-10-8	120	0.71	0.65	1.29	1.00	2.26	1.93	2.25
MRF-R-20-5	202	1.00	1.00	1.96	-	3.94	3.45	3.96
MRF-V-20-5	202	0.90	0.89	1.96	-	3.62	3.24	3.65
MRF-H-20-5	202	1.00	0.78	1.96	-	3.87	3.65	3.84
MRF-C-20-5	202	0.95	0.80	1.96	-	3.71	3.34	3.79
MRF-R-20-8	240	1.00	1.00	2.25	-	4.23	3.70	4.25
MRF-V-20-8	240	0.80	0.78	2.25	-	3.73	3.67	3.76
MRF-H-20-8	240	1.00	0.72	2.25	-	3.92	3.62	3.92
MRF-C-20-8	240	0.82	0.72	2.25	-	3.70	3.55	3.73

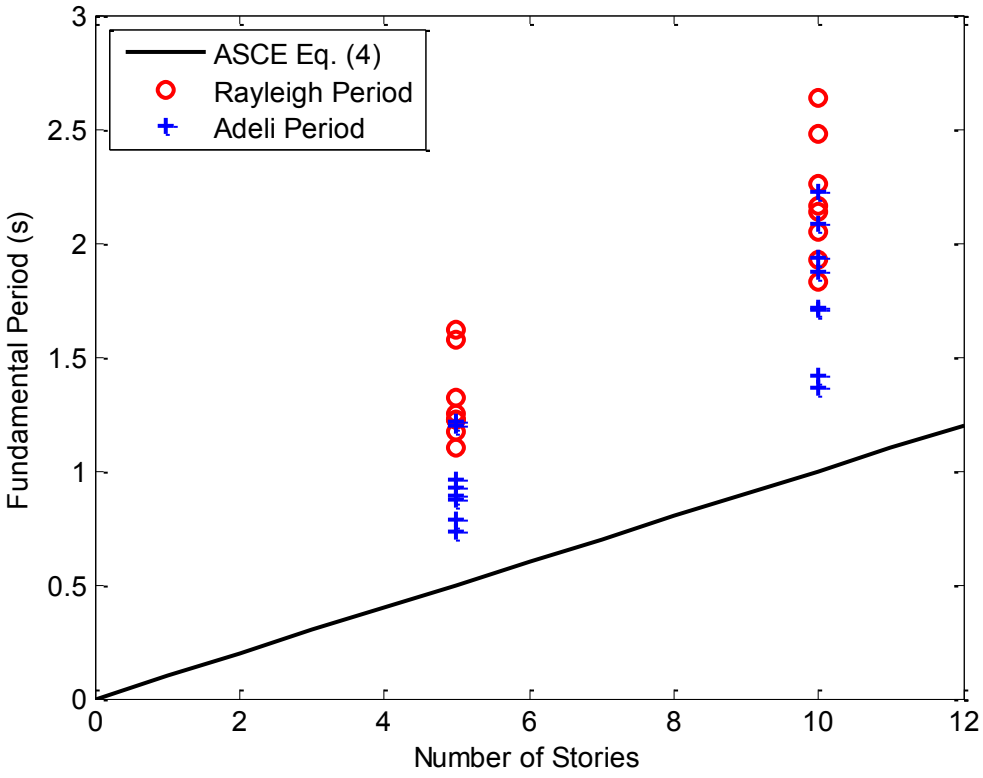

Figure 10: Fundamental periods of MRFs as a function of number of stories

Figure 11 shows the Rayleigh fundamental period plotted against height for each structure type (combination irregularity, horizontal irregularity, vertical irregularity, and no irregularity.)

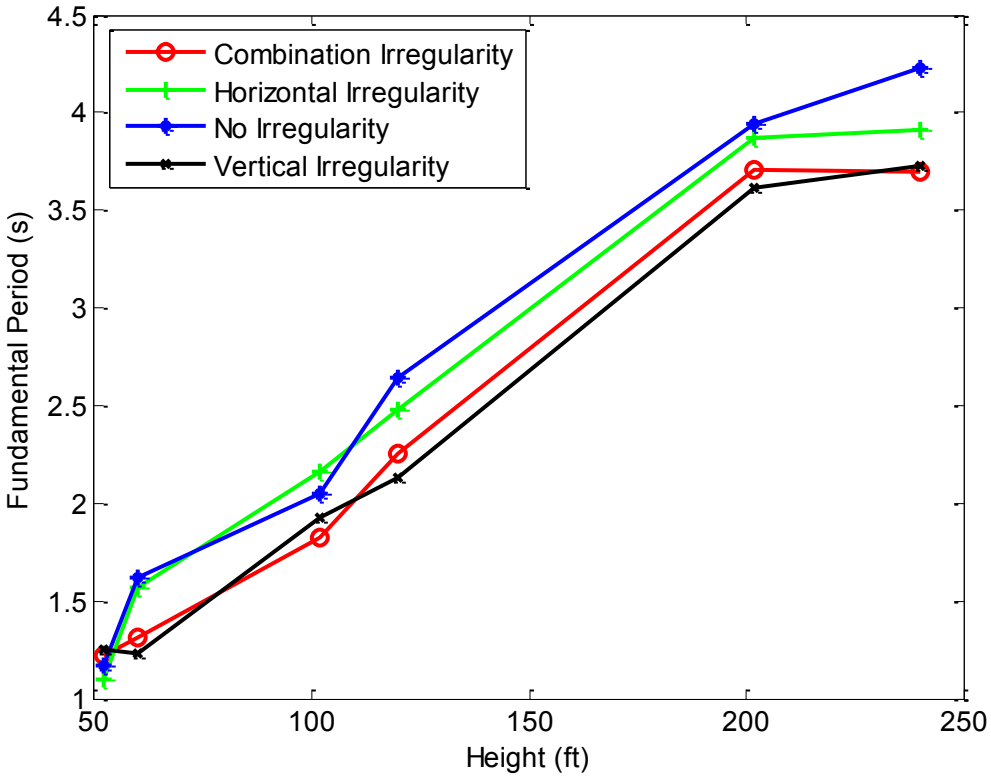

Figure 11: Rayleigh fundamental period versus height for MRFs

3.3 Analysis of Results

The ASCE Eq. (4) yields the most conservative estimate of the fundamental period for all 5 and 10 story MRFs, followed by ASCE Eq. (3). In general, the periods obtained by Rayleigh equation and ETABS modal analysis yield close values and the longest fundamental period, and Adeli equation provides a middle ground between the ASCE estimate and the Rayleigh periods. This general trend is observed in Figure 9 and Figure 10. In general, structures without irregularities tend to have a longer period compared with those with irregularities (Figure 11). Horizontally irregular structures exhibit this pattern, with their fundamental periods are only slightly shorter than regular structures for each height examined. This can be partially explained by the fact that both regular and horizontally irregular structures have $H/H_{av} = 1$, with the horizontal irregularity accounting for a decrease in weight and thus a shorter period.

For all MRFs the fundamental periods given by Rayleigh equation and ETABS modal analysis range from identical to differing by 4.99%. The largest differences are found in the combination irregularity examples, with an average of 1.84%. The smallest differences are found in the examples without irregularities with an average of 0.28%. Since the values between these two methods of calculating fundamental period appear by and large to yield close results for MRFs, in the rest of this research the period obtained from approximate and empirical equations are compared with those obtained from Rayleigh equation as a baseline.

The fundamental periods obtained from Adeli equation are consistently larger than those obtained from ASCE Eq. (3), with the largest for MRF-H-20-5 with a 60.37%

difference, and the smallest for MRF-H-5-5 with a 10.80% difference. As the height of the structure increases, the average difference between the Adeli and ASCE Eq. (3) periods increase, with average differences of 28.71%, 37.46%, and 50.77% for five, ten, and twenty story examples, respectively. When comparing the two equations for varying types of structural irregularity, the examples without irregularities yield the highest difference of 44.07%.

Compared with Rayleigh equation, Adeli equation yields a lower value for all example structures. The largest difference exists in example MRF-C-5-8, with difference of 40.14%. As the height of the structure increases, results from Adeli equation approach to those of Rayleigh equation. For five story example structures the average difference is 32.56%, whereas for twenty story structures the difference decreases to 8.43%. The ten story structures fall in between, with 20.32% average difference. When comparing Adeli equation and Rayleigh equation for irregularity type, there is no significant difference in terms of irregularity type with an average difference of 20% for each of the four structure groups. The weighted average structural properties used in Adeli equation appear to provide a reasonable, albeit a lower bound and therefore conservative estimate of the fundamental period when compared with Rayleigh equation.

Equation (3) yields an average overall underestimate of 56% for all examples compared with Rayleigh equation. There is not a large variation in average percent differences as height increases, with ten, twenty, and thirty story structures having an average difference of 59.89%, 56.74%, and 58.54%, respectively. In terms of irregularity type, ASCE Eq. (3) underestimates the period by 64.15% for examples without

irregularities and 61.16% for horizontally irregular structures. Combination irregularity and vertically irregular structures yield a slightly lower difference, with 54.66% and 53.63%, respectively.

The inability of current code equations to accurately predict the effect of irregularities on the fundamental period is highlighted when a comparison is made between two MRFs having the same height but different structural form. When comparing MRF-R-5-8 and MRF-V-5-8, ASCE Eq. (3) predicts a period of 0.74 seconds and ASCE Eq. (4) predicts a period of 0.5 seconds. However, the Rayleigh equation yields a period of 1.61 seconds and 1.23 seconds for the regular and irregular structure, respectively. Designs for both example structures are first performed using ASCE Eq. (3), and then the Rayleigh period. The difference between the designs performed with ASCE period and Rayleigh period yielded a difference in design shear of 700k for MRF-R-5-8, and 408k for MRF-V-5-8, highlighting the importance of an accurate estimation of the period.

3.4 New Equation

A goal of this research is to develop a simplified equation to allow design engineers to quickly and accurately estimate the fundamental period of MRF structures by taking into account vertical and horizontal irregularities. Irregularities are incorporated by considering not only the height (H), but also the average height (H_{av}) of lateral force resisting MRFs, as well as the depth and the average depth of lateral force resisting MRFs (D_{av}, D) in the direction of earthquake forces. Each average value

represents a weighted average value. By taking into account more structural parameters than height or number of stories, these equations will be more accurate than the current code equations (ASCE Eq. 3&4).

The proposed equation is developed by nonlinear regression analysis. The program DataFit Version 9.0.59 (Oakdale Engineering, 2011) is used to perform the regression analysis. Several equation forms were investigated, including power models of varying form, quadratic models, polynomial models, and linear models. The equations were modified to account for structural parameters in varying ways, such as including height raised to a power compared with the ratio of height over depth raised to a power. Based on extensive simulations and statistical analyses of these options, an equation of the following form was found to match the Rayleigh data the best statistically:

$$T_r = \mathrm{a}(H)^b \left(\frac{H_{av}}{H}\right)^c \left(\frac{D_{av}}{D}\right)^d \tag{12}$$

where a, b, c, and d are regression variables. This equation form will be referred to as a 3-variable power model. For a regular structure (H_{av} /H and D_{av}/D =1) Eq. (12) takes the form of the current code equation (Eq. 3). As such, the proposed 3-variable power model is a generalization of Eq. (3) intended to be used for structures with irregularities (H_{av} /H and/or D_{av}/D ≠1) as well as structures with no irregularities. The four regression parameters are obtained by minimizing the sum of the squares of the distances between the actual data points and the regression curve.

A direct comparison is made between Eq. (12), a power model ($T=aH^b$) and a linear model (T=aH) in order to highlight the benefit of using an equation of this form over the forms currently used by the code. Results are presented for the following regression

analyses with cases 1 to 4 referring to the 3-variable power model, case 5 refers to the 1-variable power model and case 6 refers to the linear model

1. Unconstrained regression analysis to determine a, b, c, and d.
2. Constrained regression analysis with b = 0.80. For a structure with no irregularity, Eq. (12) would simplify to an equation of similar form to ASCE Eq. (3), and b = 0.80 replicates the slope given in that equation.
3. Constrained regression analysis with b = 1.0, which for a structure with no irregularity would reduce to the form of linear ASCE Eq. (4).
4. Constrained regression analysis to determine a, with the values of b, c, and d rounded to the nearest 0.05 from the unconstrained regression case 1.
5. Unconstrained 1-variable nonlinear regression analysis to determine a and b.
6. Unconstrained linear regression analysis to determine a.

For each regression, the standard deviation of the residuals (σ) and r-squared (R^2) values are found. These values indicate how well the regression equation fits the sample Rayleigh data. A standard deviation of zero would indicate that the regression model accurately describes the data. It is determined by the following equation:

$$\sigma = \sqrt{\frac{S}{D_f}} \tag{13}$$

where S is the error sum-of-squares of the vertical difference between the Rayleigh data points and the regression curve, and D_f is the degrees of freedom of the model, equal to the number of data points minus the number of regression parameters. Also determined

is the correlation ratio (R^2) defined as the proportion of variability in the data set as follows:

$$R^2 = \frac{S_R}{S_T} \tag{14a}$$

$$S_R = \sum_{i=1}^{n} \left(\widehat{Y}_i - \overline{Y}\right)^2 \tag{14b}$$

$$S_T = \sum_{i=1}^{n} \left(Y_i - \overline{Y}\right)^2 \tag{14c}$$

The value of R^2 is always between 0 and 1, with higher values indicating that the regression model fits the data better. A value of R^2=1.0 means that the curve passes through every data point, whereas R^2=0 means that the regression model does not describe the data any better than a horizontal line passing through the average of the data points. For example, a value of R^2=0.95 indicates that 95% of the variation in the dependent variable is explained by the regression model. The results of the regression analyses are given in Table 4.

Table 4: Regression analysis results for MRFs

	Regression Analysis Case	Best-fit Regression Coefficients	σ	R^2
3-Variable Power Model	(1) Unconstrained	a=0.066 b=0.77 c=0.34 d=0.19	0.14	0.98
	(2) Constrained with b=0.8	a=0.055 b=0.80 c=0.31 d=0.22	0.14	0.98
	(3) Constrained with b=1.0	a=0.019 b=1.00 c=0.12 d=0.33	0.30	0.93
	(4) Constrained with b=0.75, c=0.35, d=0.20	a=0.071 b=0.75 c=0.35 d=0.20	0.13	0.98
1-Variable Power Model	(5) Unconstrained	a=0.057 b=0.78	0.21	0.97
Linear Model	(6) Unconstrained	a=0.018	0.32	0.91

The standard deviation for the constrained 3-variable power (case 4), the 1-variable power (case 5), and the linear model (case 6) are 0.13, 0.21 and 0.32, respectively. These measures indicate that case (4) provides the best fit to the data. Case (4) corresponds to

an r-squared value of 0.98, meaning that 98% of the variation in the fundamental period can be explained by this model.

In order to further compare these three possible models, an F test is conducted. The F test indicates whether the addition of variables increases the probability of decreasing the sum-of-squares of the errors and improves the fit. The F ratio is defined as:

$$F = \frac{(S_1 - S_2)/(D_{Fn})}{S_2/D_{F2}} \tag{15}$$

where subscript 1 denotes the simpler model with fewer variables and subscript 2 denotes the model with an added variable, and $D_{Fn} = D_{F1} - D_{F2}$. The result of Eq. (15) is compared with a tabulated value of F taken from an F table of sampling distributions of F. A particular value of F from the tables is specified by three quantities: (1) the numerator degrees of freedom (D_{Fn}) (2) the denominator degrees of freedom (D_{F2}), and (3) the proportion of area to the right of an ordinate (α), called the significance level of the test. Keppel and Wickens (2004) state that a confidence level of 5% is often used by researchers. The F value from the tables are reported as $F_{\alpha}(D_{Fn}, D_{F2})$ and compared with F from Eq. (15). These values are compared in order to test the null hypothesis, which in each case says that the simpler model (the equation with fewer parameters) is a statistically better model. If $F \geq F_{\alpha}(D_{Fn}, D_{F2})$, then the null hypothesis is rejected and the more complicated model is accepted. If $F < F_{\alpha}(D_{Fn}, D_{F2})$, then the simpler model is retained. However, many statistical computer programs eliminate the need for an F table by reporting the probability of a result greater than F under the null hypothesis. This

probability is called the p-value. Generally the more complicated model is accepted if the p-value is less than 0.05 (Keppel & Wickens, 2004).

The F test between the linear and 1-variable power models yields a p-value of <0.0001 indicating that the latter is a statistically more significant fit for the given set of data. The same p-value of <0.0001 is obtained when the F testis performed between the 1-variable and 3-variable power models resulting in the same conclusion that the latter is a statistically more significant fit for the given set of data.

Consequently, Eq. (12) with parameters a=0.071, b=0.75, c=0.35 and d=0.20 is proposed as the best-fit equation for determining the approximate fundamental period of MRFs:

$$T = 0.071(H)^{0.75}\left(\frac{H_{av}}{H}\right)^{0.35}\left(\frac{D_{av}}{D}\right)^{0.20} \quad (16)$$

Equation (16) results in an overall average difference of 5.36% for all examples when compared with the Rayleigh data. Equation (16) yields a closer approximation as the structure height increases, with 5, 10, and 20 story structures having average differences of 7.44%, 5.49%, and 3.14%. Results from Eq. (16) are compared with the results obtained from ASCE Eq. (3), Rayleigh, and Adeli equations in Table 5 and plotted in Figure 12 as a function of height. To illustrate the effect that irregularities introduce into the approximation, the vertical bars represent the range in period value that the 3-variable power model captures due to the effect of the H_{av}/H and D_{av}/D terms. The top of the bar represents the period for a structure with no irregularities, and the length of the

vertical bar is the difference between the largest and smallest period for each height as calculated by Eq. (16).

Table 5: Comparison of best-fit equation with ASCE, Adeli and Rayleigh period for MRFs

Building Designation	H (ft)	T_{ASCE} Eq. (3)	T_{ASCE} Eq. (4)	T_{Adeli}	$T_{Rayleigh}$	Eq. (16)
MRF-R-5-5	52	0.66	0.50	0.79	1.17	1.37
MRF-V-5-5	52	0.66	0.50	0.89	1.25	1.27
MRF-H-5-5	52	0.66	0.50	0.74	1.10	1.28
MRF-C-5-5	52	0.66	0.50	0.93	1.22	1.14
MRF-R-5-8	60	0.74	0.50	1.22	1.61	1.53
MRF-V-5-8	60	0.74	0.50	0.96	1.23	1.32
MRF-H-5-8	60	0.74	0.50	1.20	1.57	1.49
MRF-C-5-8	60	0.74	0.50	0.88	1.32	1.28
MRF-R-10-5	102	1.13	1.00	1.72	2.05	2.28
MRF-V-10-5	102	1.13	1.00	1.42	1.92	1.83
MRF-H-10-5	102	1.13	1.00	1.71	2.16	2.22
MRF-C-10-5	102	1.13	1.00	1.36	1.83	1.96
MRF-R-10-8	120	1.29	1.00	2.22	2.64	2.57
MRF-V-10-8	120	1.29	1.00	1.87	2.13	2.30
MRF-H-10-8	120	1.29	1.00	2.08	2.47	2.45
MRF-C-10-8	120	1.29	1.00	1.93	2.26	2.10
MRF-R-20-5	202	1.96	-	3.45	3.94	3.80
MRF-V-20-5	202	1.96	-	3.24	3.62	3.58
MRF-H-20-5	202	1.96	-	3.65	3.87	3.64
MRF-C-20-5	202	1.96	-	3.34	3.71	3.58
MRF-R-20-8	240	2.25	-	3.70	4.23	4.33
MRF-V-20-8	240	2.25	-	3.67	3.73	3.81
MRF-H-20-8	240	2.25	-	3.62	3.92	4.06
MRF-C-20-8	240	2.25	-	3.55	3.70	3.79

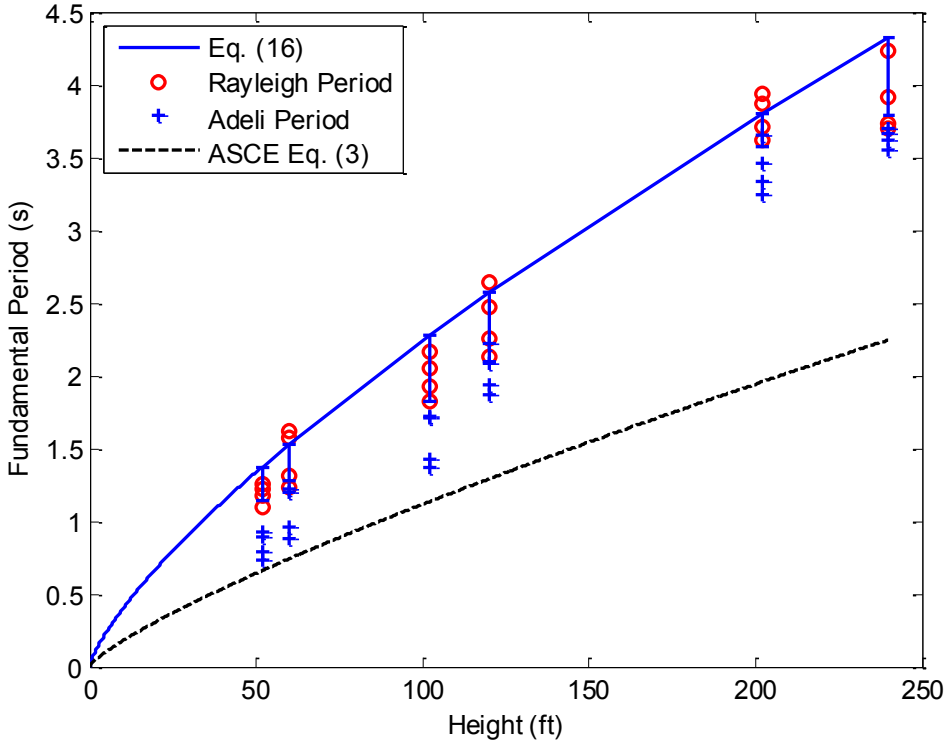

Figure 12: Comparison of results from Eq.(16) with the results obtained from ASCE Eq. (3), Rayleigh, and Adeli equation as a function of height. The top of the bar represents the period for a structure with no irregularities, and the length of the vertical bar is the difference between the largest and smallest period for each height as calculated by Eq. (16)

Equation (16) represents the best-fit to the Rayleigh period data for MRFs. However, it does not take into account nonstructural elements that add to the stiffness of the structure and thus is a non-conservative estimate. Further, the Rayleigh equation does not account for the damping of the structure. As such, the periods obtained by Eq. (16) represent an upper-bound to the permissible periods used in design as stipulated by

ASCE 7-10. Therefore, a reduction of the best-fit equation is suggested by lowering each best fit curve without changing its shape and general pattern by comparing Eq. (16) with measured period data compiled by Kwon and Kim (2010) for an assortment of structures in California without large irregularities. All structures selected for comparison with Eq. (16) have steel moment resisting frames in both longitudinal and transverse direction. This results in a total of 30 structures with periods measured in both the longitudinal and transverse directions, for a total of 60 measured periods. The building data comes from several sources: California Strong Motion Instrumentation Program (CSMIP) (11 buildings with building code beginning with C) Applied Technology Council (ATC) 3-06 (15 buildings with building code beginning with ATC) and the United States Geological Survey (4 buildings with building code beginning with U.) Limited structural details from CSMIP structures are available from the Center for Engineering Strong Motion Data's online website (USGS). Of these 11 structures, only one is considered irregular (C24566).

Table 6 gives the building designations, city, earthquake name and year it occurred with its magnitude, peak ground acceleration (PGA), and measured periods.

In order to suggest a conservative approximation for the fundamental period, a reduced form of Eq. (16) is posed by reducing the equation by the standard deviation in order to obtain an equation which yields a conservative estimate for 70-80% of the measured periods. Equation (16) resulted in a non-conservative estimate for all measured periods, so an initial modification of minus two standard deviations (best-fit -2σ) is examined, which resulted in a conservative estimation for 14 of 60 periods (23.3%). The

best-fit -3 σ curve yielded conservative results for 33 of 60 periods (55 %). Finally, the best-fit -4 σ was compared with the measured periods, which resulted in a conservative estimate for 43 of 60 periods (71.67%). This discussion is shown graphically in Figure 13.

As such, the following equation for the approximate fundamental period for MRFs is proposed for use in practice:

$$T = 0.042(H)^{0.75}\left(\frac{H_{av}}{H}\right)^{0.35}\left(\frac{D_{av}}{D}\right)^{0.20} \quad (17)$$

Equation (17) is compared with ASCE Eq. (3) and the measured period data, with results given in Table 6. Results of Table 6 are plotted in Figure 14.

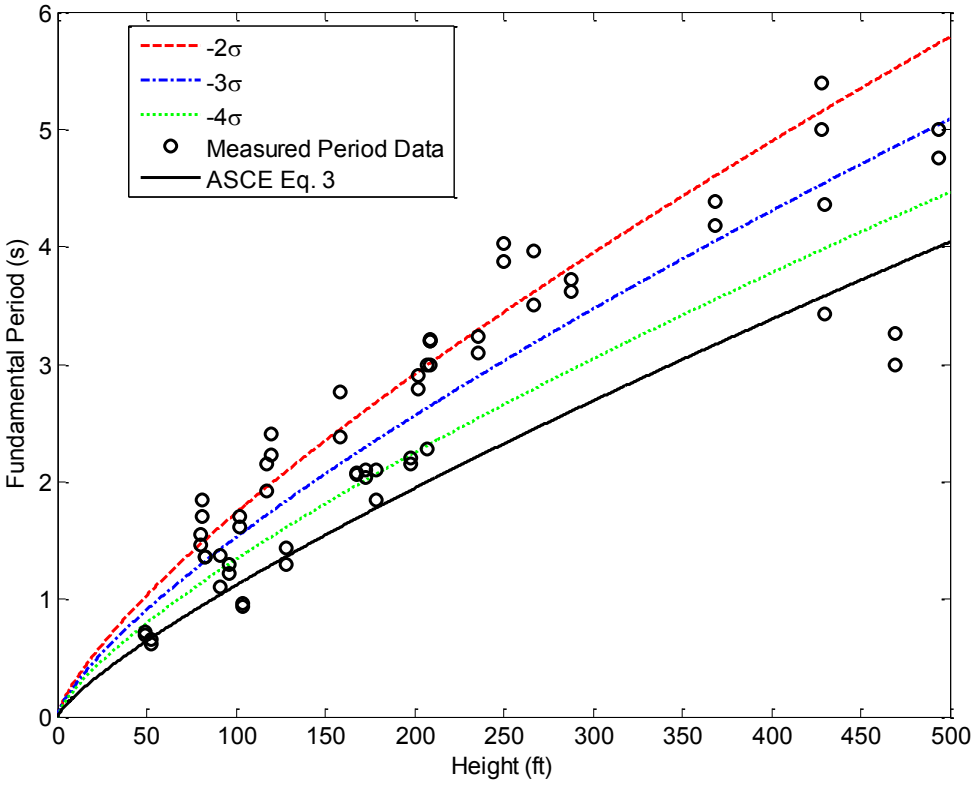

Figure 13: Reduction of best-fit Eq. (16)

Table 6: Comparison of periods from measured data with those obtained from Eq. (17) for MRFs

Building Code	City	EQ (Year)	M	H (ft)	PGA(g)	T_{Long}	T_{Trans}	Eq. 3	Eq. 17
C57562	San Jose	Loma Prieta (1989)	6.9	49.50	0.20	0.69	0.73	0.64	0.78
C58261	San Francisco	Loma Prieta (1989)	6.9	52.50	0.16	0.66	0.61	0.67	0.82
C23481	Redlands	Landers (1992)	7.3	80.00	0.07	1.46	1.55	0.93	1.12
C24370	Burbank	Northridge (1994)	6.7	82.50	0.30	1.35	1.36	0.96	1.15
C14323	Long Beach	Whittier (1987)	4.4	91.00	0.07	1.11	1.37	1.03	1.24
C23515	SanBernardino	Landers (1992)	7.3	117.60	0.08	2.16	1.92	1.27	1.50
*C24566	Pasadena	Anza (2005)	5.2	168.0	0.01	2.063	2.074	1.69	1.96
**C57357	San Jose	Loma Prieta (1989)	6.9	173.10	0.10	2.10	2.04	1.73	2.00
C24546	Pasadena	Northridge (1994)	6.7	178.80	0.17	1.85	2.10	1.77	2.05
C24569	Los Angeles	Landers (1992)	7.3	236.00	0.03	3.09	3.23	2.22	2.53
C14533	Long Beach	Whittier (1987)	4.4	288.00	0.06	3.72	3.62	2.60	2.94
ATC.ST01	Los Angeles	San Fernando (1971)	6.6	208.50	-	3.00	3.21	2.01	2.30
ATC.ST02	Pasadena	San Fernando (1971)	6.6	128.50	-	1.29	1.44	1.36	1.60
ATC.ST03	Los Angeles	San Fernando (1971)	6.6	120.00	-	2.41	2.23	1.29	1.52
ATC.ST04	Los Angeles	San Fernando (1971)	6.6	368.50	-	4.38	4.18	3.16	3.53
ATC.ST05	Los Angeles	San Fernando (1971)	6.6	267.00	-	3.97	3.50	2.45	2.77
ATC.ST06	Los Angeles	San Fernando (1971)	6.6	207.00	-	3.00	2.28	1.99	2.29
ATC.ST07	Los Angeles	San Fernando (1971)	6.6	250.00	-	4.03	3.88	2.32	2.64
ATC.ST08	Los Angeles	San Fernando (1971)	6.6	428.50	-	5.00	5.40	3.57	3.96
ATC.ST09	Los Angeles	Northridge (1994)	6.7	208.50	-	3.20	3.20	2.01	2.30
ATC.ST10	Los Angeles	San Fernando (1971)	6.6	494.00	-	5.00	4.76	4.00	4.40

Continued

Table 6 continued

Building Code	City	EQ (Year)	M	H (ft)	PGA(g)	T_{Long}	T_{Trans}	Eq. 3	Eq. 17
ATC.ST11	Los Angeles	San Fernando (1971)	6.6	202.00	-	2.91	2.79	1.96	2.25
ATC.ST12	Los Angeles	San Fernando (1971)	6.6	469.00	-	3.26	3.00	3.84	4.23
ATC.ST13	Los Angeles	San Fernando (1971)	6.6	102.00	-	1.71	1.62	1.13	1.35
ATC.ST14	Los Angeles	San Fernando (1971)	6.6	158.50	-	2.76	2.38	1.61	1.88
ATC.ST17	Los Angeles	San Fernando (1971)	6.6	81.50	-	1.85	1.71	0.95	1.14
U482	Alhambra	Northridge (1994)	6.7	198.00	*	2.15	2.20	1.93	2.22
U5208	Los Angeles	Northridge (1994)	6.7	104.00	*	0.94	0.96	1.15	1.37
U5233	Los Angeles	Northridge (1994)	6.7	430.00	*	3.43	4.36	3.58	3.97
U239	Norwalk	Whittier (1987)	4.4	96.00	*	1.30	1.22	1.08	1.29

*Indicated irregular structure with vertical irregularity: $H_{av}/H=0.7$, $D_{av}/D=0.66$
**Indicates dampers present in building
Note: Asterisks (*) denotes PGA greater or equal to 0.15g. Minus sign (-) denotes PGA less than 0.15g

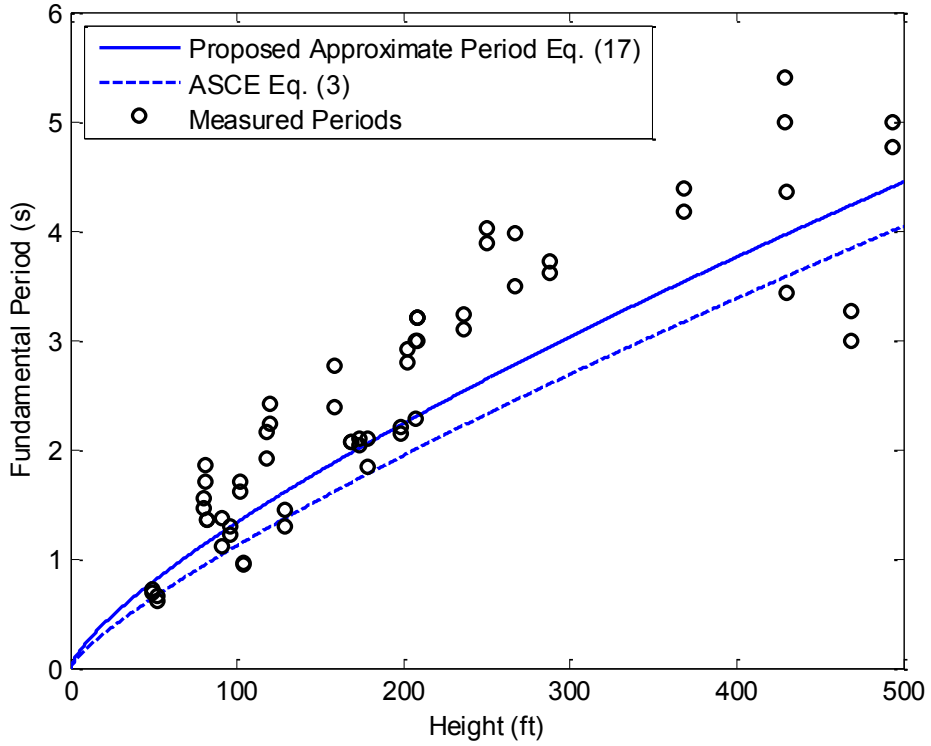

Figure 14: Comparison of periods from measured data with those obtained from Eq. (17) for MRFs

Figure 14 shows that Eq. (17) yields a less conservative result than ASCE Eq. (13), with a ratio between the two values ranging from 1.10 to 1.23. The ASCE Code specifies that the fundamental period may be either estimated from ASCE Eq. (3), or determined from an alternative substantiated analysis, such as the Rayleigh equation or normal modal analysis, but the value obtained cannot exceed an upper bound ranging from 1.4 to 1.7 times of the value obtained from ASCE Eq. (3). As such, the proposed equation satisfies this stipulation of the code. Equation (17) results in a conservative

estimate for 71.67% of measured periods, whereas ASCE Eq. (13) is conservative for 86.67% of the measured periods. The average difference between ASCE Eq. (3) and the measured periods is 30%, whereas the average difference between Eq. (17) and the measured periods is 21.4%. On the basis of this comparison, it can be concluded that ASCE Eq. (3) is overly conservative and Eq. (17) results in a more accurate approximation by considering structural irregularities.

3.5 Conclusions

Through a comparison of the fundamental period of 24 MRFs by the ASCE equations (Eq. 3 & 4), Rayleigh equation (Eq. 7), ETABS generated period, and Adeli equation (Eq. 8, 10, 11), the following conclusions are made:

1) ASCE linear Eq. (4) yields the most conservative result for all examples within its allowable range (5 and 10 story structures), followed by ASCE Eq. (3).
2) The periods resulting from the Rayleigh equation and ETABS modal analysis are nearly identical for all example buildings. The Adeli equation, in general, yields longer periods compared with ASCE Eq. (3) & (4), and shorter periods compared with Rayleigh/ETABS periods. Hence, the Adeli equation can provide a more accurate, yet generally conservative, estimate of the fundamental period for a structure past the preliminary design phase.
3) In general, structures without irregularities tend to have a longer period compared with irregular structures. Horizontally irregular structures tend to have

fundamental periods only slightly shorter than regular structures for each height examined.

4) Linear, 1-variable power, and 3-variable power regression models were developed along with several others. The results were compared through statistical methods using 24 MRFs. It is concluded that a 3-variable power model which captures structural irregularity results in a better statistically significant model of the fundamental period when compared to an equation which is based simply on its height.
5) A new equation is proposed as an approximate equation for the fundamental period of steel MRFs along the principal structural direction under consideration. Comparison with ASCE Eq. (3) and measured period data shows that the proposed equation yields a more reasonable estimation than the current code equation.

Measured fundamental period data for irregular structures is scarce. For the few that such data exist structural properties are not readily available. As such, comparison with measure data presented in this paper is limited to regular structures. Incorporating additional structural parameters which account for structural irregularities is important to obtain reasonably accurate results. The close fit of best-fit Eq. (16) with the irregular example structures shows the proposed equation incorporates the effect of irregularity properly. The comparison of measured data with the results obtained from the proposed Eq. (17) validates the merit of the proposed equation.

CHAPTER 4: CONCENTRICALLY BRACED FRAMES

4.1 Building Design Model

All CBF structures are modeled with either 30 stories, 20 stories, or 10 stories (N) and 5 bays (N_b). All structures have a uniform story height of 10 feet, with the exception of the first story which is 12 feet, and a uniform bay spacing of 25 feet. Concentric X-bracing is placed along middle bays of perimeter frames.

A total of 12 CBF structures are evaluated: 3 vertically irregular structures, 3 horizontally irregular structures, 3 vertically and horizontally irregular structures, and 3 regular reference structures. Three-dimensional models of each 10, 20, and 30 story structure are shown in Figure 15, Figure 16, and Figure 17. Each structure has a designation beginning with CBF followed by V, H, C, or R representing vertical, horizontal, or combination irregularity, respectively, or their regular counterpart, followed by a numerical designation indicating the number of stories and the number of bays. For example, CBF-V-20-5 represents a 20 story, 5 bay concentrically braced frame with a vertical irregularity. Likewise, the designation CBF-R-10-5 represents a 10 story, 5 bay concentrically braced frame with no structural irregularity. The setbacks and reentrant corner irregularities are defined in terms of the depth and height. For each structure, the criterion for irregularity is checked to ensure that an irregularity is present

as defined by the code as described in Section 1.3.2, and none falls under the classification of extreme irregularity.

As defined by ASCE 7-10, the coefficients used in Eq. (3) for steel eccentrically braced frames are $C_t = 0.02$ and $x = 0.75$. The deflection, lateral force, and weight per story used in the Rayleigh equation come directly from the structural models developed in ETABS. The period calculated from ETABS comes directly from the mode of vibration which has the largest modal participation mass ratio in the direction being considered. The geometric and property data used in the Adeli equation are all based off of weighted averages for the perimeter braced frames in the direction under consideration.

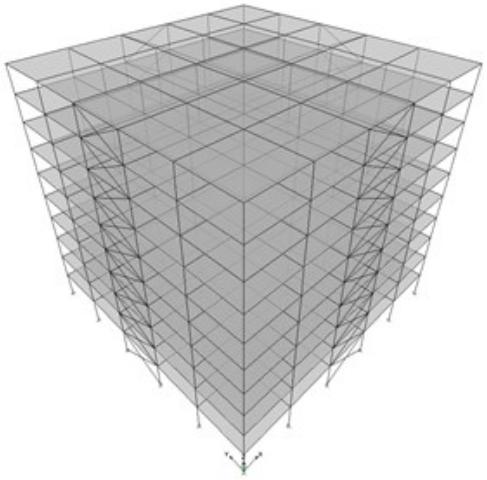

CBF-R-10-5

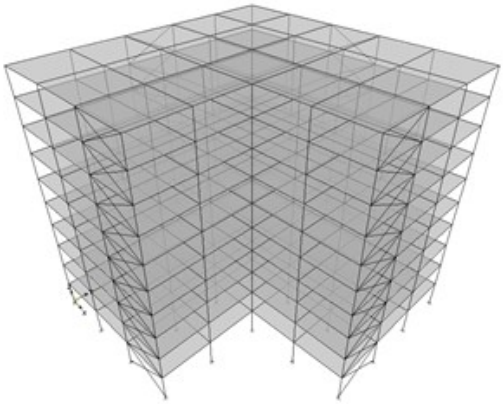

CBF-H-10-5

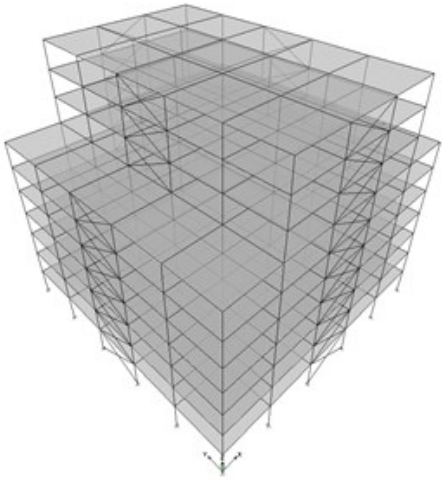

CBF-V-10-5

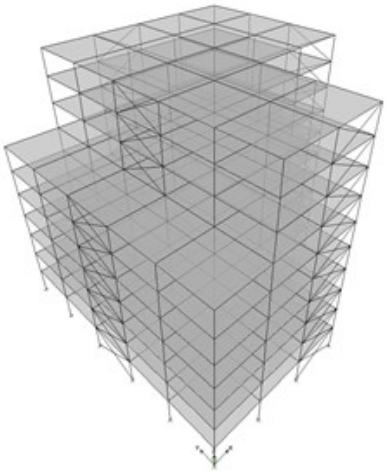

CBF-C-10-5

Figure 15: 10 Story, 5 Bay CBF Views

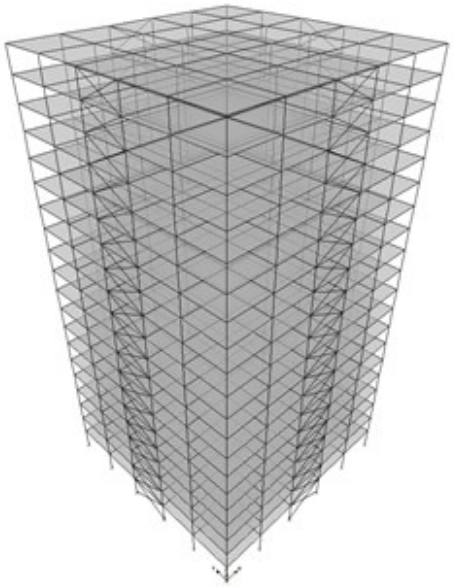

CBF-R-20-5

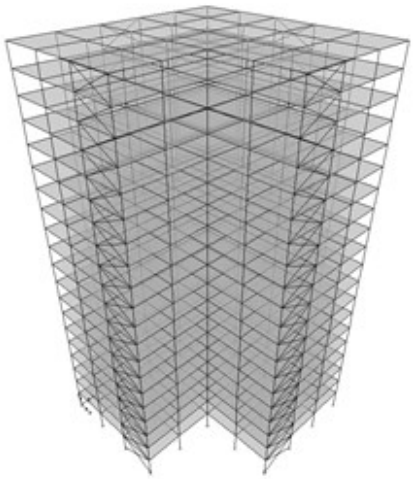

CBF-H-20-5

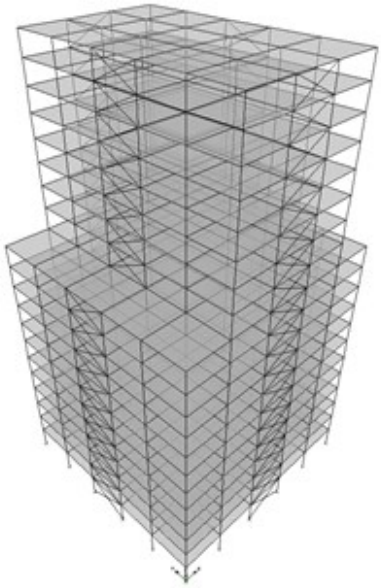

CBF-V-20-5

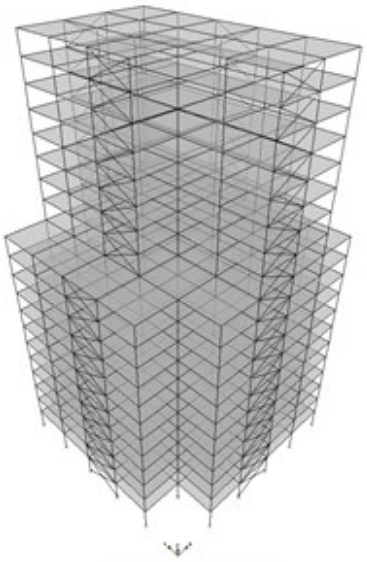

CBF-C-20-5

Figure 16: 20 Story, 5 Bay CBF Views

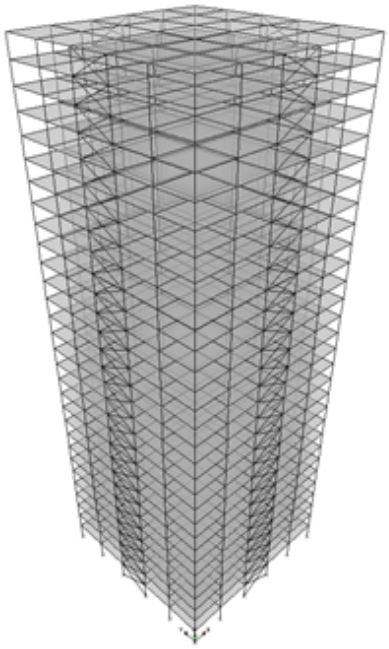

CBF-R-30-5

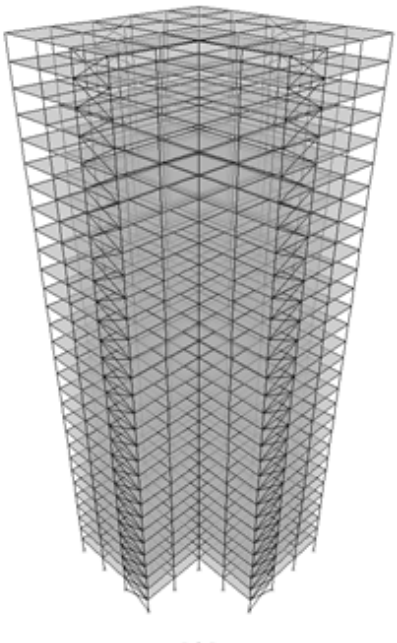

CBF-H-30-5

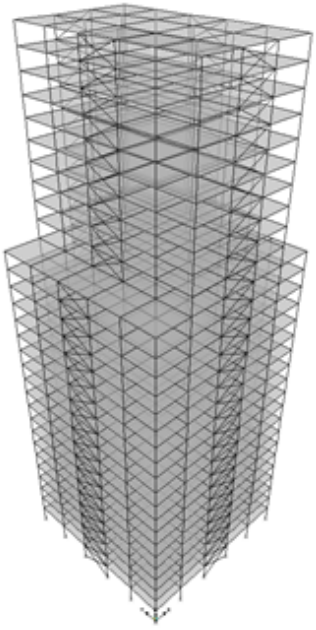

CBF-V-30-5

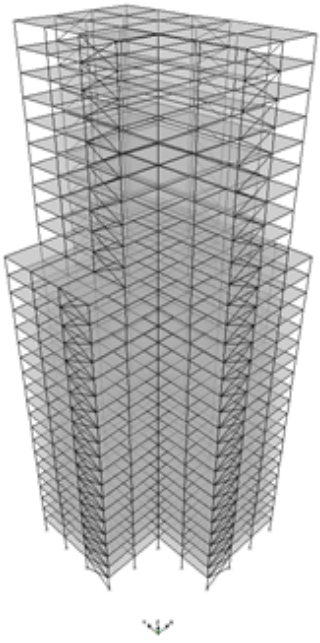

CBF-C-30-5

Figure 17: 30 Story, 5 Bay CBF Views

4.2 Results

Design and property data and loading and deflection data for concentrically braced frame structures are given in Appendix B (Table 40 to Table 51). For each story the column section, beam section, brace section, lateral deflection of each story, and weight and seismic force assigned to each story are given. This data is used in the Rayleigh and Adeli equations

The fundamental period of all CBFs using ASCE equation (Eq. 3), Rayleigh equation (Eq. 7), ETABS generated period, Adeli equations (Eq. 9-11), and Tremblay's equation (Eq. 5) are summarized in Table 7 and shown graphically in Figure 18. Table 7 also includes the ratio of the weighted average height to maximum height (H_{av}/H) and the weighted average depth to maximum depth (D_{av}/D) for all examples.

Table 7: Fundamental periods of CBFs sorted by height

Building Designation	H (ft)	H_{av}/H	D_{av}/D	T_{ASCE} Eq. 3	$T_{Rayleigh}$	T_{ADELI}	T_{ETABS}	$T_{Tremblay}$
CBF-R-10-5	102	1.00	1.00	0.64	1.73	0.87	1.73	0.78
CBF-V-10-5	102	0.90	0.88	0.64	1.56	0.75	1.57	0.78
CBF-H-10-5	102	1.00	0.80	0.64	1.64	0.80	1.65	0.78
CBF-C-10-5	102	0.94	0.74	0.64	1.57	0.74	1.57	0.78
CBF-R-20-5	202	1.00	1.00	1.07	3.25	2.36	3.25	1.54
CBF-V-20-5	202	0.87	0.84	1.07	2.88	1.89	2.89	1.54
CBF-H-20-5	202	1.00	0.80	1.07	3.08	2.24	3.09	1.54
CBF-C-20-5	202	0.85	0.74	1.07	2.88	1.85	2.88	1.54
CBF-R-30-5	302	1.00	1.00	1.45	4.77	4.69	4.77	2.30
CBF-V-30-5	302	0.89	0.87	1.45	4.00	4.06	4.00	2.30
CBF-H-30-5	302	1.00	0.80	1.45	4.30	4.57	4.31	2.30
CBF-C-30-5	302	0.93	0.70	1.45	3.85	3.98	3.85	2.30

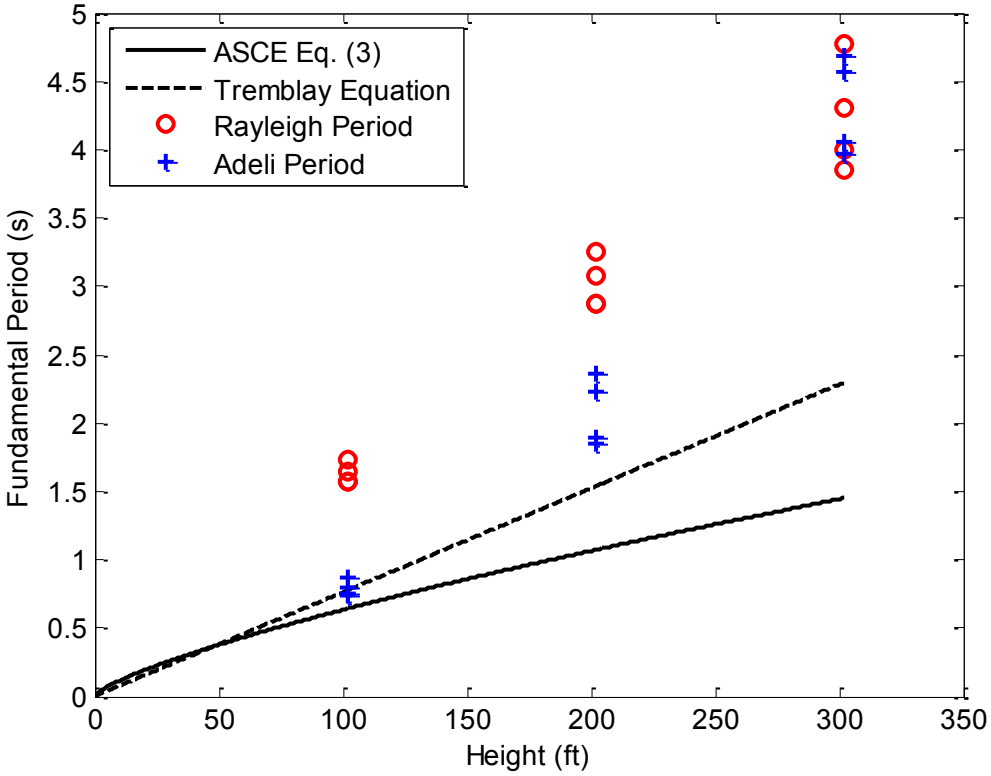

Figure 18: Fundamental period versus height for CBFs

Figure 19 shows the fundamental period versus height for each structure type (combination irregularity, horizontal irregularity, vertical irregularity, and no irregularity.)

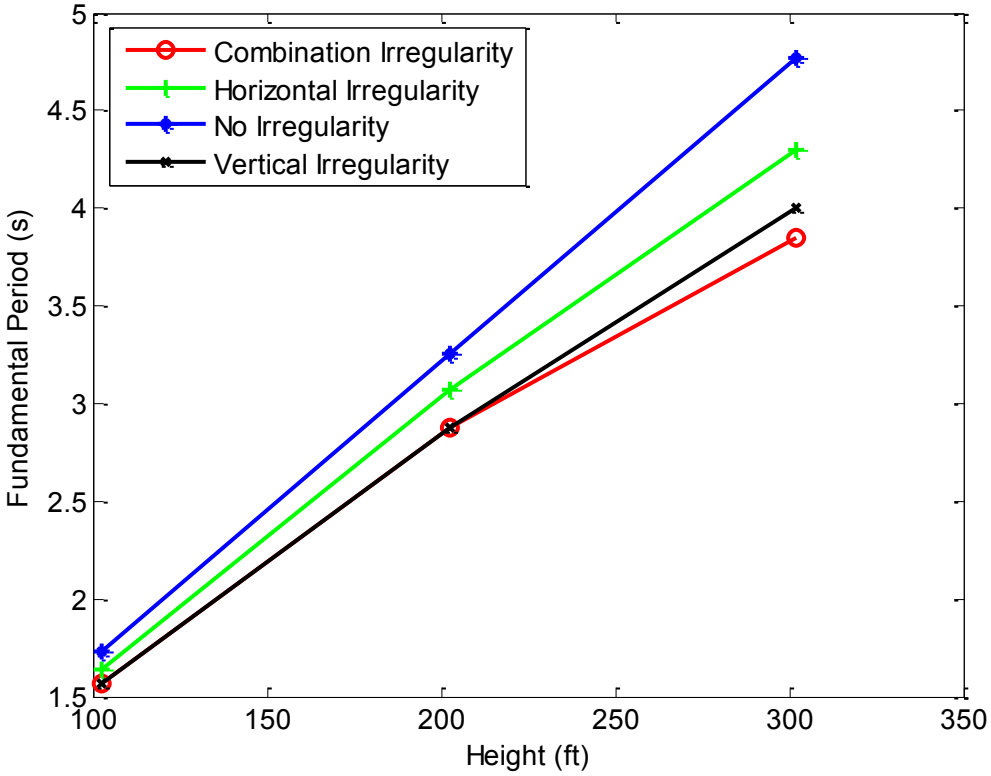

Figure 19: Rayleigh fundamental period versus height for CBFs

4.3 Analysis of Results

ASCE Eq. (3) yields the most conservative estimate of the fundamental period for all example CBFs. In general, the periods obtained by Rayleigh equation and ETABS modal analysis yield close value and the longest fundamental period, and the Adeli equation provides a middle ground between the ASCE estimate and Rayleigh periods for buildings less than 20 stories. For 30 story structures, Adeli and Rayleigh equations yield close values. When comparing the Tremblay equation and ASCE Eq. (3) for structures under 100 feet, both equations yield similar results, but as structure height increases the Tremblay equation predicts a longer period. However, the Tremblay equation is still

quite conservative when compared to Rayleigh equation. This general trend can be seen in Figure 18. In general, structures without irregularities tend to have a longer period compared with those with irregularities (Fig. 19). Horizontally irregular structures exhibit this pattern but their fundamental periods are only slightly shorter than regular structures for each height examined. This can be partially explained by the fact that both regular and horizontally irregular structures have $H/H_{av} = 1$, with the horizontal irregularity accounting for a decrease in weight and thus a shorter period.

For all CBFs, the fundamental periods given by Rayleigh equation and ETABS modal analysis range from identical to a difference of 0.36%, with an average difference of 0.15%. The largest differences are found in the horizontal irregularity examples, with an average difference of 0.21%. The smallest differences are found in the examples without irregularities with an average percent difference of 0.07%. In the rest of this research the period obtained from approximate and empirical equations are compared with those obtained from Rayleigh equation as a baseline.

The fundamental periods obtained from Adeli equation are consistently larger than those obtained from ASCE Eq. (3), with the largest for CBF-R-30-5 with a 105.59% difference, and the smallest for CBF-C-10-5with a 14.54% difference. As the height of the structure increases, the average difference between the Adeli and ASCE Eq. (3) periods increase with differences of 20.46%, 63.52%, and 99.33% for ten, twenty, and thirty story examples, respectively. When comparing the two equations for varying types of structural irregularity, the examples without irregularities yield the highest average percent difference of 70.11%. Combination and vertically irregular examples have the

lowest average difference with 53.62% and 55.23%, respectively. Horizontally irregular examples fall in the middle with an average difference of 65.45%.

Compared with Rayleigh equation, Adeli equation yields a lower value for ten and twenty story examples with average differences between the two of 69.31% and 37.08%, respectively. For thirty story example structures the Adeli equation yields a higher value in three out of four examples with an average difference of 2.27%. The largest difference exists in example CBF-C-10-5, with a difference of 71.45%. More data is needed in order to suggest whether the difference between the two equations will remain low for structures over 30 stories (302 ft). When comparing Adeli equation and Rayleigh equation for irregularity type, there is no significant difference in terms of irregularity type with an average difference of 33.39% for regular structures, whereas values of 37.27%, 31.41%, and 36.77% are obtained for combination, horizontal, and vertical irregularities, respectively. The weighted average structural properties used in Adeli equation appear to provide a reasonable, albeit a lower bound and therefore conservative estimate of the fundamental period when compared with Rayleigh equation.

ASCE Eq. (3) yields an average overall underestimate of 93.13% when compared with the Rayleigh equation. As structure height increases, the difference between the estimated periods increases, with ten, twenty, and thirty story structures having an average difference of 88.69%, 95.12%, and 97.58%, respectively. In terms of irregularity type, combination and vertically irregular have lower average percent differences (88.62% and 89.60%, respectively) than horizontally and vertically irregular examples (94.48% and 99.82%, respectively.)

Tremblay equation results in a longer estimated period for all example structures when compared with ASCE Eq. (3), with the difference increasing with structure height: the difference between the Tremblay period and the ASCE period approximation for ten, twenty, and thirty story examples are 18.81%, 35.57%, and 45.21%, respectively.

Compared with Rayleigh equations, the Tremblay equation yields a lower value for all example structures. As the height of the structure increases, the difference between the two values decreases, with average differences of 70.77%, 65.07%, and 58.92% for ten, twenty, and thirty story examples, respectively.

4.4 New Equation

A goal of this research is to develop simplified equation to allow design engineers to quickly and accurately estimate the fundamental period of CBF structures by taking into account vertical and horizontal irregularities. This goal is accomplished by considering not only the height (H), but also the average height (H_{av}) of lateral force resisting CBFs, as well as the depth and the average depth of lateral force resisting CBFs (D_{av}, D) in the direction of earthquake forces. Each average value represents a weighted average value. By taking into account more structural parameters than height or number of stories, these equations will be more accurate than the current code equations (ASCE Eq. 3).

The proposed equation is developed by nonlinear regression analysis. Several equation forms were investigated, including power models of varying form, quadratic models, polynomial models, and linear models. The equations were modified to account

for structural parameters in varying ways, such as including height raised to a power compared with the ratio of height over depth raised to a power. Based on extensive simulations and statistical analyses an equation of the following form of Eq. (12) was found to match the Rayleigh equation the best statistically. Results are presented for the following regression analyses with cases 1 to 4 referring to the 3-variable power model (Eq. 12), case 5 refers to a 1-variable power model ($T=aH^b$) and case 6 refers to a linear model (T=aH).

1. Unconstrained regression analysis to determine a, b, c, and d.
2. Constrained regression analysis with b = 0.75. For a structure with no irregularity, Eq. (12) would simplify to an equation of similar form to Eq. (3), and b = 0.75 replicates the slope given in that equation.
3. Constrained regression analysis with b = 1.0. For a structure with no irregularity, the equation would simplify into a linear equation in the form of Tremblay's proposed equation.
4. Constrained regression analysis to determine a, with the values of b, c, and d rounded to the nearest 0.05.
5. Unconstrained 1-variable nonlinear regression analysis to determine a and b.
6. Unconstrained linear regression analysis to determine a.

For each regression, the standard deviation of the residuals (σ and r-squared (R^2) values are found as defined in section 3.4. The results of these regression analyses are given in Table 8.

Table 8: Regression analysis results for CBFs

	Regression Analysis Type	Best-fit Regression Coefficients	σ	R^2
3-Variable Power Model	(1) Unconstrained	a=0.032 b=0.87 c=0.59 d=0.36	0.11	0.99
	(2) Constrained with b=0.75	a=0.062 b=0.75 c=0.62 d=0.33	0.18	0.98
	(3) Constrained with b=1.0	a=0.015 b=1.00 c=0.54 d=0.38	0.30	0.98
	(4) Constrained with b=0.85, c=0.60, d=0.35	a=0.036 b=0.85 c=0.60 d=0.35	0.10	0.99
1-Variable Power Model	(5) Unconstrained	a=0.030 b=0.87	0.25	0.96
Linear Model	(6) Unconstrained	a=0.014	0.27	0.94

The standard deviation for the constrained 3-variable power model (case 4), the 1-variable power (case 5), and the linear model (case 6) are 0.10, 0.25, and 0.27, respectively. These measures indicate that case (4) provides the best fit to the data. Case (4) corresponds to an r-squared value of 0.99, meaning that 99% of the variation in the fundamental period can be explained by this model.

In order to further compare these three possible models, an F test is conducted as described in section 3.4. The F test between the linear and 1-variable power models yields a p-value of 0.0969, indicating that the linear model is statistically more significant fit for the given set of data. A p-value of 0.0004 is obtained when the F testis performed between the linear model and 3-variable power models. Based on the statistical analysis, Eq. (12) with parameters a=0.036, b=0.85, c=0.60 and d=0.35 is proposed as the best-fit equation for determining the approximate fundamental period of CBFs:

$$T = 0.036(H)^{0.85}\left(\frac{H_{av}}{H}\right)^{0.60}\left(\frac{D_{av}}{D}\right)^{0.35} \quad (18)$$

Equation 18 results in an overall average difference of 2.91% for all examples when compared with the Rayleigh data. Equation (18) yields a closer approximation as the structure height increases, with 10, 20, and 30 story structures having average differences of 4.24%, 2.57%, and 1.92%. Results from Eq. (18) are compared with the results obtained from ASCE Eq. (3), Rayleigh, and Adeli equations in Table 9 and plotted in Figure 20 as a function of height. To illustrate the effect that irregularities introduce into the approximation, the vertical bars represent the range in period value that the 3-variable power model captures due to the effect of the H_{av}/H and D_{av}/D terms. The top of the bar represents the period for a structure with no irregularities, and the length of the vertical bar is the difference between the largest and smallest period for each height as calculated by Eq. (18).

Table 9: Comparison of best-fit equation with ASCE, Adeli, and Rayleigh period for CBFs

Building Designation	H (ft)	$T_{Tremblay}$	T_{ASCE} Eq. (3)	T_{Adeli}	$T_{Rayleigh}$	Eq. (18)
CBF-R-10-5	102	0.78	0.64	0.87	1.73	1.85
CBF-V-10-5	102	0.78	0.64	0.75	1.57	1.66
CBF-H-10-5	102	0.78	0.64	0.80	1.65	1.71
CBF-C-10-5	102	0.78	0.64	0.74	1.57	1.60
CBF-R-20-5	202	1.54	1.07	2.36	3.25	3.30
CBF-V-20-5	202	1.54	1.07	1.86	2.89	2.85
CBF-H-20-5	202	1.54	1.07	2.24	3.09	3.05
CBF-C-20-5	202	1.54	1.07	1.85	2.88	2.70
CBF-R-30-5	302	2.30	1.45	4.69	4.77	4.64
CBF-V-30-5	302	2.30	1.45	4.06	4.00	4.11
CBF-H-30-5	302	2.30	1.45	4.57	4.31	4.29
CBF-C-30-5	302	2.30	1.45	3.98	3.85	3.92

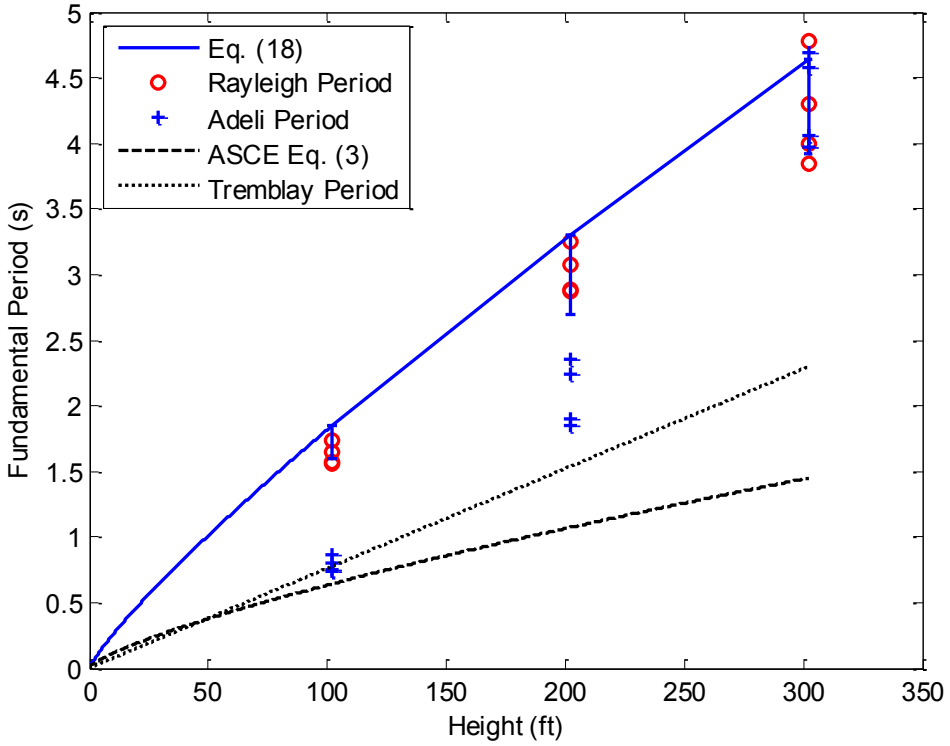

Figure 20: Comparison of results from Eq. (18) with the results obtained from ASCE Eq. (3), Rayleigh, Adeli and Tremblay equations as a function of height. The top of the bar represents the period for a structure with no irregularities, and the length of the vertical bar is the difference between the largest and smallest period for each height as calculated by Eq. (18).

Equation (18) represents the best-fit to the Rayleigh period data for CBFs. However, it does not take into account nonstructural elements that add to the stiffness of the structure and thus is a non-conservative estimate. As such, the periods obtained by Eq. (18) represent an upper-bound to the permissible periods used in design as stipulated by ASCE 7-10. Therefore, a reduction of the best-fit equation is suggested by lowering each best fit curve without changing its shape and general pattern by comparing Eq. (18)

with measured period data compiled by Kwon and Kim (2010) for an assortment of structures in California without large irregularities. All structures selected for comparison with Eq. (18) have concentrically braced frames in both longitudinal and transverse direction. This results in a total of 9 structures with periods measured in both the longitudinal and transverse directions, for a total of 18 measured periods. All measured periods come from CSMIP. Table 10 gives the building designations, city, earthquake name and year it occurred with its magnitude, peak ground acceleration (PGA), and measured periods.

In order to suggest a conservative approximation for the fundamental period, a reduced form of Eq. (18) is posed by reducing the equation by the standard deviation in order to obtain an equation which yields a conservative estimate for 70-80% of the measured periods. Since the standard deviation is relatively small (σ =0.10) the best-fit equation will have to be reduced by several standard deviations in order to reach the desired conservative estimation. Equation (18) resulted in a non-conservative estimate for all measured periods, so an initial modification of minus two standard deviations (best-fit -2σ) is examined, which resulted in a conservative estimation for only 2 of 18 periods (11.1%). It was observed from the results that there was still a large discrepancy between the measured periods and proposed equation due to the very small standard deviation for the best-fit curve. The next gradation which yielded more conservative results was the best-fit -6σ curve, which yielded conservative results for 5 of 18 periods (27.78%). Finally, the best-fit -8σ was compared with the measured periods, which

resulted in a conservative estimate for 13 of 18 periods (72.22%). This is shown in Figure 21.

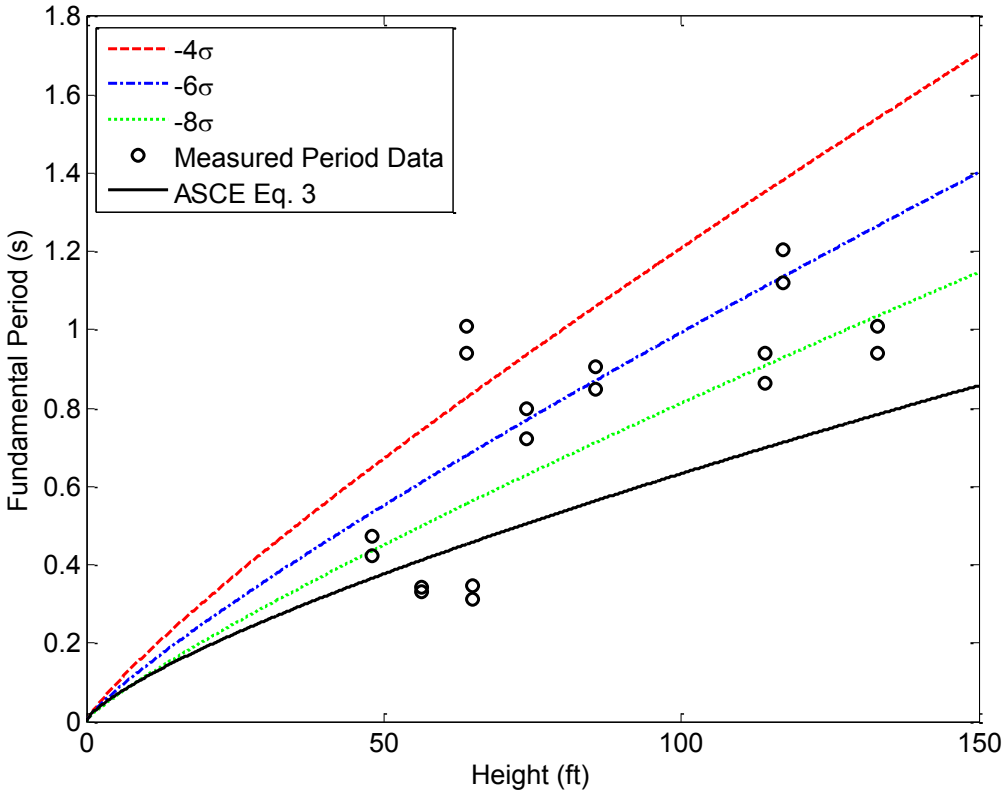

Figure 21: Reduction of best-fit Eq. (18)

As such, the following equation for the approximate fundamental period for CBFs is proposed for use in practice:

$$T = 0.015(H)^{0.85}\left(\frac{H_{av}}{H}\right)^{0.60}\left(\frac{D_{av}}{D}\right)^{0.35} \quad (19)$$

Since there were a limited number of measured periods available, Eq. (19) is also compared with the database of period data for CBFs compiled by Tremblay (2005). The database contained 195 CBFs compiled from 35 different sources. The majority of examples were designed under recent versions (1980 or later) of the Canadian Design Code. No data is available on structural configuration, so all structures are assumed to have no plan or vertical irregularity. Equation (19) is compared with ASCE Eq. (3) and the measured period data, with results given in Table 10. Results of Table 10 are plotted in Figure 22, in addition to periods from the Tremblay database and Eq. (18).

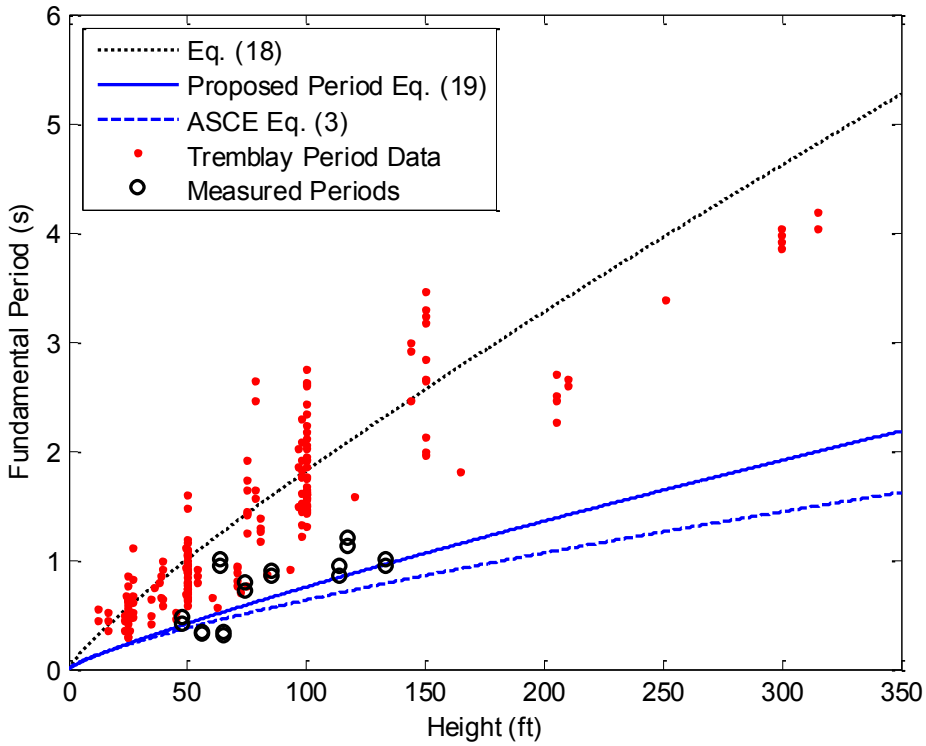

Figure 22: Comparison of periods from measured and example data with those obtained from Eqs. (18 & 19) for CBFs

Table 10: Comparison of periods from measured data with those obtained from Eq. (19) for CBFs

Building Code	City	EQ (Year)	M	H (ft)	PGA(g)	T_{Long}	T_{Trans}	Eq. 3	Eq. 19
C24053	Los Angeles	Yucaipa (2005)	4.9	48.0	0.01	0.42	0.47	0.36	0.35
C58769	Hayward	Berkeley (2003)	3.9	56.3	0.01	0.34	0.33	0.41	0.46
C13214	Costa Mesa	Yucaipa (2005)	4.9	64.0	0.02	0.94	1.01	0.45	0.51
C47796	Sanlinas	Aromas (2007)	4.3	65.0	0.02	0.31	0.35	0.46	0.52
C23497	Rancho Cucamong	Hector Mine (1999)	7.1	74.0	0.03	0.80	0.72	0.50	0.58
C24652	Los Angeles	Northridge (1994)	6.7	85.5	0.24	0.85	0.91	0.56	0.66
C24713	Los Angeles	Big Bear City (2003)	5.4	114.0	0.01	0.94	0.86	0.70	0.84
C24605	Los Angeles	Landers (1992)	7.3	117.0	0.04	1.12	1.20	0.71	0.86
C13702	Riverside	Anza (2005)	5.2	133.0	0.02	0.94	1.01	0.78	0.96

Figure 22 shows that Eq. (19) yields a less conservative result than ASCE Eq. (13), for all but one structure, with a ratio ranging from 0.97 to 1.22. The ASCE Code specifies that the fundamental period may be either estimated from ASCE Eq. (3), or determined from an alternative substantiated analysis, such as the Rayleigh equation or normal modal analysis. This result may be used as long as its value does not exceed a coefficient ranging from 1.4 to 1.7 multiplied by the result from ASCE Eq. (3). We can see that with a ratio ranging from 1.10 to 1.23 the proposed equation falls in the range of what is currently deemed acceptable by the code. Equation (19) results in a conservative estimate for 72.22% of measured periods, whereas ASCE Eq. (13) is conservative for 77.78% of the measured periods. The average difference between ASCE Eq. (3) and the measured periods is 36.14%, whereas the average difference between Eq. (19) and the measured periods is 28.51%.

Eq. (18) results in a satisfactory approximation of the data when compared with the Tremblay period database. Equation (18) yields an un-conservative estimation of the fundamental period for 119 of the 195 examples with an average difference of 24.27%. For the remaining 76 examples Eq. (18) yields a conservative estimate with an average difference of 74.68%. Equation (19) results in a conservative approximation for all 195 Tremblay examples with an average difference of 75%. It is shown that ASCE Eq. (3) also yields a conservative estimation for all 195 examples, with an average difference of 85.35%.

It can be observed that Eq. (19) yields a better fit to the measured periods for structures subjected to a stronger PGA. For structure C24652 subjected to the Northridge

earthquake (M6.7, PGA 0.24) the difference in measured longitudinal and transverse periods and Eq. (19) are 25.34% and 31.6% on the conservative side, respectively, compared with 40.62% and 46.7% on the conservative side when compared with ASCE Eq. (3).

Fundamental period data for irregular concentrically braced frame structures is scarce. The fit of best-fit Eq. (18) with the irregular example CBF structures highlights the importance of incorporating additional structural parameters which account for structural irregularities, and comparison with the Tremblay database validates the accuracy of this approximation. The comparison of measured data with the results obtained from the proposed Eq. (19) validates the merit of the proposed equation.

4.5 Conclusions

Through a comparison of the fundamental period of 12 CBFs by the ASCE equation (Eq. 3), Tremblay equation (Eq. 5) Rayleigh equation (Eq. 7), ETABS generated period, and Adeli equation (Eq. 8, 10, 11), the following conclusions are made:

1) ASCE Eq. (3) equation yields a much more conservative estimate when compared with the periods obtained from the Rayleigh equation and modal analysis.
2) The periods resulting from the Rayleigh equation and ETABS modal analysis are nearly identical for all example buildings. The Adeli equation yields a longer period when compared with ASCE Eq. (3), and a shorter period when compared with the results of the Rayleigh/ETABS periods. Hence, the Adeli equation can

provide an accurate, yet generally conservative, estimate of the fundamental period for a structure past the preliminary design phase.

3) Structures without irregularities tend to have a longer period in comparison with irregular structures. Horizontally irregular structures tend to have fundamental periods only slightly shorter than regular structures for each height examined. Structures with vertical and combination irregularities exhibit very similar periods.
4) Linear, 1-variable power, and 3-variable power regression models were developed along with several others. The results were compared through statistical methods using 12 CBFs. It is concluded that a 3-variable power model which captures structural irregularity results in a better statistically significant model of the fundamental period when compared to an equation which is based simply on its height.
5) A new equation is proposed as an approximate equation for the fundamental period of steel CBFs along the principal structural direction under consideration. Comparison with ASCE Eq. (3) and measured period data shows that the proposed equation yields a more reasonable estimation than the current code equation.

Fundamental period data for irregular concentrically braced frame structures is scarce. The fit of best-fit Eq. (18) with the irregular example CBF structures highlights the importance of incorporating additional structural parameters which account for

structural irregularities, and comparison with the Tremblay database validates the accuracy of this approximation. The comparison of measured data with the results obtained from the proposed Eq. (19) validates the merit of the proposed equation.

CHAPTER 5: ECCENTRICALLY BRACED FRAMES

5.1 Building Design Model

Eccentrically brace frames of type shown in Figure 23 are considered. All EBF structures are modeled with either 30 stories, 20 stories, or 10 stories (N) and 5 bays (N_b). with a uniform story height of 10 feet, with the exception of 12 feet for the first story, and a uniform bay spacing of 25 feet. An eccentricity (e) of 5 ft is used in all examples. The locations of bracings for each 10, 20, and 30 story structure are the same as those shown in Figure 15, Figure 16, and Figure 17 for CBFs with the replacement of bracings as shown in Figure 23.

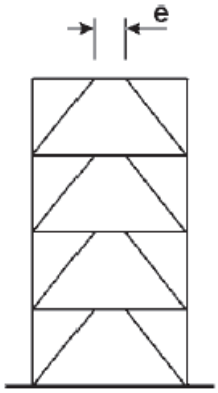

Figure 23: Eccentrically Brace Frame (EBF)

A total of 12 EBF structures are evaluated: 3 vertically irregular structures, 3 horizontally irregular structures, 3 vertically and horizontally irregular structures, and 3

regular reference structures. The irregularities of irregular structures can be seen in Figs. 14 to 16. Each structure has a designation beginning with EBF followed by V, H, C, or R representing vertical, horizontal, or combination irregularity, respectively, or their regular counterpart, followed by a numerical designation indicating the number of stories and the number of bays. For example, EBF-V-20-5 represents a 20 story, 5 bay concentrically braced frame with a vertical irregularity. Likewise, the designation EBF-R-10-5 represents a 10 story, 5 bay concentrically braced frame with no structural irregularity. The setbacks and reentrant corner irregularities are defined in terms of depth and height. For each structure, the criterion for irregularity is checked to ensure that an irregularity is present as defined by the code as described in Section 1.3.2, and none falls under the classification of extreme irregularity.

As defined by ASCE 7-10, the coefficients used in Eq. (3) for steel eccentrically braced frames are $C_t = 0.03$ and $x = 0.75$. The deflection, lateral force, and weight per story used in the Rayleigh equation come directly from the structural models developed in ETABS. The period calculated from ETABS comes directly from the mode of vibration which has the largest modal participation mass ratio in the direction being considered.

5.2 Results

Design, loading, and deflection data for EBFs are given in Appendix C (Table 52 to Table 63). For each story the column section, beam section, bracing section, lateral deflection of each story, and weight and seismic force assigned to each story are given.

The fundamental period of all EBFs using ASCE equation (Eq. 3), Rayleigh equation (Eq. 7), ETABS generated period, and Adeli equation (Eq. 9-11) are summarized in Table 11 and shown graphically in Figure 24. Table 11 also includes the ratio of the weighted average height to maximum height (H_{av}/H) and the weighted average depth to maximum depth (D_{av}/D) for all examples.

Table 11: Fundamental periods of EBFs sorted by height

Building Designation	H (ft)	H_{av}/H	D_{av}/D	T_{ASCE} Eq. 3	$T_{Rayleigh}$	T_{ADELI}	T_{ETABS}
EBF-R-10-5	102	1.00	1.00	0.96	2.12	1.01	2.16
EBF-V-10-5	102	0.90	0.88	0.96	1.94	0.87	1.94
EBF-H-10-5	102	1.00	0.80	0.96	2.10	0.97	2.10
EBF-C-10-5	102	0.94	0.74	0.96	1.96	0.86	1.96
EBF-R-20-5	202	1.00	1.00	1.61	3.87	2.77	3.87
EBF-V-20-5	202	0.87	0.84	1.61	3.15	2.17	3.21
EBF-H-20-5	202	1.00	0.80	1.61	3.43	2.54	3.47
EBF-C-20-5	202	0.85	0.74	1.61	3.12	1.83	3.18
EBF-R-30-5	302	1.00	1.00	2.17	5.55	5.39	5.56
EBF-V-30-5	302	0.89	0.87	2.17	4.61	4.30	4.63
EBF-H-30-5	302	1.00	0.80	2.17	5.22	4.97	5.23
EBF-C-30-5	302	0.93	0.70	2.17	4.64	4.07	4.66

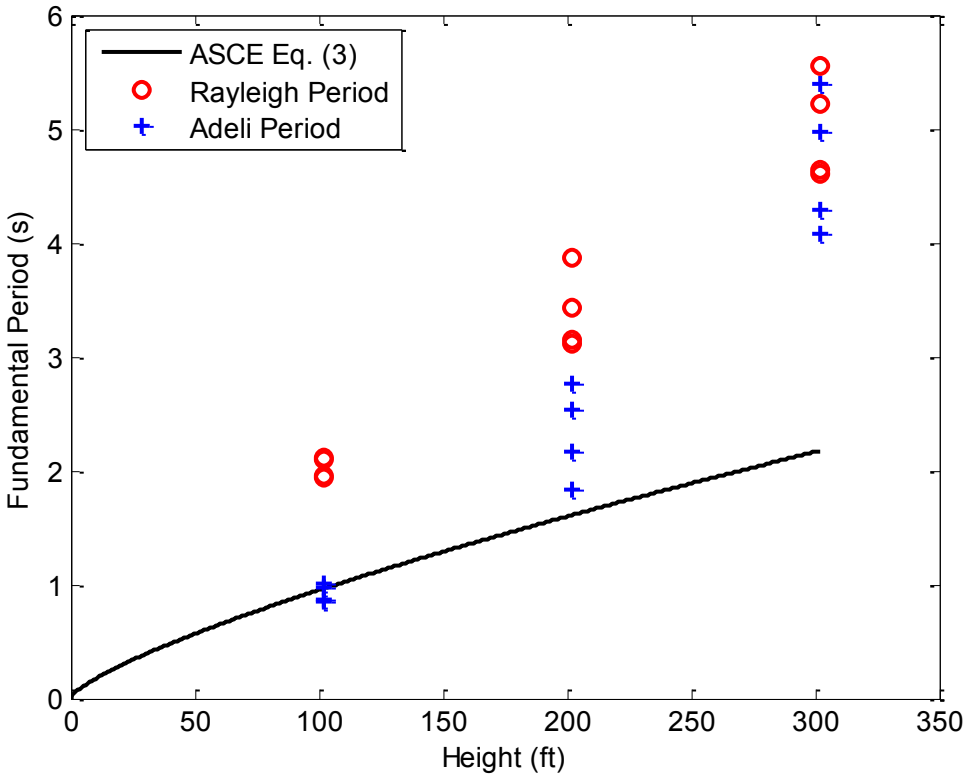

Figure 24: Fundamental period versus height for EBFs

Figure 25 shows the fundamental period versus height for each structure type (combination irregularity, horizontal irregularity, vertical irregularity, and no irregularity.)

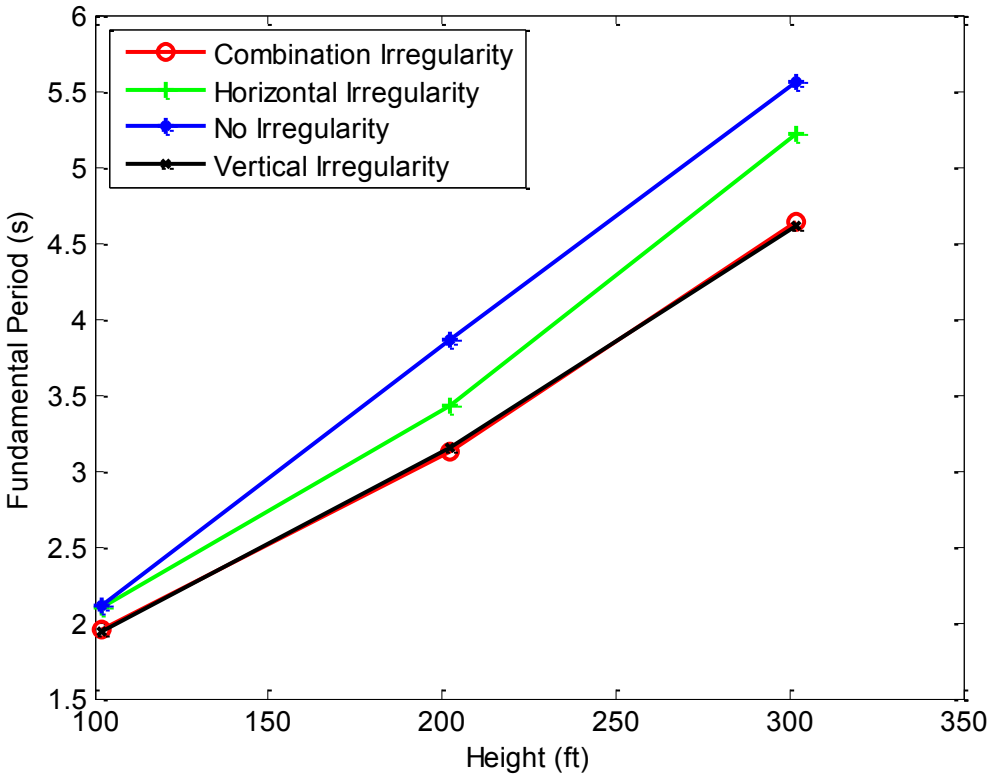

Figure 25: Rayleigh fundamental period versus height for CBFs

5.3 Analysis of Results

ASCE Eq. (3) yields the most conservative estimate of the fundamental period for all example EBFs with the exception of examples EBF-C-10-5 and EBF-V-10-5. In general, the periods obtained by Rayleigh equation and ETABS modal analysis yield close values and the longest fundamental period. Adeli equation, in general, yields values closer to ASCE Eq. (3) for 10 story structures, values closer to Rayleigh equation for 30 story structures, and a middle ground between the two for 20 story structures. In general, structures without irregularities have the longest period, followed by horizontally irregular structures, with vertically and combination irregular structures having the

shortest period (Figure 25). This can be partially explained by the fact that irregularities result in a decrease in weight and thus a shorter period.

For all EBFs, the fundamental periods given by Rayleigh equation and ETABS modal analysis range from identical to a difference of 2.15%, with an average difference of 0.72%. The smallest differences are found in the horizontal irregularity examples, with an average difference of 0.45%. Combination irregular, regular, and vertically irregular structures have an average difference of 0.76%, 0.83%, and 0.84%, respectively. Since the values between these two methods of calculating fundamental period appear by and large to yield close results for EBFs, in the rest of this research the period obtained from approximate and empirical equations are compared with those obtained from Rayleigh equation as a baseline.

The fundamental periods obtained from Adeli equation are consistently larger for twenty and thirty story structures than those obtained from ASCE Eq. (3). For ten story structures, Adeli equation yields a lower estimate for examples EBF-C-10-5 and EBF-V-10-5, with underestimations of 11.58% and 10.13%, respectively. As the height of the structure increases, the average difference between Adeli equation and ASCE Eq. (3) periods increase with differences of 6.86%, 35.18%, and 72.45% for ten, twenty, and thirty story examples, respectively. When comparing the two equations for varying types of structural irregularity, the examples without irregularities yield the highest average percent difference of 47.7%. Combination, vertical, and horizontally irregular structures yield average differences of 28.54%, 35.17%, and 41.23%.

Compared with Rayleigh equation, Adeli equation yields a lower value for ten, twenty, and thirty story structures with average differences of 74.67%, 37.97%, and 7.01%. The largest difference exists in example EBF-C-10-5, with a difference of 78.28%. More data is needed in order to suggest whether the difference between the two equations will remain low for structures over 30 stories (302 ft). When comparing Adeli equation and Rayleigh equations for irregularity type, combination irregular structures have the largest average difference with 47.75%. For horizontal and vertical irregularities and regular structures, differences of 36.16%, 40.01%, and 35.61% are obtained, respectively.

ASCE Eq. (3) yields an average overall underestimate of 73.55% when compared with the Rayleigh equation. As structure height increases, the difference between the estimated periods increases, with ten, twenty, and thirty story structures having an average difference of 70.91%, 71.19%, and 78.55%, respectively. In terms of irregularity type, combination and vertically irregular have lower average percent differences (68.24% and 68.00%, respectively) than horizontally and vertically irregular examples (76.28% and 81.69%, respectively.)

5.4 New Equation

A goal of this research is to develop simplified equations to allow design engineers to quickly and accurately estimate the fundamental period of EBF structures by taking into account vertical and horizontal irregularities. The goal is to develop equations which take into account structural irregularities by considering not only the height (H),

but also the average height (H_{av}) of lateral force resisting EBFs, as well as the depth and the average depth of lateral force resisting EBFs (D_{av}, D) in the direction of earthquake forces. Each average value represents a weighted average value. By taking into account more structural parameters than height or number of stories, this equation will be more accurate than the current code equations.

The proposed equation is developed by nonlinear regression analysis. Several equation forms were investigated, including power models of varying form, quadratic models, polynomial models, and linear models. The equations were modified to account for structural parameters in varying ways, such as including height raised to a power compared with the ratio of height over depth raised to a power. Based on extensive simulations and statistical analyses an equation of the following form of Eq. (12) was found to match the Rayleigh equation the best statistically. Results are presented for the following regression analyses with cases 1 to 4 referring to the 3-variable power model (Eq. 12), case 5 refers to a 1-variable power model ($T=aH^b$) and case 6 refers to a linear model (T=aH).

Based on extensive simulations and statistical analyses an equation of the form of Eq. (12) was found to match the Rayleigh equation the best statistically. Results are presented for the following regression analyses with cases 1 to 5 referring to the 3-variable power model (Eq. 12), case 6 refers to a 1-variable power model ($T=aH^b$) and case 7 refers to a linear model (T=aH).

1. Unconstrained regression analysis to determine a, b, c, and d.

2. Constrained regression analysis with b = 0.75. For a structure with no irregularity, Eq. (12) would simplify to an equation of similar form to Eq. (3), and b = 0.75 replicates the slope given in that equation.
3. Constrained regression analysis with b = 1.0. For a structure with no irregularity, the equation would simplify into a linear equation.
4. Constrained regression analysis to determine a, with the values of b, c, and d rounded to the nearest 0.05.
5. Constrained regression analysis with b=0.85, c=0.60, and d=0.35, which are the coefficients from the CBF case; similar coefficients EBFs would simplify calculations and imitates current code equations for braced frames.
6. Unconstrained 1-variable nonlinear regression analysis to determine a and b.
7. Unconstrained linear regression analysis to determine a.

For each regression, the standard deviation of the residuals (σ) and r-squared (R^2) values are found as defined in section 3.4. The results of these regression analyses are given in Table 12.

Table 12: Regression analysis results for EBFs

	Regression Analysis Type	Best-fit Regression Coefficients	σ	R^2
3-Variable Power Model	(1) Unconstrained	a=0.042 b=0.85 c=1.02 d=0.26	0.11	0.99
	(2) Constrained with b=0.75	a=0.073 b=0.75 c=1.04 d=0.25	0.18	0.97
	(3) Constrained with b=1.0	a=0.019 b=1.00 c=0.96 d=0.29	0.22	0.96
	(4) Constrained with b=0.85, c=1.05, d=0.25	a=0.0417 b=0.85 c=1.05 d=0.25	0.10	0.99
	(5) Constrained with b=0.85, c=0.60, d=0.35	a=0.0423 b=0.85 c=0.60 d=0.35	0.13	0.99
1-Variable Power Model	(5) Unconstrained	a=0.037 b=0.86	0.33	0.94
Linear Model	(6) Unconstrained	a=0.017	0.36	0.92

The standard deviation of case (4), case (5), the 1-variable power (case 6), and the linear model (case 7) are 0.10, 0.13, 0.33, and 0.36, respectively. Even though case (4) has the lowest standard deviation, case (5) is chosen as the best fit 3-variable power

model in order to maintain consistency between CBF and EBF proposed equations. Case (5) corresponds to an r-squared value of 0.99, meaning that 99% of the variation in the fundamental period can be explained by this model.

The F test between the linear and 1-variable power models yields a p-value of 0.1167, indicating that the linear model is statistically more significant fit for the given set of data. A p-value of 0.0005 is obtained when the F test is performed between the linear model and 3-variable power models. Based on the statistical analysis, Eq. (12) with parameters a=0.042, b=0.85, c=0.60 and d=0.35 is proposed as the best-fit equation for determining the approximate fundamental period of EBFs:

$$T = 0.042(H)^{0.85}\left(\frac{H_{av}}{H}\right)^{0.60}\left(\frac{D_{av}}{D}\right)^{0.35} \quad (20)$$

Equation 20 results in an overall average difference of 3.02% for all examples when compared with the Rayleigh data. The average difference for 10, 20, and 30 story structures is 3.37%, 2.36%, and 3.31%, respectively. Results from Eq. (20) are compared with the results obtained from ASCE Eq. (3), Rayleigh, and Adeli equations in Table 13 and plotted in Figure 26 as a function of height. To illustrate the effect that irregularities introduce into the approximation, the vertical bars represent the range in period value that the 3-variable power model captures due to the effect of the H_{av}/H and D_{av}/D terms. The top of the bar represents the period for a structure with no irregularities, and the length of the vertical bar is the difference between the largest and smallest period for each height as calculated by Eq. (20).

Table 13: Comparison of best-fit equation with ASCE, Adeli, and Rayleigh period for EBFs

Building Designation	H (ft)	T_{ASCE} Eq. (3)	T_{Adeli}	$T_{Rayleigh}$	Eq. (20)
EBF-R-10-5	102	0.96	1.01	2.12	2.14
EBF-V-10-5	102	0.96	0.87	1.94	1.92
EBF-H-10-5	102	0.96	0.97	2.10	1.98
EBF-C-10-5	102	0.96	0.86	1.96	1.85
EBF-R-20-5	202	1.61	2.77	3.87	3.83
EBF-V-20-5	202	1.61	2.17	3.15	3.30
EBF-H-20-5	202	1.61	2.54	3.43	3.54
EBF-C-20-5	202	1.61	1.83	3.12	3.13
EBF-R-30-5	302	2.17	5.39	5.55	5.39
EBF-V-30-5	302	2.17	4.30	4.61	4.77
EBF-H-30-5	302	2.17	4.97	5.22	4.98
EBF-C-30-5	302	2.17	4.07	4.64	4.55

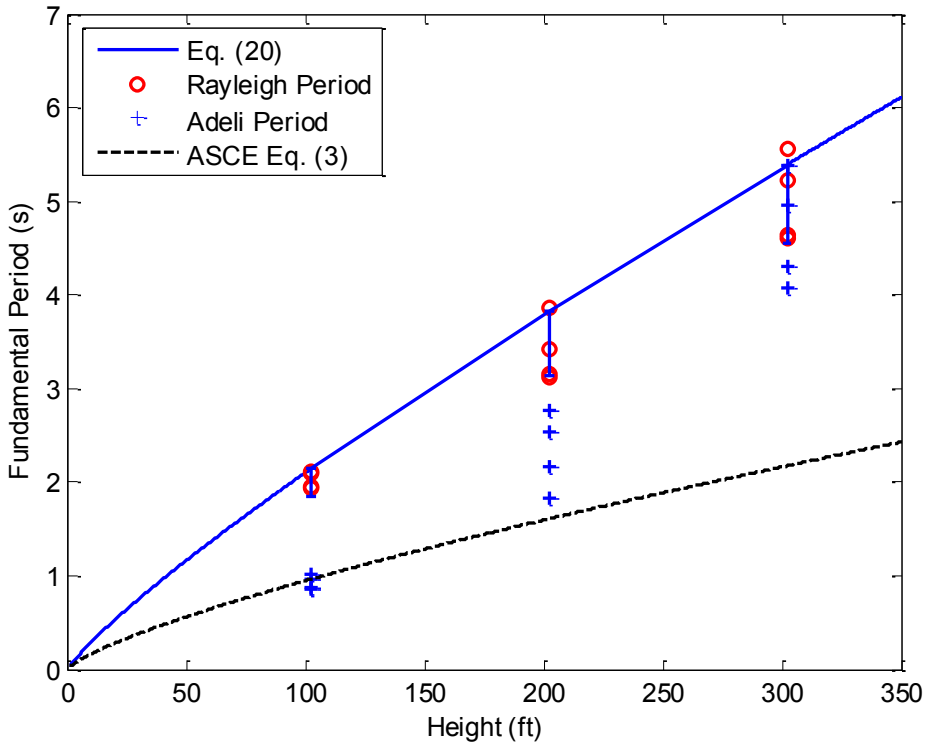

Figure 26: Comparison of results from Eq. (20) with the results obtained from ASCE Eq. (3), Rayleigh, and Adeli equations as a function of height. The top of the bar represents the period for a structure with no irregularities, and the length of the vertical bar is the difference between the largest and smallest period for each height as calculated by Eq. (20)

Equation (20) represents the best-fit to the Rayleigh period data for EBFs. However, it does not take into account nonstructural elements that add to the stiffness of the structure and thus is a non-conservative estimate. As such, the periods obtained by Eq. (20) represent an upper-bound to the permissible periods used in design as stipulated by ASCE 7-10. Therefore, a reduction of the best-fit equation is suggested by lowering each best fit curve without changing its shape and general pattern by comparing Eq. (20)

with measured period data compiled by Kwon and Kim (2010) for an assortment of structures in California without large irregularities. All structures selected for comparison with Eq. (20) have steel eccentric bracing in both longitudinal and transverse direction which results in a total of 3 structures with periods measured in both the longitudinal and transverse directions, for a total of 6 measured periods. All measured periods come from CSMIP. Table 14 gives the building designations, city, earthquake name and year it occurred with its magnitude, peak ground acceleration (PGA), and measured periods.

In order to suggest a conservative approximation for the fundamental period, a reduced form of Eq. (20) is posed by reducing the equation by the standard deviation in order to obtain an equation which yields a conservative estimate for 50-60% of the measured periods. For this case, 50-60% is the target due to the small sample size in which 4 out of the 6 data points are for structures under 5 stories. Equation (20) resulted in a non-conservative estimate for all measured periods. Equation (20) remained un-conservative until it was reduced by four standard deviations (best-fit -4σ), which resulted in a conservative estimation for only 1 of 6 periods (16.67%). It was observed from the results that there was still a large discrepancy between the measured periods and proposed equation due to the very small standard deviation for the best-fit curve. The next step which yielded more conservative results was the best-fit -6σ curve, which yielded conservative results for 3 of 6 periods (50%). At this point, no further reduction is attempted. This is shown in Figure 27.

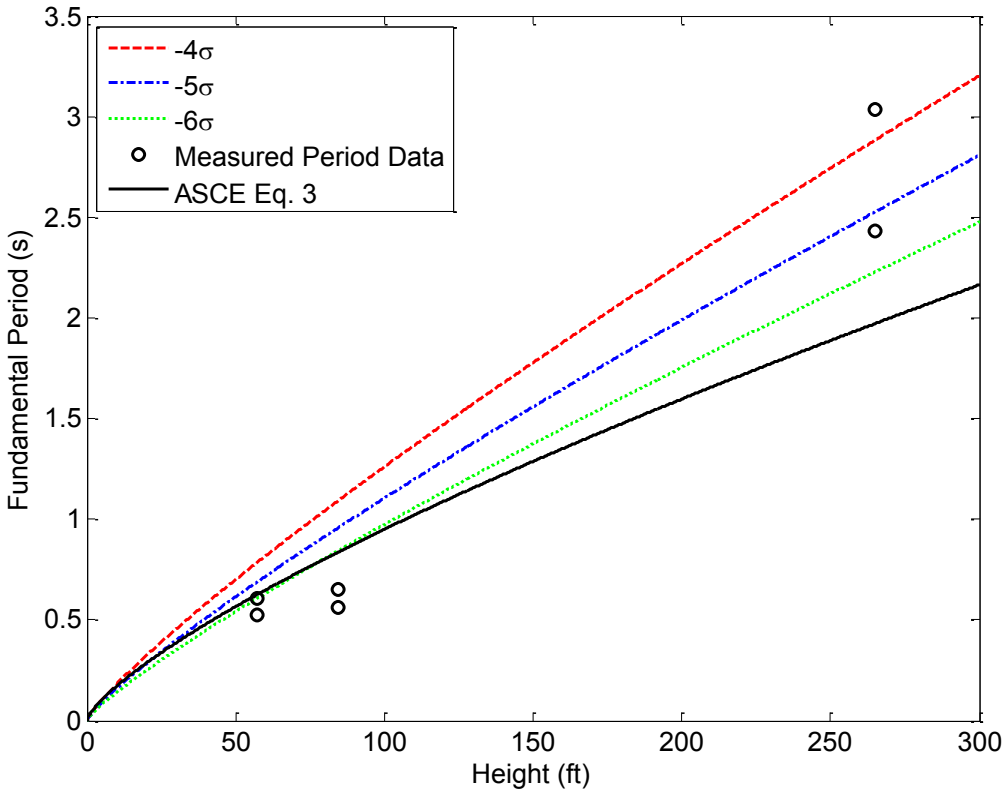

Figure 27: Reduction of best-fit Eq. (20)

As such, the following equation for the approximate fundamental period for EBFs is proposed for use in practice:

$$T = 0.02(H)^{0.85}\left(\frac{H_{av}}{H}\right)^{0.60}\left(\frac{D_{av}}{D}\right)^{0.35} \quad (21)$$

Since there were a limited number of measured periods available, Eq. (21) is also compared with the database of period data for EBFs compiled by Tremblay (2005). The database contained 25 EBFs compiled from 11 different sources. The majority of

examples were designed under recent versions (1980 or later) of the Canadian Design Code. No data is available on structural configuration, so all structures are assumed to have no plan or vertical irregularity. Equation (21) is compared with ASCE Eq. (3) and the measured period data, with results given in Table 14. Results of Table 14 are plotted in Figure 28.

Table 14: Comparison of periods from measured data with those obtained from Eq. (21) for EBFs

Building Code	City	EQ (Year)	M	H (ft)	PGA (g)	T_{Long}	T_{Trans}	Eq. 3	Eq. 21
C03603	San Diego	San Clemente (2004)	5.2	265	0.02	3.03	2.43	1.97	2.30
C58593	Stanford	Alum Rock (2007)	5.4	57	0.01	0.53	0.61	0.62	0.62
C57594	San Jose	Alum Rock (2007)	5.4	84.5	0.07	0.66	0.56	0.84	0.87

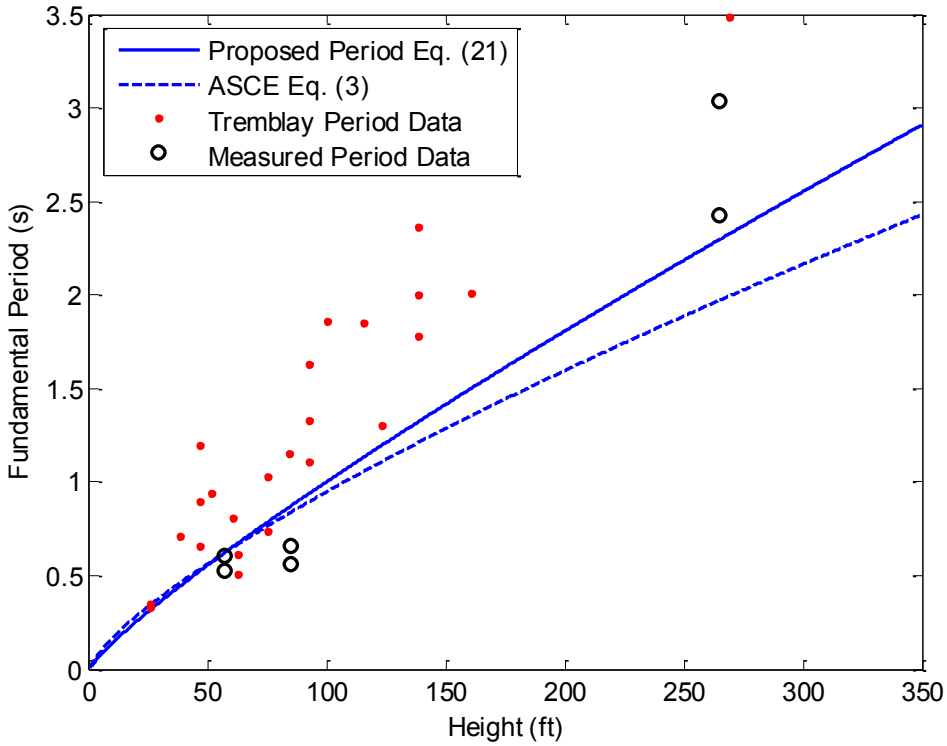

Figure 28: Comparison of periods from measured and example data with those obtained from Eqs. (21) for EBFs

Figure 28 shows that ASCE Eq. (3) and Eq. (21) yield very similar results for structures under 100 feet. As the height of the structure increases, the differences in the periods approximated by the two equations also increases. The ratio of Eq. (21) to ASCE Eq. (3) ranges from 1.00 to 1.16. The ASCE Code specifies that the fundamental period may be either estimated from ASCE Eq. (3), or determined from an alternative substantiated analysis, such as the Rayleigh equation or normal modal analysis. This result may be used as long as its value does not exceed a coefficient ranging from 1.4 to 1.7 multiplied by the result from ASCE Eq. (3). We can see that with a ratio ranging

from 1.10 to 1.23 the proposed equation falls in the range of what is currently deemed acceptable by the code.

Equation (21) results in a satisfactory conservative approximation of the data when compared with the Tremblay period database. Equation (21) yields an un-conservative estimation of the fundamental period for 3 of the 25 examples with an average difference of 13.77%. For the remaining 22 examples Eq. (21) yields a conservative estimate with an average difference of 37.49%. It is shown that ASCE Eq. (3) yields a conservative estimation for 21 examples, with an average difference of 42.71%. In comparison with the measured data, Equation (21) yields an average difference of 20.57%. A slightly larger difference exists between ASCE Eq. (3) and the measure data, with a difference of 24.36%.

5.5 Conclusions

Through a comparison of the fundamental period of 12 eccentrically braced frame structures by the ASCE equation (Eq. 3), Rayleigh equation (Eq. 7), ETABS generated period, and Adeli equations (Eq. 8, 10, 11), the following conclusions are made:

1) ASCE Eq. (3) equation yields a more conservative estimate when compared with the periods obtained from the Rayleigh equation and modal analysis.
2) The periods resulting from the Rayleigh equation and ETABS modal analysis are nearly identical for all example buildings. The Adeli equation yields longer periods when compared with ASCE Eq. (3) for 20 and 30 story structures, and shorter periods when compared with the results of the Rayleigh/ETABS period

for 10 and 20 story structures. Hence, the Adeli equation can provide an estimate of the fundamental period for a structure past the preliminary design phase. Further evaluation of the proposed Adeli equation for EBFs presented in this paper should be conducted on varying EBF configurations to verify its applicability for a number of formations.

3) Structures without irregularities tend to have a longer period in comparison with irregular structures. Horizontally irregular structures tend to have fundamental periods only slightly shorter than regular structures for each height examined. Structures with vertical and combination irregularities exhibit very similar periods.
4) Linear, 1-variable power, and 3-variable power regression models were developed along with several others. The results were compared through statistical methods using 12 EBFs. It is concluded that a 3-variable power model which captures structural irregularity results in a better statistically significant model of the fundamental period when compared to an equation which is based simply on its height.
5) A new equation is proposed as an approximate equation for the fundamental period of steel EBFs along the principal structural direction under consideration. Comparison with ASCE Eq. (3) and measured period data shows that the proposed equation yields a more reasonable estimation than the current code equation.

Fundamental period data for irregular EBF structures is scarce. The fit of best-fit Eq. (20) with the irregular example EBF structures highlights the importance of incorporating additional structural parameters which account for structural irregularities, and comparison with the Tremblay database validates the accuracy of this approximation. The comparison of measured data with the results obtained from the proposed Eq. (21) validates the merit of the proposed equation.

CHAPTER 6: CONCLUSION

6.1 Summary and Conclusions

A study has been conducted on the fundamental period of irregular steel structures. A total of 24 MRFs, 12 CBFs, and 12 EBFs were designed and their fundamental periods analyzed by several different methods. Based on these analyses, empirical equations based on a 3-variable power model are suggested to improve the accuracy of the fundamental period approximation and account for the effect of irregularities on the period. These values of the four regression parameters are summarized in Table 15. The proposed equations for MRFs, CBFs, and EBFs are plotted in Figure 29 along with the ASCE eq. (3) for each structure type.

Table 15: Proposed equation parameters

	MRF		CBF		EBF	
	Eq. (17)	Eq. (3)	Eq. (19)	Eq. (3)	Eq. (21)	Eq. (3)
a	0.042	0.028	0.015	0.020	0.020	0.030
b	0.75	0.80	0.85	0.75	0.85	0.75
c	0.35	-	0.60	-	0.60	-
d	0.20	-	0.35	-	0.35	-

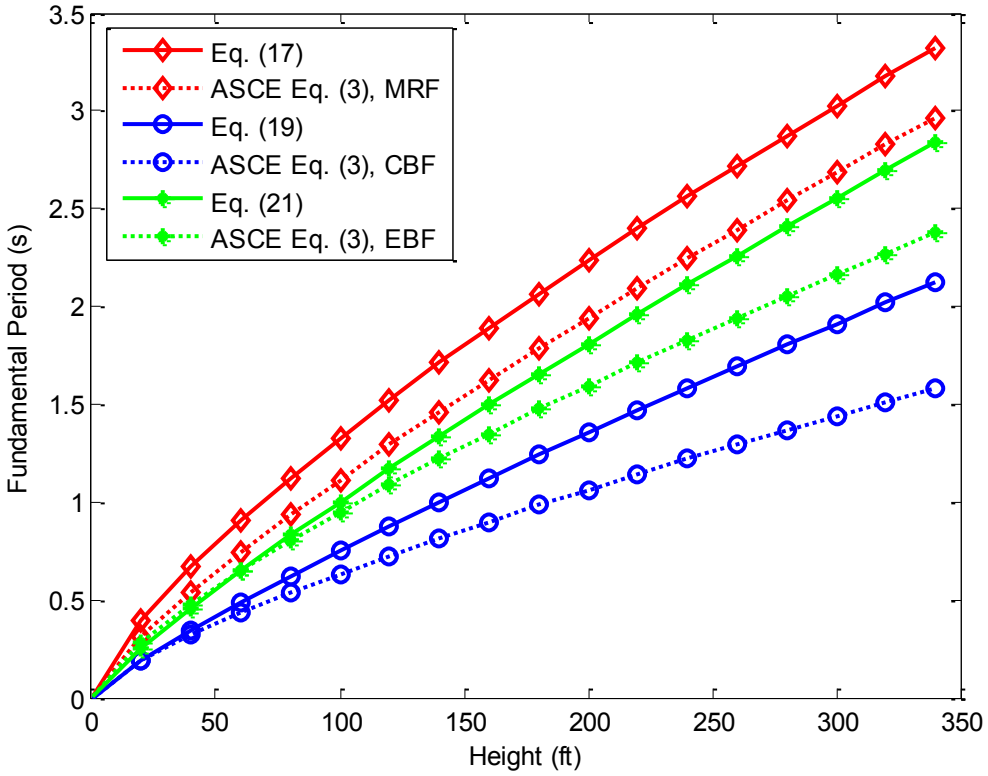

Figure 29: Comparison of proposed equations with ASCE Eq. (3)

The proposed equations were shown to accurately predict the variation in fundamental period that results from horizontal or vertically irregularities, or a combination of the two. The current code equations are unable to predict this variation. It was shown that structures with irregularities exhibit a shorter period than their regular counterparts. The proposed equations accurately predict this variation, resulting in models that can predict a more accurate initial fundamental period. Once the preliminary design is complete, other equations which utilize structural properties such as the Adeli equation may be used to further refine the fundamental period estimation.

6.2 Suggestions for Further Studies

The models used to derive these equations fail to account for partition walls, structural walls, and other structural elements which add to the stiffness of a structure. Further studies may be conducted which account for these elements. Furthermore, models of varying heights and configurations can be added to this database in order to further refine these proposed equations.

The validation of the proposed equations with measured periods were limited to the available data from instrumented structures, of which did not include information on complete structural dimensions or existing irregularities. Therefore, the proposed equations were compared with the measured fundamental periods of structures without irregularities. As more measured data becomes available, further comparison should be conducted with refinement of the proposed equations as needed.

Another study could be done on the difference in cost that results from using this more accurate fundamental period approximation.

BIBLIOGRAPHY

Adeli, H. (1985). Approximate Formulae for Period of Vibrations of Building Systems. *Civil Engineering for Practicing and Design Engineers, 4*, 93-128.

AISC. (2005). *ANSI/AISC 360-05: An American National Standard - Specification for Structural Steel Building* (13th ed.). Chicago, Illinois.

ASCE. (2010). *Minimum Design Loads for Buildings and Other Structures - SEI/ASCE Standatd No. 7-10.* American Society of Civil Engineers. Reston, VA: American Society of Civil Engineers.

Chopra, A. K., & Goel, R. K. (2000). Building Period Formula for Estimating Seismic Displacements. *Earthquake Spectra, 6*(2), 533-536.

Comite Europeen de Normalisation (CEN). (2004). *Eurocode 8: Design of Structure for Earthquake Resistance.*

Computers and Structures Inc. (2010). ETABS Nonlinear Version 9.7.2.

Goel, R. K., & Chopra, A. K. (1997). Period Formulas for Moment-Resisting Frame Buildings. *Journal of Structural Engineering, 123*(11), 1454-1461.

Gong, M., Sun, J., & Xue, L. (2011). Emperical Formula of Fundamental Period for Steel Structure Based on Seismic Response Record. *2011 International Conference on Civil Engineering (ICETCE)*, (pp. 283-286). Lushan, China.

Gong, M., Sun, J., & Xue, L. (22-24 April 2011). Emperical Formula of Fundamental Period for Steel Structure Based on Seismic Response Record. *2011 International Conference on Civil Engineering (ICETCE)*, (pp. 283-286). Lushan, China.

Hsiao, J. K. (2009). Computation of Fundamental Periods for Moment Frames Using a Hand-Calculated Approach. *Electronic Journal of Structural Engineering, 9*, 16-28.

IBC. (2006). *International Building Code.* International Code Council.

Keppel, G., & Wickens, T. D. (2004). *Design and Analysis: A Researcher's Handbook 4th ed.* Prentice Hall.

Kwon, O.-S., & Kim, E. S. (2010). Evaluation of building period formulas for seismic design. *Earthquake Engineering and Structural Dynamics, 39*, 1569-1583.

Oakdale Engineering. (2011). DataFit Version 9.0.59.

Tremblay, R. (2005). Fundamental Periods of Vibration of Braced Steel Frames for Seismic Design. *Earthquake Spectra, 21*(5), 833-860.

Tremblay, R., & Poncet, L. (2005). Seismic Performance of Concentrically Braced Steel Frames in Multistory Buildings with Mass Irregularity. *Journal of Structural Engineering, 131*(9), 1363-1375.

USGS. (n.d.). *Center for Engineering Strong Motion Data*. Retrieved August 2011, from http://strongmotioncenter.org/

APPENDIX A: TABLES OF DESIGN DATA, LOADS, AND DEFLECTIONS – MOMENT RESISTING FRAMES

Table 16: MRF-R-5-5 Design, load, and deflection data

Story (i)	Column Section	L_c (in)	Beam Section - Interior	L_g (in)	Beam Section - Perimeter	L_g (in)	Weight (k)	δ (in)	Lateral Force (k)
5	W16X26	120	W16X26	180	W16X26	180	658.90	1.13	66.98
4	W16X26	120	W16X26	180	W16X26	180	663.53	1.01	53.56
3	W16X50	120	W21X44	180	W21X44	180	682.83	0.85	41.09
2	W16X50	120	W21X44	180	W21X44	180	687.08	0.73	27.58
1	W16X50	144	W21X44	180	W21X44	180	688.62	0.55	14.36

Table 17: MRF-V-5-5 Design, load, and deflection data

Story (i)	Column Section	L_c (in)	Beam Section - Interior	L_g (in)	Beam Section - Perimeter	L_g (in)	Weight (k)	δ (in)	Lateral Force (k)
5	W16X26	120	W16X31	180	W16X26	180	397.97	1.36	44.56
4	W16X26	120	W16X31	180	W16X26	180	401.05	1.24	35.66
3	W14X61	120	W16X31	180	W16X26	180	670.87	1.05	44.46
2	W14X61	120	W16X31	180	W16X26	180	678.59	0.88	30.01
1	W14X61	144	W16X31	180	W16X26	180	680.52	0.63	15.64

Table 18: MRF-H-5-5 Design, load, and deflection data

Story (i)	Column Section	L_c (in)	Beam Section - Interior	L_g (in)	Beam Section - Perimeter	L_g (in)	Weight (k)	δ (in)	Lateral Force (k)
5	W16X26	120	W16X26	180	W16X26	180	423.44	0.63	28.61
4	W16X26	120	W16X26	180	W16X26	180	426.92	0.56	21.92
3	W16X50	120	W21X44	180	W21X44	180	440.81	0.47	15.95
2	W16X50	120	W21X44	180	W21X44	180	443.90	0.40	9.92
1	W16X50	144	W21X44	180	W21X44	180	445.44	0.30	4.57

Table 19: MRF-C-5-5 Design, load, and deflection data

Story (i)	Column Section	L_c (in)	Beam Section - Interior	L_g (in)	Beam Section - Perimeter	L_g (in)	Weight (k)	δ (in)	Lateral Force (k)
5	W14X34	120	W14X26	180	W14X22	180	106.61	1.51	14.20
4	W14X34	120	W14X26	180	W14X22	180	108.16	1.37	11.44
3	W12X65	120	W14X26	180	W14X22	180	560.47	1.07	44.20
2	W12X65	120	W14X26	180	W14X22	180	569.35	0.90	29.95
1	W12X65	144	W14X26	180	W14X22	180	571.67	0.64	15.62

Table 20: MRF-R-10-5 Design, load, and deflection data

Story (i)	Column Section	L_c (in)	Beam Section - Interior	L_g (in)	Beam Section - Perimeter	L_g (in)	Weight (k)	δ (in)	Lateral Force (k)
10	W16X26	120	W16X26	180	W16X26	180	658.90	2.45	47.62
9	W16X26	120	W16X26	180	W16X26	180	663.53	2.35	41.87
8	W16X26	120	W16X26	180	W16X26	180	663.53	2.18	35.99
7	W16X40	120	W16X26	180	W16X26	180	665.85	1.95	30.43
6	W16X40	120	W16X26	180	W16X26	180	668.55	1.70	25.09
5	W16X40	120	W16X26	180	W16X26	180	668.55	1.43	19.91
4	W18X76	120	W18X35	180	W18X35	180	681.68	1.17	15.33
3	W18X76	120	W18X35	180	W18X35	180	688.24	0.97	10.82
2	W18X76	120	W18X35	180	W18X35	180	688.24	0.77	6.61
1	W18X76	144	W18X35	180	W18X35	180	690.94	0.52	2.99

Table 21: MRF-V-10-5 Design, load, and deflection data

Story (i)	Column Section	L_c (in)	Beam Section - Interior	L_g (in)	Beam Section - Perimeter	L_g (in)	Weight (k)	δ (in)	Lateral Force (k)
10	W16X26	120	W16X26	180	W16X26	180	239.51	2.81	23.06
9	W16X26	120	W16X26	180	W16X26	180	241.56	2.67	20.31
8	W16X26	120	W16X26	180	W16X26	180	241.56	2.43	17.45
7	W16X40	120	W16X26	180	W16X26	180	242.14	2.10	14.74
6	W16X40	120	W16X26	180	W16X26	180	242.79	1.78	12.14
5	W16X40	120	W16X26	180	W16X26	180	668.55	1.49	26.52
4	W18X76	120	W18X35	180	W18X35	180	672.80	1.29	20.15
3	W18X76	120	W18X35	180	W18X35	180	676.27	1.07	14.16
2	W18X76	120	W18X35	180	W18X35	180	680.13	0.86	8.70
1	W18X76	144	W18X35	180	W18X35	180	682.45	0.60	3.93

Table 22: MRF-H-10-5 Design, load, and deflection data

Story (i)	Column Section	L_c (in)	Beam Section - Interior	L_g (in)	Beam Section - Perimeter	L_g (in)	Weight (k)	δ (in)	Lateral Force (k)
10	W16X26	120.00	W16X36	180	W16X26	180	558.54	2.56	40.33
9	W16X26	120.00	W16X36	180	W16X26	180	562.79	2.47	35.47
8	W16X26	120.00	W16X36	180	W16X26	180	562.79	2.33	30.48
7	W16X40	120.00	W16X36	180	W16X26	180	564.72	2.12	25.78
6	W16X40	120.00	W16X36	180	W16X26	180	567.03	1.92	21.25
5	W16X40	120.00	W16X36	180	W16X26	180	567.03	1.69	16.86
4	W14X74	120.00	W16X40	180	W16X31	180	575.14	1.44	12.91
3	W14X74	120.00	W16X40	180	W16X31	180	580.16	1.22	9.11
2	W14X74	120.00	W16X40	180	W16X31	180	580.16	0.98	5.56
1	W14X74	144.00	W16X40	180	W16X31	180	582.47	0.69	2.51

Table 23: MRF-C-10-5 Design, load, and deflection data

Story (i)	Column Section	L_c (in)	Beam Section - Interior	L_g (in)	Beam Section - Perimeter	L_g (in)	Weight (k)	δ (in)	Lateral Force (k)
10	W16X26	120	W16X26	180	W16X36	180	213.96	2.37	19.73
9	W16X26	120	W16X26	180	W16X36	180	215.93	2.26	17.38
8	W16X26	120	W16X26	180	W16X36	180	215.93	2.09	14.94
7	W16X36	120	W16X26	180	W16X36	180	216.62	1.86	12.63
6	W16X36	120	W16X26	180	W16X36	180	217.36	1.61	10.41
5	W14X43	120	W16X26	180	W16X36	180	509.91	1.34	19.37
4	W14X43	120	W16X26	180	W16X36	180	513.38	1.16	14.73
3	W14X74	120	W16X26	180	W16X36	180	518.01	0.96	10.39
2	W14X74	120	W16X26	180	W16X36	180	522.64	0.76	6.40
1	W14X74	144	W16X26	180	W16X36	180	524.96	0.52	2.89

Table 24: MRF-R-20-5 Design, load, and deflection data

Story (i)	Column Section	L_c (in)	Beam Section - Interior	L_g (in)	Beam Section - Perimeter	L_g (in)	Weight (k)	δ (in)	Lateral Force (k)
20	W14X30	120	W12X58	180	W14X22	180	676.27	3.70	22.40
19	W14X30	120	W12X58	180	W14X22	180	681.68	3.63	20.69
18	W14X30	120	W12X58	180	W14X22	180	681.68	3.52	18.86
17	W14X30	120	W12X58	180	W14X22	180	681.68	3.39	17.10
16	W14X48	120	W12X58	180	W14X22	180	684.76	3.22	15.49
15	W14X48	120	W12X58	180	W14X22	180	687.85	3.08	13.94
14	W14X48	120	W12X58	180	W14X22	180	687.85	2.93	12.39
13	W14X48	120	W12X58	180	W14X22	180	687.85	2.76	10.92
12	W16X67	120	W12X58	180	W14X22	180	690.94	2.58	9.57
11	W16X67	120	W12X58	180	W14X22	180	694.41	2.39	8.30
10	W16X67	120	W12X58	180	W14X22	180	694.41	2.20	7.06
9	W16X67	120	W12X58	180	W14X22	180	694.41	1.99	5.91
8	W14X82	120	W12X58	180	W14X22	180	697.12	1.79	4.86
7	W14X82	120	W12X58	180	W14X22	180	699.82	1.58	3.90
6	W14X82	120	W12X58	180	W14X22	180	699.82	1.36	3.01
5	W14X82	120	W12X58	180	W14X22	180	699.82	1.15	2.22
4	W18X119	120	W12X58	180	W16X26	180	706.77	0.94	1.55
3	W18X119	120	W12X58	180	W16X26	180	713.71	0.76	0.98
2	W18X119	120	W12X58	180	W16X26	180	713.71	0.58	0.51
1	W18X119	144	W12X58	180	W16X26	180	717.96	0.36	0.18

Table 25: MRF-V-20-5 Design, load, and deflection data

Story (i)	Column Section	L_c (in)	Beam Section - Interior	L_g (in)	Beam Section - Perimeter	L_g (in)	Weight (k)	δ (in)	Lateral Force (k)
20	W12X26	120	W14X22	180	W14X22	180	158.57	7.56	12.77
19	W12X26	120	W14X22	180	W14X22	180	160.11	7.36	11.81
18	W12X26	120	W14X22	180	W14X22	180	160.11	7.05	10.77
17	W12X40	120	W14X22	180	W14X22	180	160.92	6.65	9.81
16	W12X40	120	W14X22	180	W14X22	180	161.73	6.21	8.89
15	W12X40	120	W14X22	180	W14X22	180	161.73	5.71	7.97
14	W12X40	120	W12X26	180	W14X22	180	400.67	5.24	17.54
13	W12X40	120	W12X26	180	W14X22	180	404.14	4.91	15.60
12	W12X40	120	W12X26	180	W14X22	180	404.14	4.54	13.61
11	W12X65	120	W16X26	180	W14X22	180	405.69	4.16	11.79
10	W12X65	120	W16X26	180	W14X22	180	407.62	3.79	10.08
9	W12X65	120	W16X26	180	W14X22	180	407.62	3.41	8.43
8	W12X65	120	W16X26	180	W14X22	180	407.62	3.01	6.91
7	W12X72	120	W14X22	180	W14X22	180	671.25	2.61	9.09
6	W12X72	120	W14X22	180	W14X22	180	676.27	2.29	7.07
5	W12X72	120	W14X22	180	W14X22	180	676.27	1.95	5.22
4	W18X119	120	W12X26	180	W12X26	180	687.85	1.60	3.67
3	W18X119	120	W12X26	180	W12X26	180	696.34	1.28	2.32
2	W18X119	120	W12X26	180	W12X26	180	696.34	0.95	1.21
1	W18X119	144	W12X26	180	W12X26	180	700.59	0.57	0.43

Table 26: MRF-H-20-5 Design, load, and deflection data

Story (i)	Column Section	L_c (in)	Beam Section - Interior	L_g (in)	Beam Section - Perimeter	L_g (in)	Weight (k)	δ (in)	Lateral Force (k)
20	W12X30	120	W14X22	180	W14X22	180	499.87	4.06	18.21
19	W12X30	120	W14X22	180	W14X22	180	504.12	3.97	16.60
18	W12X30	120	W14X22	180	W14X22	180	504.12	3.83	14.91
17	W12X30	120	W14X22	180	W14X22	180	504.12	3.64	13.32
16	W14X48	120	W14X22	180	W14X22	180	506.82	3.41	11.88
15	W14X48	120	W14X22	180	W14X22	180	509.52	3.19	10.51
14	W14X48	120	W14X22	180	W14X22	180	509.52	2.94	9.17
13	W14X48	120	W14X22	180	W14X22	180	509.52	2.68	7.93
12	W14X61	120	W16X26	180	W16X26	180	514.15	2.43	6.83
11	W14X61	120	W16X26	180	W16X26	180	516.08	2.20	5.78
10	W14X61	120	W16X26	180	W16X26	180	516.08	1.97	4.79
9	W14X61	120	W16X26	180	W16X26	180	516.08	1.73	3.90
8	W24X84	120	W16X26	180	W16X26	180	519.17	1.49	3.12
7	W24X84	120	W16X26	180	W16X26	180	522.64	1.29	2.42
6	W24X84	120	W16X26	180	W16X26	180	522.64	1.09	1.79
5	W24X84	120	W16X26	180	W16X26	180	522.64	0.90	1.26
4	W21X122	120	W18X35	180	W18X35	180	533.84	0.73	0.84
3	W21X122	120	W18X35	180	W18X35	180	539.63	0.58	0.49
2	W21X122	120	W18X35	180	W18X35	180	539.63	0.43	0.23
1	W21X122	144	W18X35	180	W18X35	180	543.10	0.27	0.07

Table 27: MRF-C-20-5 Design, load, and deflection data

Story (i)	Column Section	L_c (in)	Beam Section - Interior	L_g (in)	Beam Section - Perimeter	L_g (in)	Weight (k)	δ (in)	Lateral Force (k)
20	W14X30	120	W14X22	180	W14X22	180	237.39	6.81	15.97
19	W14X30	120	W14X22	180	W14X22	180	239.78	6.66	14.77
18	W14X30	120	W14X22	180	W14X22	180	239.78	6.44	13.47
17	W14X30	120	W14X22	180	W14X22	180	239.78	6.14	12.22
16	W14X53	120	W14X22	180	W14X22	180	241.60	5.76	11.10
15	W14X53	120	W14X22	180	W14X22	180	243.45	5.38	10.02
14	W14X53	120	W14X22	180	W14X22	180	243.45	4.96	8.90
13	W14X53	120	W14X22	180	W14X22	180	243.45	4.51	7.85
12	W14X61	120	W16X26	180	W14X22	180	509.91	3.96	14.35
11	W14X61	120	W16X26	180	W14X22	180	514.92	3.70	12.50
10	W14X61	120	W16X26	180	W14X22	180	514.92	3.43	10.63
9	W14X61	120	W16X26	180	W14X22	180	514.92	3.14	8.90
8	W18X76	120	W14X22	180	W14X22	180	515.31	2.80	7.30
7	W18X76	120	W14X22	180	W14X22	180	517.63	2.46	5.85
6	W18X76	120	W14X22	180	W14X22	180	517.63	2.11	4.52
5	W18X76	120	W14X22	180	W14X22	180	517.63	1.76	3.34
4	W18X119	120	W14X30	180	W14X30	180	529.21	1.44	2.36
3	W18X119	120	W14X30	180	W14X30	180	535.77	1.15	1.49
2	W18X119	120	W14X30	180	W14X30	180	535.77	0.86	0.78
1	W18X119	144	W14X30	180	W14X30	180	539.24	0.52	0.28

Table 28: MRF-R-5-8 Design, load, and deflection data

Story (i)	Column Section	L_c (in)	Beam Section - Interior	L_g (in)	Beam Section - Perimeter	L_g (in)	Weight (k)	δ (in)	Lateral Force (k)
5	W21X48	144	W21X55	300	W16X40	300	4693.76	2.09	441.29
4	W21X48	144	W21X55	300	W16X40	300	4716.92	1.86	345.38
3	W30X99	144	W21X57	300	W21X48	300	4747.80	1.48	251.88
2	W30X99	144	W21X57	300	W21X48	300	4774.82	1.11	160.76
1	W30X99	144	W21X57	300	W21X48	300	4774.82	0.65	73.94

Table 29: MRF-V-5-8 Design, load, and deflection data

Story (i)	Column Section	L_c (in)	Beam Section - Interior	L_g (in)	Beam Section - Perimeter	L_g (in)	Weight (k)	δ (in)	Lateral Force (k)
5	W24X62	144	W21X55	300	W16X40	300	4693.76	1.11	444.51
4	W24X62	144	W21X55	300	W16X40	300	4716.92	0.91	347.89
3	W24X103	144	W21X68	300	W21X68	300	4909.92	0.65	262.24
2	W24X103	144	W21X68	300	W21X68	300	4933.08	0.51	167.34
1	W24X103	144	W21X68	300	W21X68	300	4933.08	0.33	76.97

Table 30: MRF-H-5-8 Design, load, and deflection data

Story (i)	Column Section	L_c (in)	Beam Section - Interior	L_g (in)	Beam Section - Perimeter	L_g (in)	Weight (k)	δ (in)	Lateral Force (k)
5	W21X48	144	W21X55	300	W16X40	300	4037.56	1.97	379.83
4	W21X48	144	W21X55	300	W16X40	300	4056.86	1.75	297.33
3	W24X104	144	W21X62	300	W21X48	300	4099.32	1.41	217.72
2	W24X104	144	W21X62	300	W21X48	300	4126.34	1.07	139.04
1	W24X104	144	W21X62	300	W21X48	300	4126.34	0.64	63.96

Table 31: MRF-C-5-8 Design, load, and deflection data

Story (i)	Column Section	L_c (in)	Beam Section - Interior	L_g (in)	Beam Section - Perimeter	L_g (in)	Weight (k)	δ (in)	Lateral Force (k)
5	W24X62	144	W21X62	300	W16X45	300	1185.41	1.62	139.60
4	W24X62	144	W21X62	300	W16X45	300	1194.67	1.42	109.57
3	W14X132	144	W21X68	300	W24X68	300	3612.19	1.09	240.03
2	W14X132	144	W21X68	300	W24X68	300	3654.26	0.88	154.17
1	W14X132	144	W21X68	300	W24X68	300	3654.26	0.59	70.91

Table 32: MRF-R-10-8 Design, load, and deflection data

Story (i)	Column Section	L_c (in)	Beam Section - Interior	L_g (in)	Beam Section - Perimeter	L_g (in)	Weight (k)	δ (in)	Lateral Force (k)
10	W21X55	144	W21X55	300	W21X44	300	4701.48	3.66	311.74
9	W21X55	144	W21X55	300	W21X44	300	4728.50	3.51	270.66
8	W21X55	144	W21X55	300	W21X44	300	4728.50	3.26	229.66
7	W18X97	144	W24X55	300	W18X55	300	4755.52	2.91	191.77
6	W18X97	144	W24X55	300	W18X55	300	4774.82	2.55	155.33
5	W18X97	144	W24X55	300	W18X55	300	4774.82	2.14	120.45
4	W27X161	144	W24X62	300	W24X55	300	4821.14	1.71	89.07
3	W27X161	144	W24X62	300	W24X55	300	4852.02	1.36	60.02
2	W27X161	144	W24X62	300	W24X55	300	4852.02	0.98	34.09
1	W27X161	144	W24X62	300	W24X55	300	4852.02	0.56	12.96

Table 33: MRF-V-10-8 Design, load, and deflection data

Story (i)	Column Section	L_c (in)	Beam Section - Interior	L_g (in)	Beam Section - Perimeter	L_g (in)	Weight (k)	δ (in)	Lateral Force (k)
10	W18X60	144	W21X55	300	W21X48	300	2953.29	2.88	219.86
9	W18X60	144	W21X55	300	W21X48	300	2972.59	2.71	191.05
8	W18X60	144	W21X55	300	W21X48	300	2972.59	2.42	162.11
7	W30X99	144	W18X55	300	W21X48	300	4740.08	2.03	214.60
6	W30X99	144	W18X55	300	W21X48	300	4770.96	1.71	174.12
5	W30X99	144	W18X55	300	W21X48	300	4770.96	1.38	135.02
4	W27X161	144	W27X84	300	W21X50	300	4879.04	1.09	101.14
3	W27X161	144	W27X84	300	W21X50	300	4906.06	0.87	68.13
2	W27X161	144	W27X84	300	W21X50	300	4906.06	0.64	38.70
1	W27X161	144	W27X84	300	W21X50	300	4906.06	0.37	14.72

Table 34: MRF-H-10-8 Design, load, and deflection data

Story (i)	Column Section	L_c (in)	Beam Section - Interior	L_g (in)	Beam Section - Perimeter	L_g (in)	Weight (k)	δ (in)	Lateral Force (k)
10	W14X61	144	W21X55	300	W16X40	300	3530.74	3.48	235.09
9	W14X61	144	W21X55	300	W16X40	300	3554.29	3.29	204.32
8	W14X61	144	W21X55	300	W16X40	300	3554.29	2.95	173.37
7	W30X116	144	W21X55	300	W14X38	300	3570.50	2.48	144.56
6	W30X116	144	W21X55	300	W14X38	300	3592.12	2.11	117.29
5	W30X116	144	W21X55	300	W14X38	300	3592.12	1.73	90.95
4	W21X182	144	W27X84	300	W16X36	300	3675.88	1.39	68.18
3	W21X182	144	W27X84	300	W16X36	300	3701.74	1.10	45.96
2	W21X182	144	W27X84	300	W16X36	300	3701.74	0.81	26.11
1	W21X182	144	W27X84	300	W16X36	300	3701.74	0.48	9.93

Table 35: MRF-C-10-8 Design, load, and deflection data

Story (i)	Column Section	L_c (in)	Beam Section - Interior	L_g (in)	Beam Section - Perimeter	L_g (in)	Weight (k)	δ (in)	Lateral Force (k)
10	W27X84	144	W21X62	300	W21X48	300	3261.31	2.85	225.32
9	W27X84	144	W21X62	300	W21X48	300	3292.19	2.73	196.36
8	W27X84	144	W21X62	300	W21X48	300	3292.19	2.53	166.61
7	W33X130	144	W21X48	300	W18X40	300	3863.86	2.20	162.28
6	W33X130	144	W21X48	300	W18X40	300	3887.02	1.87	131.66
5	W33X130	144	W21X48	300	W18X40	300	3887.02	1.53	102.10
4	W33X141	144	W27X84	300	W18X35	300	3960.36	1.22	76.23
3	W33X141	144	W27X84	300	W18X35	300	3964.22	0.96	51.09
2	W33X141	144	W27X84	300	W18X35	300	3964.22	0.69	29.02
1	W33X141	144	W27X84	300	W18X35	300	3964.22	0.40	11.04

Table 36: MRF-R-20-8 Design, load, and deflection data

Story (i)	Column Section	L_c (in)	Beam Section - Interior	L_g (in)	Beam Section - Perimeter	L_g (in)	Weight (k)	δ (in)	Lateral Force (k)
20	W16X67	144	W21X55	300	W16X40	300	4705.34	6.43	227.59
19	W16X67	144	W21X55	300	W16X40	300	4736.22	6.30	208.17
18	W16X67	144	W21X55	300	W16X40	300	4736.22	6.06	188.12
17	W16X67	144	W21X55	300	W16X40	300	4736.22	5.74	169.02
16	W24X117	144	W24X68	300	W16X36	300	4790.26	5.38	152.56
15	W24X117	144	W24X68	300	W16X36	300	4813.42	5.09	135.88
14	W24X117	144	W24X68	300	W16X36	300	4813.42	4.78	119.41
13	W24X117	144	W24X68	300	W16X36	300	4813.42	4.44	103.93
12	W30X173	144	W24X68	300	W16X36	300	4836.58	4.07	89.92
11	W30X173	144	W24X68	300	W16X36	300	4867.46	3.72	76.83
10	W30X173	144	W24X68	300	W16X36	300	4867.46	3.35	64.27
9	W30X173	144	W24X68	300	W16X36	300	4867.46	2.97	52.76
8	W33X221	144	W24X68	300	W16X36	300	4886.76	2.59	42.51
7	W33X221	144	W24X68	300	W16X36	300	4909.92	2.21	33.26
6	W33X221	144	W24X68	300	W16X36	300	4909.92	1.85	24.92
5	W33X221	144	W24X68	300	W16X36	300	4909.92	1.51	17.71
4	W12X305	144	W30X99	300	W30X99	300	5087.48	1.23	12.08
3	W12X305	144	W30X99	300	W30X99	300	5126.08	0.98	7.10
2	W12X305	144	W30X99	300	W30X99	300	5126.08	0.74	3.32
1	W12X305	144	W30X99	300	W30X99	300	5126.08	0.48	0.91

Table 37: MRF-V-20-8 Design, load, and deflection data

Story (i)	Column Section	L_c (in)	Beam Section - Interior	L_g (in)	Beam Section - Perimeter	L_g (in)	Weight (k)	δ (in)	Lateral Force (k)
20	W18X76	144	W21X55	300	W16X40	300	1770.97	6.32	114.11
19	W18X76	144	W21X55	300	W16X40	300	1787.57	6.14	104.61
18	W18X76	144	W21X55	300	W16X40	300	1787.57	5.87	94.54
17	W18X76	144	W21X55	300	W16X40	300	1787.57	5.50	84.94
16	W24X117	144	W24X68	300	W16X36	300	2992.27	5.13	126.93
15	W24X117	144	W24X68	300	W16X36	300	3013.50	4.87	113.29
14	W24X117	144	W24X68	300	W16X36	300	3013.50	4.58	99.56
13	W24X117	144	W24X68	300	W16X36	300	3013.50	4.25	86.66
12	W21X166	144	W21X62	300	W16X36	300	4207.40	3.88	104.18
11	W21X166	144	W21X62	300	W16X36	300	4242.14	3.52	89.22
10	W21X166	144	W21X62	300	W16X36	300	4242.14	3.14	74.64
9	W21X166	144	W21X62	300	W16X36	300	4242.14	2.75	61.27
8	W27X217	144	W24X68	300	W16X36	300	4875.18	2.38	56.47
7	W27X217	144	W24X68	300	W16X36	300	4909.92	2.07	44.28
6	W27X217	144	W24X68	300	W16X36	300	4909.92	1.77	33.18
5	W27X217	144	W24X68	300	W16X36	300	4909.92	1.47	23.58
4	W24X279	144	W24X84	300	W21X48	300	4990.98	1.19	15.78
3	W24X279	144	W24X84	300	W21X48	300	5018.00	0.93	9.26
2	W24X279	144	W24X84	300	W21X48	300	5018.00	0.66	4.33
1	W24X279	144	W24X84	300	W21X48	300	5018.00	0.37	1.18

Table 38: MRF-H-20-8 Design, load, and deflection data

Story (i)	Column Section	L_c (in)	Beam Section - Interior	L_g (in)	Beam Section - Perimeter	L_g (in)	Weight (k)	δ (in)	Lateral Force (k)
20	W16X67	144	W21X55	300	W16X40	300	3239.31	5.71	156.86
19	W16X67	144	W21X55	300	W16X40	300	3264.02	5.56	143.57
18	W16X67	144	W21X55	300	W16X40	300	3264.02	5.33	129.74
17	W16X67	144	W21X55	300	W16X40	300	3264.02	5.01	116.57
16	W30X124	144	W24X68	300	W16X36	300	3300.69	4.64	105.24
15	W30X124	144	W24X68	300	W16X36	300	3321.53	4.36	93.84
14	W30X124	144	W24X68	300	W16X36	300	3321.53	4.07	82.47
13	W30X124	144	W24X68	300	W16X36	300	3321.53	3.75	71.78
12	W30X173	144	W24X68	300	W24X68	300	3362.45	3.43	62.55
11	W30X173	144	W24X68	300	W24X68	300	3380.20	3.14	53.43
10	W30X173	144	W24X68	300	W24X68	300	3380.20	2.83	44.69
9	W30X173	144	W24X68	300	W24X68	300	3380.20	2.51	36.69
8	W24X229	144	W21X68	300	W24X76	300	3407.61	2.18	29.66
7	W24X229	144	W21X68	300	W24X76	300	3427.68	1.84	23.24
6	W24X229	144	W21X68	300	W24X76	300	3427.68	1.50	17.41
5	W24X229	144	W21X68	300	W24X76	300	3427.68	1.17	12.37
4	W40X297	144	W30X90	300	W27X84	300	3489.05	0.89	8.29
3	W40X297	144	W30X90	300	W27X84	300	3514.14	0.69	4.87
2	W40X297	144	W30X90	300	W27X84	300	3514.14	0.48	2.28
1	W40X297	144	W30X90	300	W27X84	300	3514.14	0.26	0.62

Table 39: MRF-C-20-8 Design, load, and deflection data

Story (i)	Column Section	L_c (in)	Beam Section - Interior	L_g (in)	Beam Section - Perimeter	L_g (in)	Weight (k)	δ (in)	Lateral Force (k)
20	W14X74	144	W21X55	300	W16X40	300	2202.52	6.10	133.00
19	W14X74	144	W21X55	300	W16X40	300	2222.20	5.90	121.89
18	W14X74	144	W21X55	300	W16X40	300	2222.20	5.57	110.15
17	W14X74	144	W21X55	300	W16X40	300	2222.20	5.12	98.97
16	W27X129	144	W21X68	300	W24X68	300	2280.49	4.66	90.67
15	W27X129	144	W21X68	300	W24X68	300	2294.77	4.38	80.85
14	W27X129	144	W21X68	300	W24X68	300	2294.77	4.07	71.05
13	W27X129	144	W21X68	300	W24X68	300	2294.77	3.75	61.84
12	W21X166	144	W24X68	300	W24X76	300	4168.80	3.44	96.70
11	W21X166	144	W24X68	300	W24X76	300	4207.40	3.19	82.90
10	W21X166	144	W24X68	300	W24X76	300	4207.40	2.94	69.35
9	W21X166	144	W24X68	300	W24X76	300	4207.40	2.66	56.93
8	W33X221	144	W21X62	300	W24X68	300	4226.70	2.38	45.90
7	W33X221	144	W21X62	300	W24X68	300	4253.72	2.12	35.95
6	W33X221	144	W21X62	300	W24X68	300	4253.72	1.85	26.93
5	W33X221	144	W21X62	300	W24X68	300	4253.72	1.59	19.14
4	W12X305	144	W24X76	300	W24X68	300	4338.64	1.34	12.86
3	W12X305	144	W24X76	300	W24X68	300	4377.24	1.07	7.57
2	W12X305	144	W24X76	300	W24X68	300	4377.24	0.80	3.54
1	W12X305	144	W24X76	300	W24X68	300	4377.24	0.49	0.97

APPENDIX B: TABLES OF DESIGN DATA, LOADS, AND DEFLECTIONS – CONCENTRICALLY BRACED FRAMES

Table 40: CBF-R-10-5 Design, load, and deflection data

Story (i)	Column Section	L_c (in)	Beam - Interior	L_g (in)	Beam - Perimeter	L_g (in)	Bracing Section	Weight (k)	δ (in)	Lateral Force (k)
10	W14X53	120	W14X48	300	W14X38	300	W14X68	1836.97	3.70	227.70
9	W14X53	120	W14X48	300	W14X38	300	W14X68	1853.57	3.35	205.74
8	W14X53	120	W14X48	300	W14X38	300	W14X68	1853.57	2.95	181.89
7	W18X97	120	W14X43	300	W14X34	300	W14X68	1853.96	2.51	158.26
6	W18X97	120	W14X43	300	W14X34	300	W14X68	1861.68	2.07	135.41
5	W18X97	120	W14X43	300	W14X34	300	W14X68	1861.68	1.64	112.16
4	W12X190	120	W14X43	300	W14X34	300	W12X96	1881.75	1.22	90.19
3	W12X190	120	W14X43	300	W14X34	300	W12X96	1901.44	0.86	68.11
2	W12X190	120	W14X43	300	W14X34	300	W12X96	1901.44	0.53	45.59
1	W12X190	144	W14X43	300	W14X34	300	W12X96	1908.38	0.26	23.91

Table 41: CBF-V-10-5 Design, load, and deflection data

Story (i)	Column Section	L_c (in)	Beam - Interior	L_g (in)	Beam - Perimeter	L_g (in)	Bracing Section	Weight (k)	δ (in)	Lateral Force (k)
10	W12X53	120	W14X48	300	W14X38	300	W12X45	1104.35	3.35	150.08
9	W12X53	120	W14X48	300	W14X38	300	W12X45	1115.54	3.03	135.73
8	W12X53	120	W14X48	300	W14X38	300	W12X45	1115.54	2.65	120.00
7	W12X96	120	W14X43	300	W14X34	300	W14X68	1848.55	2.25	172.98
6	W12X96	120	W14X43	300	W14X34	300	W14X68	1862.06	1.88	148.45
5	W12X96	120	W14X43	300	W14X34	300	W14X68	1862.06	1.50	122.96
4	W12X170	120	W12X40	300	W14X34	300	W12X96	1875.19	1.11	98.51
3	W12X170	120	W12X40	300	W14X34	300	W12X96	1891.40	0.79	74.26
2	W12X170	120	W12X40	300	W14X34	300	W12X96	1891.40	0.49	49.72
1	W12X170	144	W12X40	300	W14X34	300	W12X96	1897.96	0.23	26.06

Table 42: CBF-H-10-5 Design, load, and deflection data

Story (i)	Column Section	L_c (in)	Beam - Interior	L_g (in)	Beam - Perimeter	L_g (in)	Bracing Section	Weight (k)	δ (in)	Lateral Force (k)
10	W12X53	120	W14X48	300	W14X38	300	W14X68	1545.54	3.36	191.70
9	W12X53	120	W14X48	300	W14X38	300	W14X68	1561.37	3.02	173.39
8	W12X53	120	W14X48	300	W14X38	300	W14X68	1561.37	2.65	153.29
7	W12X106	120	W14X43	300	W14X34	300	W14X68	1563.69	2.25	133.56
6	W12X106	120	W14X43	300	W14X34	300	W14X68	1572.18	1.86	114.41
5	W12X106	120	W14X43	300	W14X34	300	W14X68	1572.18	1.46	94.77
4	W12X190	120	W14X43	300	W14X34	300	W12X96	1588.39	1.07	76.17
3	W12X190	120	W14X43	300	W14X34	300	W12X96	1604.60	0.75	57.51
2	W12X190	120	W14X43	300	W14X34	300	W12X96	1604.60	0.46	38.50
1	W12X190	144	W14X43	300	W14X34	300	W12X96	1611.16	0.22	20.20

Table 43: CBF-C-10-5 Design, load, and deflection data

Story (i)	Column Section	L_c (in)	Beam - Interior	L_g (in)	Beam - Perimeter	L_g (in)	Bracing Section	Weight (k)	δ (in)	Lateral Force (k)
10	W12X53	120	W14X38	300	W14X48	300	W14X68	1180.77	3.21	153.92
9	W12X53	120	W14X38	300	W14X48	300	W14X68	1195.06	2.89	139.47
8	W12X53	120	W14X38	300	W14X48	300	W14X68	1195.06	2.54	123.30
7	W12X106	120	W14X43	300	W14X34	300	W14X68	1562.14	2.17	140.24
6	W12X106	120	W14X43	300	W14X34	300	W14X68	1572.18	1.81	120.25
5	W12X106	120	W14X43	300	W14X34	300	W14X68	1572.18	1.44	99.61
4	W12X170	120	W14X43	300	W14X34	300	W18X86	1584.14	1.07	79.85
3	W12X170	120	W14X43	300	W14X34	300	W18X86	1596.50	0.76	60.13
2	W12X170	120	W14X43	300	W14X34	300	W18X86	1596.50	0.47	40.25
1	W12X170	144	W14X43	300	W14X34	300	W18X86	1601.90	0.23	21.11

Table 44: CBF-R-20-5 Design, load, and deflection data

Story (i)	Column Section	L_c (in)	Beam - Interior	L_g (in)	Beam - Perimeter	L_g (in)	Bracing Section	Weight (k)	δ (in)	Lateral Force (k)
20	W12X72	120	W21X48	300	W12X35	300	W12X45	1835.82	8.53	159.95
19	W12X72	120	W21X48	300	W12X35	300	W12X45	1853.57	8.18	151.28
18	W12X72	120	W21X48	300	W12X35	300	W12X45	1853.57	7.77	141.23
17	W12X72	120	W21X48	300	W12X35	300	W12X45	1853.57	7.32	131.33
16	W24X117	120	W21X55	300	W12X35	300	W14X68	1869.40	6.82	122.64
15	W24X117	120	W21X55	300	W12X35	300	W14X68	1880.21	6.37	113.64
14	W24X117	120	W21X55	300	W12X35	300	W14X68	1880.21	5.89	104.12
13	W24X117	120	W21X55	300	W12X35	300	W14X68	1880.21	5.40	94.79
12	W30X173	120	W21X55	300	W14X34	300	W14X68	1888.70	4.89	86.05
11	W30X173	120	W21X55	300	W14X34	300	W14X68	1899.12	4.40	77.50
10	W30X173	120	W21X55	300	W14X34	300	W14X68	1899.12	3.90	68.72
9	W30X173	120	W21X55	300	W14X34	300	W14X68	1899.12	3.42	60.18
8	W14X283	120	W21X55	300	W14X34	300	W18X86	1922.28	2.94	52.54
7	W14X283	120	W21X55	300	W14X34	300	W18X86	1943.90	2.49	44.95
6	W14X283	120	W21X55	300	W14X34	300	W18X86	1943.90	2.06	37.09
5	W14X283	120	W21X55	300	W14X34	300	W18X86	1943.90	1.65	29.58
4	W14X500	120	W12X40	300	W14X34	300	W12X96	1968.99	1.26	22.77
3	W14X500	120	W12X40	300	W14X34	300	W12X96	2008.74	0.91	16.38
2	W14X500	120	W12X40	300	W14X34	300	W12X96	2008.74	0.58	10.11
1	W14X500	144	W12X40	300	W14X34	300	W12X96	2027.27	0.30	4.68

Table 45: CBF-V-20-5 Design, load, and deflection data

Story (i)	Column Section	L_c (in)	Beam - Interior	L_g (in)	Beam - Perimeter	L_g (in)	Bracing Section	Weight (k)	δ (in)	Lateral Force (k)
20	W12X65	120	W21X48	300	W14X38	300	W12X45	1105.89	7.82	110.36
19	W12X65	120	W21X48	300	W14X38	300	W12X45	1118.24	7.46	104.56
18	W12X65	120	W21X48	300	W14X38	300	W12X45	1118.24	7.05	97.61
17	W12X65	120	W21X48	300	W14X38	300	W12X45	1118.24	6.61	90.77
16	W24X117	120	W21X55	300	W12X35	300	W21X68	1128.66	6.13	84.82
15	W24X117	120	W21X55	300	W12X35	300	W21X68	1137.54	5.70	78.75
14	W24X117	120	W21X55	300	W12X35	300	W21X68	1137.54	5.24	72.15
13	W24X117	120	W21X55	300	W12X35	300	W21X68	1137.54	4.77	65.69
12	W14X159	120	W21X55	300	W14X38	300	W14X68	1882.91	4.32	98.26
11	W14X159	120	W21X55	300	W14X38	300	W14X68	1897.58	3.89	88.71
10	W14X159	120	W21X55	300	W14X38	300	W14X68	1897.58	3.45	78.66
9	W14X159	120	W21X55	300	W14X38	300	W14X68	1897.58	3.01	68.88
8	W12X252	120	W21X55	300	W14X38	300	W18X86	1914.17	2.58	59.94
7	W12X252	120	W21X55	300	W14X38	300	W18X86	1933.09	2.19	51.20
6	W12X252	120	W21X55	300	W14X38	300	W18X86	1933.09	1.81	42.25
5	W12X252	120	W21X55	300	W14X38	300	W18X86	1933.09	1.45	33.70
4	W14X426	120	W12X40	300	W14X38	300	W12X96	1950.07	1.11	25.83
3	W14X426	120	W12X40	300	W14X38	300	W12X96	1982.11	0.79	18.51
2	W14X426	120	W12X40	300	W14X38	300	W12X96	1982.11	0.50	11.43
1	W14X426	144	W12X40	300	W14X38	300	W12X96	1997.55	0.25	5.29

Table 46: CBF-H-20-5 Design, load, and deflection data

Story (i)	Column Section	L_c (in)	Beam - Interior	L_g (in)	Beam - Perimeter	L_g (in)	Bracing Section	Weight (k)	δ (in)	Lateral Force (k)
20	W12X72	120	W21X48	300	W12X35	300	W12X45	1105.89	7.82	110.36
19	W12X72	120	W21X48	300	W12X35	300	W12X45	1118.24	7.46	104.56
18	W12X72	120	W21X48	300	W12X35	300	W12X45	1118.24	7.05	97.61
17	W12X72	120	W21X48	300	W12X35	300	W12X45	1118.24	6.61	90.77
16	W14X120	120	W21X55	300	W21X48	300	W14X68	1128.66	6.13	84.82
15	W14X120	120	W21X55	300	W21X48	300	W14X68	1137.54	5.70	78.75
14	W14X120	120	W21X55	300	W21X48	300	W14X68	1137.54	5.24	72.15
13	W14X120	120	W21X55	300	W21X48	300	W14X68	1137.54	4.77	65.69
12	W30X173	120	W21X55	300	W21X48	300	W14X68	1882.91	4.32	98.26
11	W30X173	120	W21X55	300	W21X48	300	W14X68	1897.58	3.89	88.71
10	W30X173	120	W21X55	300	W21X48	300	W14X68	1897.58	3.45	78.66
9	W30X173	120	W21X55	300	W21X48	300	W14X68	1897.58	3.01	68.88
8	W12X279	120	W21X55	300	W12X35	300	W18X86	1914.17	2.58	59.94
7	W12X279	120	W21X55	300	W12X35	300	W18X86	1933.09	2.19	51.20
6	W12X279	120	W21X55	300	W12X35	300	W18X86	1933.09	1.81	42.25
5	W12X279	120	W21X55	300	W12X35	300	W18X86	1933.09	1.45	33.70
4	W14X455	120	W12X40	300	W14X34	300	W12X96	1950.07	1.11	25.83
3	W14X455	120	W12X40	300	W14X34	300	W12X96	1982.11	0.79	18.51
2	W14X455	120	W12X40	300	W14X34	300	W12X96	1982.11	0.50	11.43
1	W14X455	144	W12X40	300	W14X34	300	W12X96	1997.55	0.25	5.29

Table 47: CBF-C-20-5 Design, load, and deflection data

Story (i)	Column Section	L_c (in)	Beam - Interior	L_g (in)	Beam - Perimeter	L_g (in)	Bracing Section	Weight (k)	δ (in)	Lateral Force (k)
20	W12X65	120	W14X48	300	W12X40	300	W12X45	960.75	8.33	98.50
19	W12X65	120	W14X48	300	W12X40	300	W12X45	972.72	7.87	93.41
18	W12X65	120	W14X48	300	W12X40	300	W12X45	972.72	7.37	87.21
17	W12X65	120	W14X48	300	W12X40	300	W12X45	972.72	6.84	81.09
16	W24X104	120	W14X43	300	W12X40	300	W14X68	976.58	6.29	75.38
15	W24X104	120	W14X43	300	W12X40	300	W14X68	983.53	5.76	69.94
14	W24X104	120	W14X43	300	W12X40	300	W14X68	983.53	5.22	64.08
13	W24X104	120	W14X43	300	W12X40	300	W14X68	983.53	4.69	58.34
12	W14X145	120	W21X55	300	W21X55	300	W18X86	1812.27	4.20	97.16
11	W14X145	120	W21X55	300	W21X55	300	W18X86	1826.17	3.79	87.71
10	W14X145	120	W21X55	300	W21X55	300	W18X86	1826.17	3.37	77.77
9	W14X145	120	W21X55	300	W21X55	300	W18X86	1826.17	2.97	68.11
8	W12X252	120	W14X43	300	W21X48	300	W12X96	1832.73	2.55	58.95
7	W12X252	120	W14X43	300	W21X48	300	W12X96	1853.19	2.15	50.43
6	W12X252	120	W14X43	300	W21X48	300	W12X96	1853.19	1.76	41.61
5	W12X252	120	W14X43	300	W21X48	300	W12X96	1853.19	1.40	33.19
4	W14X426	120	W12X40	300	W14X34	300	W12X96	1874.80	1.06	25.51
3	W14X426	120	W12X40	300	W14X34	300	W12X96	1906.07	0.75	18.28
2	W14X426	120	W12X40	300	W14X34	300	W12X96	1906.07	0.48	11.29
1	W14X426	144	W12X40	300	W14X34	300	W12X96	1921.12	0.24	5.22

Table 48: CBF-R-30-5 Design, load, and deflection data

Story (i)	Column Section	L_c (in)	Beam - Interior	L_g (in)	Beam - Perimeter	L_g (in)	Bracing Section	Weight (k)	δ (in)	Lateral Force (k)
30	W14X99	120	W21X55	300	W14X38	300	W12X45	1848.55	14.81	134.07
29	W14X99	120	W21X55	300	W14X38	300	W12X45	1869.78	14.45	129.04
28	W14X99	120	W21X55	300	W14X38	300	W12X45	1869.78	14.04	122.58
27	W14X99	120	W21X55	300	W14X38	300	W12X45	1869.78	13.59	116.22
26	W14X99	120	W21X55	300	W14X38	300	W12X45	1869.78	13.10	109.98
25	W14X159	120	W18X60	300	W14X43	300	W14X68	1891.01	12.55	105.02
24	W14X159	120	W18X60	300	W14X43	300	W14X68	1904.14	12.00	99.62
23	W14X159	120	W18X60	300	W14X43	300	W14X68	1904.14	11.41	93.61
22	W14X159	120	W18X60	300	W14X43	300	W14X68	1904.14	10.79	87.73
21	W14X159	120	W18X60	300	W14X43	300	W14X68	1904.14	10.15	81.96
20	W30X211	120	W18X60	300	W12X35	300	W14X68	1908.38	9.48	76.49
19	W30X211	120	W18X60	300	W12X35	300	W14X68	1917.65	8.82	71.32
18	W30X211	120	W18X60	300	W12X35	300	W14X68	1917.65	8.15	65.91
17	W30X211	120	W18X60	300	W12X35	300	W14X68	1917.65	7.48	60.65
16	W30X211	120	W18X60	300	W12X35	300	W14X68	1917.65	6.80	55.52
15	W14X257	120	W21X62	300	W14X53	300	W18X86	1940.04	6.16	51.13
14	W14X257	120	W21X62	300	W14X53	300	W18X86	1950.07	5.52	46.49
13	W14X257	120	W21X62	300	W14X53	300	W18X86	1950.07	4.91	41.74
12	W14X257	120	W21X62	300	W14X53	300	W18X86	1950.07	4.31	37.17
11	W14X257	120	W21X62	300	W14X53	300	W18X86	1950.07	3.73	32.76

Continued

Table 48 continued

Story (i)	Column Section	L_c (in)	Beam - Interior	L_g (in)	Beam - Perimeter	L_g (in)	Bracing Section	Weight (k)	δ (in)	Lateral Force (k)
10	W14X455	120	W18X50	300	W14X38	300	W12X96	1967.83	3.16	28.80
9	W14X455	120	W18X50	300	W14X38	300	W12X96	2004.50	2.61	25.20
8	W14X455	120	W18X50	300	W14X38	300	W12X96	2004.50	2.08	21.27
7	W14X455	120	W18X50	300	W14X38	300	W12X96	2004.50	1.59	17.56
6	W14X455	120	W18X50	300	W14X38	300	W12X96	2004.50	1.14	14.08
5	W27X539	120	W30X211	300	W14X211	300	W12X96	2246.13	0.83	12.17
4	W27X539	120	W30X211	300	W14X211	300	W12X96	2261.19	0.64	8.95
3	W27X539	120	W30X211	300	W14X211	300	W12X96	2261.19	0.48	5.99
2	W27X539	120	W30X211	300	W14X211	300	W12X96	2261.19	0.33	3.45
1	W27X539	144	W30X211	300	W14X211	300	W12X96	2281.26	0.19	1.42

Table 49: CBF-V-30-5 Design, load, and deflection data

Story (i)	Column Section	L_c (in)	Beam - Interior	L_c (in)	Beam - Perimeter	L_c (in)	Bracing Section	Weight (k)	δ (in)	Lateral Force (k)
30	W12X79	120	W21X48	300	W12X35	300	W12X45	1106.28	11.92	92.05
29	W12X79	120	W21X48	300	W12X35	300	W12X45	1120.56	11.56	88.71
28	W12X79	120	W21X48	300	W12X35	300	W12X45	1120.56	11.15	84.27
27	W12X79	120	W21X48	300	W12X35	300	W12X45	1120.56	10.71	79.90
26	W12X79	120	W21X48	300	W12X35	300	W12X45	1120.56	10.25	75.61
25	W14X145	120	W21X55	300	W21X55	300	W14X68	1141.79	9.77	72.76
24	W14X145	120	W21X55	300	W21X55	300	W14X68	1152.21	9.33	69.17
23	W14X145	120	W21X55	300	W21X55	300	W14X68	1152.21	8.87	64.99
22	W14X145	120	W21X55	300	W21X55	300	W14X68	1152.21	8.39	60.91
21	W14X145	120	W21X55	300	W21X55	300	W14X68	1152.21	7.91	56.90
20	W30X191	120	W24X76	300	W14X38	300	W14X68	1909.54	7.43	87.82
19	W30X191	120	W24X76	300	W14X38	300	W14X68	1926.53	7.04	82.21
18	W30X191	120	W24X76	300	W14X38	300	W14X68	1926.53	6.62	75.98
17	W30X191	120	W24X76	300	W14X38	300	W14X68	1926.53	6.19	69.90
16	W30X191	120	W24X76	300	W14X38	300	W14X68	1926.53	5.75	64.00
15	W24X250	120	W18X60	300	W12X35	300	W14X74	1922.28	5.27	58.12
14	W24X250	120	W18X60	300	W12X35	300	W14X74	1933.47	4.76	52.88
13	W24X250	120	W18X60	300	W12X35	300	W14X74	1933.47	4.24	47.48
12	W24X250	120	W18X60	300	W12X35	300	W14X74	1933.47	3.72	42.27
11	W24X250	120	W18X60	300	W12X35	300	W14X74	1933.47	3.21	37.26
10	W27X368	120	W21X55	300	W14X34	300	W14X74	1948.91	2.72	32.72

Continued

Table 49 continued

Story (i)	Column Section	L_c (in)	Beam - Interior	L_c (in)	Beam - Perimeter	L_c (in)	Bracing Section	Weight (k)	δ (in)	Lateral Force (k)
9	W27X368	120	W21X55	300	W14X34	300	W14X74	1969.76	2.26	28.41
8	W27X368	120	W21X55	300	W14X34	300	W14X74	1969.76	1.82	23.98
7	W27X368	120	W21X55	300	W14X34	300	W14X74	1969.76	1.41	19.79
6	W27X368	120	W21X55	300	W14X34	300	W14X74	1969.76	1.05	15.88
5	W14X398	120	W30X191	300	W30X191	300	W12X96	2180.90	0.79	13.56
4	W14X398	120	W30X191	300	W30X191	300	W12X96	2189.01	0.61	9.93
3	W14X398	120	W30X191	300	W30X191	300	W12X96	2189.01	0.45	6.65
2	W14X398	120	W30X191	300	W30X191	300	W12X96	2189.01	0.32	3.83
1	W14X398	144	W30X191	300	W30X191	300	W12X96	2203.67	0.19	1.58

Table 50: CBF-H-30-5 Design, load, and deflection data

Story (i)	Column Section	L_c (in)	Beam - Interior	L_g (in)	Beam - Perimeter	L_g (in)	Bracing Section	Weight (k)	δ (in)	Lateral Force (k)
30	W14X99	120	W21X55	300	W21X48	300	W12X45	1561.37	11.68	112.03
29	W14X99	120	W21X55	300	W21X48	300	W12X45	1580.67	11.41	107.92
28	W14X99	120	W21X55	300	W21X48	300	W12X45	1580.28	11.09	102.50
27	W14X99	120	W21X55	300	W21X48	300	W12X45	1580.28	10.74	97.18
26	W14X99	120	W21X55	300	W21X48	300	W12X45	1580.28	10.36	91.96
25	W14X159	120	W21X62	300	W21X55	300	W14X68	1601.13	9.95	87.98
24	W14X159	120	W21X62	300	W21X55	300	W14X68	1613.09	9.55	83.51
23	W14X159	120	W21X62	300	W21X55	300	W14X68	1613.09	9.11	78.47
22	W14X159	120	W21X62	300	W21X55	300	W14X68	1613.09	8.66	73.53
21	W14X159	120	W21X62	300	W21X55	300	W14X68	1613.09	8.19	68.70
20	W14X211	120	W21X62	300	W21X55	300	W14X68	1620.04	7.70	64.25
19	W14X211	120	W21X62	300	W21X55	300	W14X68	1627.76	7.21	59.90
18	W14X211	120	W21X62	300	W21X55	300	W14X68	1627.76	6.72	55.36
17	W14X211	120	W21X62	300	W21X55	300	W14X68	1627.76	6.21	50.93
16	W14X211	120	W21X62	300	W21X55	300	W14X68	1627.76	5.70	46.63
15	W14X257	120	W21X62	300	W21X55	300	W18X86	1638.18	5.19	42.72
14	W14X257	120	W21X62	300	W21X55	300	W18X86	1648.22	4.69	38.88
13	W14X257	120	W21X62	300	W21X55	300	W18X86	1648.22	4.19	34.91
12	W14X257	120	W21X62	300	W21X55	300	W18X86	1648.22	3.70	31.08
11	W14X257	120	W21X62	300	W21X55	300	W18X86	1648.22	3.22	27.40
10	W30X391	120	W21X55	300	W21X48	300	W18X86	1659.03	2.75	24.02

Continued

Table 50 continued

Story (i)	Column Section	L_c (in)	Beam - Interior	L_g (in)	Beam - Perimeter	L_g (in)	Bracing Section	Weight (k)	δ (in)	Lateral Force (k)
9	W30X391	120	W21X55	300	W21X48	300	W18X86	1680.26	2.32	20.90
8	W30X391	120	W21X55	300	W21X48	300	W18X86	1680.26	1.91	17.64
7	W30X391	120	W21X55	300	W21X48	300	W18X86	1680.26	1.51	14.56
6	W30X391	120	W21X55	300	W21X48	300	W18X86	1680.26	1.17	11.68
5	W14X455	120	W40X199	300	W14X34	300	W12X96	1794.51	0.90	9.62
4	W14X455	120	W40X199	300	W14X34	300	W12X96	1806.09	0.68	7.07
3	W14X455	120	W40X199	300	W14X34	300	W12X96	1806.09	0.50	4.73
2	W14X455	120	W40X199	300	W14X34	300	W12X96	1806.09	0.35	2.72
1	W14X455	144	W40X199	300	W14X34	300	W12X96	1820.76	0.20	1.12

Table 51: CBF-C-30-5 Design, load, and deflection data

Story (i)	Column Section	L_c (in)	Beam - Interior	L_g (in)	Beam - Perimeter	L_g (in)	Bracing Section	Weight (k)	δ (in)	Lateral Force (k)
30	W12X79	120	W21X48	300	W21X48	300	W12X45	965.39	10.65	79.19
29	W12X79	120	W21X48	300	W21X48	300	W12X45	978.90	10.34	76.40
28	W12X79	120	W21X48	300	W21X48	300	W12X45	978.90	9.99	72.58
27	W12X79	120	W21X48	300	W21X48	300	W12X45	978.90	9.62	68.81
26	W12X79	120	W21X48	300	W21X48	300	W12X45	978.90	9.23	65.12
25	W14X159	120	W21X55	300	W21X55	300	W12X50	993.56	8.81	62.41
24	W14X159	120	W21X55	300	W21X55	300	W12X50	1002.83	8.41	59.34
23	W14X159	120	W21X55	300	W21X55	300	W12X50	1002.83	8.00	55.76
22	W14X159	120	W21X55	300	W21X55	300	W12X50	1002.83	7.56	52.25
21	W14X159	120	W21X55	300	W21X55	300	W12X50	1002.83	7.12	48.82
20	W30X191	120	W30X90	300	W12X35	300	W14X68	1617.73	6.70	73.34
19	W30X191	120	W30X90	300	W12X35	300	W14X68	1632.78	6.38	68.69
18	W30X191	120	W30X90	300	W12X35	300	W14X68	1632.78	6.05	63.48
17	W30X191	120	W30X90	300	W12X35	300	W14X68	1632.78	5.70	58.40
16	W30X191	120	W30X90	300	W12X35	300	W14X68	1632.78	5.34	53.47
15	W24X250	120	W21X55	300	W21X48	300	W14X68	1623.13	4.95	48.39
14	W24X250	120	W21X55	300	W21X48	300	W14X68	1632.39	4.53	44.02
13	W24X250	120	W21X55	300	W21X48	300	W14X68	1632.39	4.09	39.53
12	W24X250	120	W21X55	300	W21X48	300	W14X68	1632.39	3.65	35.19
11	W24X250	120	W21X55	300	W21X48	300	W14X68	1632.39	3.21	31.02

Continued

Table 51 continued

Story (i)	Column Section	L_c (in)	Beam - Interior	L_g (in)	Beam - Perimeter	L_g (in)	Bracing Section	Weight (k)	δ (in)	Lateral Force (k)
10	W14X342	120	W21X55	300	W12X35	300	W18X86	1643.97	2.77	27.21
9	W14X342	120	W21X55	300	W12X35	300	W18X86	1660.96	2.34	23.61
8	W14X342	120	W21X55	300	W12X35	300	W18X86	1660.96	1.92	19.93
7	W14X342	120	W21X55	300	W12X35	300	W18X86	1660.96	1.53	16.45
6	W14X342	120	W21X55	300	W12X35	300	W18X86	1660.96	1.16	13.20
5	W14X455	120	W30X191	300	W14X34	300	W12X96	1781.39	0.88	10.92
4	W14X455	120	W30X191	300	W14X34	300	W12X96	1800.30	0.67	8.06
3	W14X455	120	W30X191	300	W14X34	300	W12X96	1800.30	0.49	5.39
2	W14X455	120	W30X191	300	W14X34	300	W12X96	1800.30	0.33	3.10
1	W14X455	144	W30X191	300	W14X34	300	W12X96	1815.36	0.19	1.28

APPENDIX C: TABLES OF DESIGN DATA, LOADS, AND DEFLECTIONS – ECCENTRICALLY BRACED FRAMES

Table 52: EBF-R-10-5 Design, load, and deflection data

Story (i)	Column Section	L_c (in)	Beam - Interior	L_g (in)	Beam - Perimeter	L_g (in)	Bracing Section	Weight (k)	δ (in)	Lateral Force (k)
10	W14X68	120	W14X48	300	W14X38	300	W12X30	1833.50	3.56	161.92
9	W14X68	120	W14X48	300	W14X38	300	W12X30	1847.40	3.37	143.68
8	W14X68	120	W14X48	300	W14X38	300	W12X30	1847.40	3.08	124.70
7	W12X96	120	W14X43	300	W12X45	300	W12X30	1850.48	2.69	106.43
6	W12X96	120	W14X43	300	W12X45	300	W12X30	1855.50	2.22	88.77
5	W12X96	120	W14X43	300	W12X45	300	W12X30	1855.50	1.71	71.48
4	W12X152	120	W14X43	300	W16X77	300	W12X50	1881.75	1.24	55.72
3	W12X152	120	W14X43	300	W16X77	300	W12X50	1892.94	0.94	40.10
2	W12X152	120	W14X43	300	W16X77	300	W12X50	1892.94	0.67	25.28
1	W12X152	144	W14X43	300	W16X77	300	W12X50	1898.73	0.40	12.02

Table 53: EBF-V-10-5 Design, load, and deflection data

Story (i)	Column Section	L_c (in)	Beam - Interior	L_g (in)	Beam - Perimeter	L_g (in)	Bracing Section	Weight (k)	δ (in)	Lateral Force (k)
10	W21X62	120	W14X53	300	W16X40	300	W12X30	1105.50	3.12	108.39
9	W21X62	120	W14X53	300	W16X40	300	W12X30	1114.77	2.97	96.24
8	W21X62	120	W14X53	300	W16X40	300	W12X30	1114.77	2.75	83.53
7	W12X96	120	W14X43	300	W12X45	300	W14X34	1846.24	2.47	117.88
6	W12X96	120	W14X43	300	W12X45	300	W14X34	1856.27	2.12	98.59
5	W12X96	120	W14X43	300	W12X45	300	W14X34	1856.27	1.71	79.39
4	W12X152	120	W14X43	300	W21X68	300	W12X40	1877.50	1.31	61.73
3	W12X152	120	W14X43	300	W21X68	300	W12X40	1887.93	1.01	44.41
2	W12X152	120	W14X43	300	W21X68	300	W12X40	1887.93	0.73	28.00
1	W12X152	144	W14X43	300	W21X68	300	W12X40	1893.72	0.44	13.31

Table 54: EBF-H-10-5 Design, load, and deflection data

Story (i)	Column Section	L_c (in)	Beam - Interior	L_c (in)	Beam - Perimeter	L_c (in)	Bracing Section	Weight (k)	δ (in)	Lateral Force (k)
10	W21X62	120	W14X48	300	W16X40	300	W12X30	1541.68	3.40	136.07
9	W21X62	120	W14X48	300	W16X40	300	W12X30	1553.26	3.22	120.73
8	W21X62	120	W14X48	300	W16X40	300	W12X30	1553.26	2.98	104.78
7	W16X89	120	W14X43	300	W12X45	300	W12X30	1555.97	2.64	89.43
6	W16X89	120	W14X43	300	W12X45	300	W12X30	1560.21	2.23	74.60
5	W16X89	120	W14X43	300	W12X45	300	W12X30	1560.21	1.77	60.07
4	W12X136	120	W14X43	300	W21X68	300	W12X40	1579.51	1.35	46.75
3	W12X136	120	W14X43	300	W21X68	300	W12X40	1587.62	1.03	33.62
2	W12X136	120	W14X43	300	W21X68	300	W12X40	1587.62	0.73	21.19
1	W12X136	144	W14X43	300	W21X68	300	W12X40	1592.25	0.44	10.07

Table 55: EBF-C-10-5 Design, load, and deflection data

Story (i)	Column Section	L_c (in)	Beam - Interior	L_g (in)	Beam - Perimeter	L_g(in)	Bracing Section	Weight (k)	δ (in)	Lateral Force (k)
10	W14X68	120	W14X38	300	W14X48	300	W12X30	1176.53	3.16	110.13
9	W14X68	120	W14X38	300	W14X48	300	W12X30	1186.56	2.99	97.82
8	W14X68	120	W14X38	300	W14X48	300	W12X30	1186.56	2.73	84.90
7	W12X96	120	W14X43	300	W12X45	300	W14X34	1555.97	2.41	94.86
6	W12X96	120	W14X43	300	W12X45	300	W14X34	1563.30	2.04	79.27
5	W12X96	120	W14X43	300	W12X45	300	W14X34	1563.30	1.62	63.83
4	W12X152	120	W14X43	300	W21X68	300	W12X40	1583.76	1.23	49.71
3	W12X152	120	W14X43	300	W21X68	300	W12X40	1593.02	0.94	35.77
2	W12X152	120	W14X43	300	W21X68	300	W12X40	1593.02	0.67	22.55
1	W12X152	144	W14X43	300	W21X68	300	W12X40	1598.04	0.40	10.72

Table 56: EBF-R-20-5 Design, load, and deflection data

Story (i)	Column Section	L_c (in)	Beam - Interior	L_g (in)	Beam - Perimeter	L_g (in)	Bracing Section	Weight (k)	δ (in)	Lateral Force (k)
20	W16X77	120	W14X48	120	W14X38	120	W16X26	1834.66	7.72	117.79
19	W16X77	120	W14X48	120	W14X38	120	W16X26	1850.10	7.52	109.76
18	W16X77	120	W14X48	120	W14X38	120	W16X26	1850.10	7.25	101.01
17	W16X77	120	W14X48	120	W14X38	120	W16X26	1850.10	6.91	92.52
16	W18X130	120	W21X55	120	W12X35	120	W12X30	1864.77	6.55	84.96
15	W18X130	120	W21X55	120	W12X35	120	W12X30	1874.42	6.20	77.36
14	W18X130	120	W21X55	120	W12X35	120	W12X30	1874.42	5.82	69.60
13	W18X130	120	W21X55	120	W12X35	120	W12X30	1874.42	5.41	62.13
12	W21X182	120	W21X55	120	W12X45	120	W12X30	1887.54	4.97	55.36
11	W21X182	120	W21X55	120	W12X45	120	W12X30	1897.19	4.54	48.72
10	W21X182	120	W21X55	120	W12X45	120	W12X30	1897.19	4.09	42.13
9	W21X182	120	W21X55	120	W12X45	120	W12X30	1897.19	3.64	35.89
8	W12X230	120	W21X55	120	W14X48	120	W14X38	1908.77	3.18	30.20
7	W12X230	120	W21X55	120	W14X48	120	W14X38	1917.65	2.72	24.79
6	W12X230	120	W21X55	120	W14X48	120	W14X38	1917.65	2.26	19.65
5	W12X230	120	W21X55	120	W14X48	120	W14X38	1917.65	1.81	14.95
4	W14X283	120	W21X48	120	W18X86	120	W12X53	1938.88	1.40	10.85
3	W14X283	120	W21X48	120	W18X86	120	W12X53	1948.91	1.07	7.15
2	W14X283	120	W21X48	120	W18X86	120	W12X53	1948.91	0.76	3.99
1	W14X283	144	W21X48	144	W18X86	144	W12X53	1959.72	0.45	1.57

Table 57: EBF-V-20-5 Design, load, and deflection data

Story (i)	Column Section	L_c (in)	Beam - Interior	L_c (in)	Beam - Perimeter	L_c (in)	Bracing Section	Weight (k)	δ (in)	Lateral Force (k)
20	W14X74	120	W14X48	120	W14X38	120	W12X30	1103.57	6.55	83.27
19	W14X74	120	W14X48	120	W14X38	120	W12X30	1114.38	6.34	77.69
18	W14X74	120	W14X48	120	W14X38	120	W12X30	1114.38	6.06	71.49
17	W14X74	120	W14X48	120	W14X38	120	W12X30	1114.38	5.71	65.48
16	W18X130	120	W18X50	120	W12X35	120	W12X30	1120.56	5.32	59.99
15	W18X130	120	W18X50	120	W12X35	120	W12X30	1127.12	4.92	54.66
14	W18X130	120	W18X50	120	W12X35	120	W12X30	1127.12	4.49	49.18
13	W18X130	120	W18X50	120	W12X35	120	W12X30	1127.12	4.05	43.90
12	W30X173	120	W21X55	120	W16X40	120	W12X30	1874.80	3.64	64.62
11	W30X173	120	W21X55	120	W16X40	120	W12X30	1890.63	3.33	57.05
10	W30X173	120	W21X55	120	W16X40	120	W12X30	1890.63	3.00	49.33
9	W30X173	120	W21X55	120	W16X40	120	W12X30	1890.63	2.67	42.03
8	W24X229	120	W21X55	120	W12X45	120	W14X34	1903.37	2.32	35.39
7	W24X229	120	W21X55	120	W12X45	120	W14X34	1913.79	1.95	29.07
6	W24X229	120	W21X55	120	W12X45	120	W14X34	1913.79	1.59	23.04
5	W24X229	120	W21X55	120	W12X45	120	W14X34	1913.79	1.24	17.53
4	W12X279	120	W21X48	120	W27X94	120	W12X53	1941.97	0.94	12.77
3	W12X279	120	W21X48	120	W27X94	120	W12X54	1952.00	0.70	8.41
2	W12X279	120	W21X48	120	W27X94	120	W12X55	1952.00	0.50	4.70
1	W12X279	144	W21X48	144	W27X94	144	W12X56	1962.04	0.30	1.84

Table 58: EBF-H-20-5 Design, load, and deflection data

Story (i)	Column Section	L_c (in)	Beam - Interior	L_g (in)	Beam - Perimeter	L_g (in)	Bracing Section	Weight (k)	δ (in)	Lateral Force (k)
20	W16X77	120	W21X55	300	W14X38	300	W12X30	1548.63	6.37	99.59
19	W16X77	120	W21X55	300	W14X38	300	W12X30	1562.91	6.22	92.86
18	W16X77	120	W21X55	300	W14X38	300	W12X30	1562.91	6.01	85.46
17	W16X77	120	W21X55	300	W14X38	300	W12X30	1562.91	5.75	78.27
16	W24X131	120	W21X55	300	W12X35	300	W12X30	1568.70	5.43	71.60
15	W24X131	120	W21X55	300	W12X35	300	W12X30	1577.58	5.11	65.20
14	W24X131	120	W21X55	300	W12X35	300	W12X30	1577.58	4.75	58.66
13	W24X131	120	W21X55	300	W12X35	300	W12X30	1577.58	4.36	52.37
12	W12X190	120	W21X55	300	W12X45	300	W14X34	1592.64	3.96	46.78
11	W12X190	120	W21X55	300	W12X45	300	W14X34	1602.29	3.51	41.21
10	W12X190	120	W21X55	300	W12X45	300	W14X34	1602.29	3.06	35.64
9	W12X190	120	W21X55	300	W12X45	300	W14X34	1602.29	2.60	30.36
8	W12X230	120	W21X55	300	W21X68	300	W12X40	1620.04	2.18	25.67
7	W12X230	120	W21X55	300	W21X68	300	W12X40	1626.99	1.84	21.06
6	W12X230	120	W21X55	300	W21X68	300	W12X40	1626.99	1.52	16.69
5	W12X230	120	W21X55	300	W21X68	300	W12X40	1626.99	1.21	12.70
4	W14X283	120	W21X48	300	W27X94	300	W12X58	1642.82	0.93	9.20
3	W14X283	120	W21X48	300	W27X94	300	W12X58	1652.08	0.71	6.07
2	W14X283	120	W21X48	300	W27X94	300	W12X58	1652.08	0.50	3.39
1	W14X283	144	W21X48	300	W27X94	300	W12X58	1661.73	0.30	1.33

Table 59: EBF-C-20-5 Design, load, and deflection data

Story (i)	Column Section	L_c (in)	Beam - Interior	L_g (in)	Beam - Perimeter	L_g(in)	Bracing Section	Weight (k)	δ (in)	Lateral Force (k)
20	W14X74	120	W14X48	300	W16X40	300	W12X30	958.05	6.53	74.51
19	W14X74	120	W14X48	300	W16X40	300	W12X30	966.93	6.32	69.51
18	W14X74	120	W14X48	300	W16X40	300	W12X30	966.93	6.05	63.96
17	W14X74	120	W14X48	300	W16X40	300	W12X30	966.93	5.73	58.59
16	W21X111	120	W21X48	300	W12X45	300	W14X34	971.95	5.36	53.65
15	W21X111	120	W21X48	300	W12X45	300	W14X34	976.19	5.00	48.80
14	W21X111	120	W21X48	300	W12X45	300	W14X34	976.19	4.60	43.90
13	W21X111	120	W21X48	300	W12X45	300	W14X34	976.19	4.19	39.20
12	W14X159	120	W18X60	300	W12X45	300	W14X34	1803.01	3.79	64.06
11	W14X159	120	W18X60	300	W12X45	300	W14X34	1819.60	3.42	56.60
10	W14X159	120	W18X60	300	W12X45	300	W14X34	1819.60	3.04	48.95
9	W14X159	120	W18X60	300	W12X45	300	W14X34	1819.60	2.65	41.70
8	W24X207	120	W21X55	300	W12X45	300	W12X53	1822.69	2.24	34.93
7	W24X207	120	W21X55	300	W12X45	300	W12X53	1830.80	1.88	28.67
6	W24X207	120	W21X55	300	W12X45	300	W12X53	1830.80	1.52	22.72
5	W24X207	120	W21X55	300	W12X45	300	W12X53	1830.80	1.18	17.29
4	W14X257	120	W21X48	300	W27X94	300	W12X96	1857.43	0.89	12.59
3	W14X257	120	W21X48	300	W27X94	300	W12X96	1867.47	0.66	8.29
2	W14X257	120	W21X48	300	W27X94	300	W12X96	1867.47	0.47	4.63
1	W14X257	144	W21X48	300	W27X94	300	W12X96	1876.73	0.28	1.82

Table 60: EBF-R-30-5 Design, load, and deflection data

Story (i)	Column Section	L_c (in)	Beam - Interior	L_c (in)	Beam - Perimeter	L_c (in)	Bracing Section	Weight (k)	δ (in)	Lateral Force (k)
30	W12X96	120	W21X48	300	W12X35	300	W16X26	1836.97	13.04	100.69
29	W12X96	120	W21X48	300	W12X35	300	W16X26	1855.12	12.85	95.58
28	W12X96	120	W21X48	300	W12X35	300	W16X26	1855.12	12.59	89.66
27	W12X96	120	W21X48	300	W12X35	300	W16X26	1855.12	12.27	83.90
26	W12X96	120	W21X48	300	W12X35	300	W16X26	1855.12	11.90	78.32
25	W18X143	120	W21X55	300	W12X35	300	W16X26	1870.17	11.48	73.52
24	W18X143	120	W21X55	300	W12X35	300	W16X26	1878.66	11.08	68.56
23	W18X143	120	W21X55	300	W12X35	300	W16X26	1878.66	10.66	63.45
22	W18X143	120	W21X55	300	W12X35	300	W16X26	1878.66	10.20	58.52
21	W18X143	120	W21X55	300	W12X35	300	W16X26	1878.66	9.71	53.77
20	W14X193	120	W18X60	300	W12X45	300	W12X30	1896.03	9.19	49.66
19	W14X193	120	W18X60	300	W12X45	300	W12X30	1906.07	8.65	45.48
18	W14X193	120	W18X60	300	W12X45	300	W12X30	1906.07	8.10	41.22
17	W14X193	120	W18X60	300	W12X45	300	W12X30	1906.07	7.53	37.16
16	W14X193	120	W18X60	300	W12X45	300	W12X30	1906.07	6.96	33.29
15	W12X252	120	W18X60	300	W12X45	300	W12X30	1917.65	6.37	29.79
14	W12X252	120	W18X60	300	W12X45	300	W12X30	1927.30	5.74	26.42
13	W12X252	120	W18X60	300	W12X45	300	W12X30	1927.30	5.11	23.11
12	W12X252	120	W18X60	300	W12X45	300	W12X30	1927.30	4.48	19.99
11	W12X252	120	W18X60	300	W12X45	300	W12X30	1927.30	3.84	17.09

Continued

Table 60 continued

Story (i)	Column Section	L_c (in)	Beam - Interior	L_c (in)	Beam - Perimeter	L_c (in)	Bracing Section	Weight (k)	δ (in)	Lateral Force (k)
10	W33X318	120	W21X48	300	W12X45	300	W12X30	1925.37	3.22	14.37
9	W33X318	120	W21X48	300	W12X45	300	W12X30	1937.33	2.67	11.97
8	W33X318	120	W21X48	300	W12X45	300	W12X30	1937.33	2.14	9.69
7	W33X318	120	W21X48	300	W12X45	300	W12X30	1937.33	1.65	7.63
6	W33X318	120	W21X48	300	W12X45	300	W12X30	1937.33	1.22	5.80
5	W14X370	120	W14X193	300	W33X201	300	W12X58	2160.44	0.90	4.68
4	W14X370	120	W14X193	300	W33X201	300	W12X58	2171.64	0.69	3.18
3	W14X370	120	W14X193	300	W33X201	300	W12X58	2171.64	0.53	1.93
2	W14X370	120	W14X193	300	W33X201	300	W12X58	2171.64	0.39	0.97
1	W14X370	120	W14X193	300	W33X201	300	W12X58	2185.15	0.25	0.32

Table 61: EBF-V-30-5 Design, load, and deflection data

Story (i)	Column Section	L_c (in)	Beam - Interior	L_g (in)	Beam - Perimeter	L_g (in)	Bracing Section	Weight (k)	δ (in)	Lateral Force (k)
30	W14X82	120	W14X48	300	W14X38	300	W12X30	1103.96	9.98	71.64
29	W14X82	120	W14X48	300	W14X38	300	W12X30	1114.38	9.76	67.99
28	W14X82	120	W14X48	300	W14X38	300	W12X30	1114.38	9.49	63.78
27	W14X82	120	W14X48	300	W14X38	300	W12X30	1114.38	9.15	59.68
26	W14X82	120	W14X48	300	W14X38	300	W12X30	1114.38	8.77	55.72
25	W27X161	120	W21X55	300	W12X35	300	W16X26	1125.19	8.37	52.38
24	W27X161	120	W21X55	300	W12X35	300	W16X26	1134.84	8.00	49.03
23	W27X161	120	W21X55	300	W12X35	300	W16X26	1134.84	7.63	45.38
22	W27X161	120	W21X55	300	W12X35	300	W16X26	1134.84	7.25	41.85
21	W27X161	120	W21X55	300	W12X35	300	W16X26	1134.84	6.89	38.45
20	W14X193	120	W40X149	300	W12X35	300	W12X30	1969.37	6.64	61.07
19	W14X193	120	W40X149	300	W12X35	300	W12X30	1985.58	6.46	56.09
18	W14X193	120	W40X149	300	W12X35	300	W12X30	1985.58	6.28	50.85
17	W14X193	120	W40X149	300	W12X35	300	W12X30	1985.58	6.09	45.83
16	W14X193	120	W40X149	300	W12X35	300	W12X30	1985.58	5.88	41.06
15	W24X250	120	W21X55	300	W12X45	300	W12X30	1910.70	5.55	35.14
14	W24X250	120	W21X55	300	W12X45	300	W12X30	1920.74	5.13	31.18
13	W24X250	120	W21X55	300	W12X45	300	W12X30	1920.74	4.69	27.26
12	W24X250	120	W21X55	300	W12X45	300	W12X30	1920.74	4.23	23.59
11	W24X250	120	W21X55	300	W12X45	300	W12X30	1920.74	3.75	20.16

Continued

Table 61 continued

Story (i)	Column Section	L_c (in)	Beam - Interior	L_g (in)	Beam - Perimeter	L_g (in)	Bracing Section	Weight (k)	δ (in)	Lateral Force (k)
10	W33X318	120	W21X48	300	W12X45	300	W12X30	1924.98	3.27	17.02
9	W33X318	120	W21X48	300	W12X45	300	W12X30	1937.33	2.79	14.17
8	W33X318	120	W21X48	300	W12X45	300	W12X30	1937.33	2.32	11.47
7	W33X318	120	W21X48	300	W12X45	300	W12X30	1937.33	1.88	9.03
6	W33X318	120	W21X48	300	W12X45	300	W12X30	1937.33	1.48	6.86
5	W24X370	120	W14X193	300	W14X193	300	W12X50	2152.72	1.15	5.52
4	W24X370	120	W14X193	300	W14X193	300	W12X50	2163.14	0.89	3.75
3	W24X370	120	W14X193	300	W14X193	300	W12X50	2163.14	0.68	2.27
2	W24X370	120	W14X193	300	W14X193	300	W12X50	2163.14	0.48	1.14
1	W24X370	144	W14X193	300	W14X193	300	W12X50	2177.04	0.28	0.38

Table 62: EBF-H-30-5 Design, load, and deflection data

Story (i)	Column Section	L_g (in)	Beam - Interior	L_g (in)	Beam - Perimeter	L_c (in)	Bracing Section	Weight (k)	δ (in)	Lateral Force (k)
30	W12X96	120	W21X55	300	W12X45	300	W12X30	1556.74	11.50	84.82
29	W12X96	120	W21X55	300	W12X45	300	W12X30	1572.18	11.32	80.54
28	W12X96	120	W21X55	300	W12X45	300	W12X30	1571.79	11.07	75.53
27	W12X96	120	W21X55	300	W12X45	300	W12X30	1571.79	10.78	70.69
26	W12X96	120	W21X55	300	W12X45	300	W12X30	1571.79	10.44	65.99
25	W14X145	120	W18X60	300	W18X50	300	W12X30	1585.69	10.07	61.97
24	W14X145	120	W18X60	300	W18X50	300	W12X30	1593.41	9.70	57.81
23	W14X145	120	W18X60	300	W18X50	300	W12X30	1593.41	9.32	53.50
22	W14X145	120	W18X60	300	W18X50	300	W12X30	1593.41	8.90	49.34
21	W14X145	120	W18X60	300	W18X50	300	W12X30	1593.41	8.46	45.34
20	W33X201	120	W21X55	300	W16X40	300	W12X30	1591.86	7.99	41.44
19	W33X201	120	W21X55	300	W16X40	300	W12X30	1600.36	7.54	37.95
18	W33X201	120	W21X55	300	W16X40	300	W12X30	1600.36	7.08	34.40
17	W33X201	120	W21X55	300	W16X40	300	W12X30	1600.36	6.60	31.01
16	W33X201	120	W21X55	300	W16X40	300	W12X30	1600.36	6.11	27.78
15	W12X252	120	W18X60	300	W14X48	300	W14X34	1618.50	5.61	24.99
14	W12X252	120	W18X60	300	W14X48	300	W14X34	1626.99	5.06	22.17
13	W12X252	120	W18X60	300	W14X48	300	W14X34	1626.99	4.49	19.39
12	W12X252	120	W18X60	300	W14X48	300	W14X34	1626.99	3.93	16.78
11	W12X252	120	W18X60	300	W14X48	300	W14X34	1626.99	3.37	14.34

Continued

Table 62 continued

Story (i)	Column Section	L_g (in)	Beam - Interior	L_g (in)	Beam - Perimeter	L_c (in)	Bracing Section	Weight (k)	δ (in)	Lateral Force (k)
10	W33X318	120	W18X60	300	W18X50	300	W12X40	1633.55	2.85	12.12
9	W33X318	120	W18X60	300	W18X50	300	W12X40	1644.75	2.41	10.10
8	W33X318	120	W18X60	300	W18X50	300	W12X40	1644.75	1.99	8.18
7	W33X318	120	W18X60	300	W18X50	300	W12X40	1644.75	1.60	6.44
6	W33X318	120	W18X60	300	W18X50	300	W12X40	1644.75	1.26	4.89
5	W14X370	120	W30X191	300	W16X77	300	W12X50	1769.81	1.00	3.81
4	W14X370	120	W30X191	300	W16X77	300	W12X50	1778.69	0.79	2.59
3	W14X370	120	W30X191	300	W16X77	300	W12X50	1778.69	0.63	1.57
2	W14X370	120	W30X191	300	W16X77	300	W12X50	1778.69	0.48	0.79
1	W14X370	144	W30X191	300	W16X77	300	W12X50	1791.04	0.31	0.26

Table 63: EBF-C-30-5 Design, load, and deflection data

Story (i)	Column Section	L_c (in)	Beam - Interior	L_g (in)	Beam - Perimeter	L_g (in)	Bracing Section	Weight (k)	δ (in)	Lateral Force (k)
30	W18X86	120	W14X48	300	W12X45	300	W12X30	960.75	10.55	61.55
29	W18X86	120	W14X48	300	W12X45	300	W12X30	970.79	10.31	58.47
28	W18X86	120	W14X48	300	W12X45	300	W12X30	970.79	10.01	54.85
27	W18X86	120	W14X48	300	W12X45	300	W12X30	970.79	9.66	51.33
26	W18X86	120	W14X48	300	W12X45	300	W12X30	970.79	9.26	47.92
25	W30X173	120	W21X48	300	W16X40	518	W12X30	977.74	8.86	44.93
24	W30X173	120	W21X48	300	W16X40	518	W12X30	987.39	8.49	42.12
23	W30X173	120	W21X48	300	W16X40	518	W12X30	987.39	8.10	38.98
22	W30X173	120	W21X48	300	W16X40	518	W12X30	987.39	7.71	35.95
21	W30X173	120	W21X48	300	W16X40	518	W12X30	987.39	7.33	33.03
20	W14X211	120	W24X76	300	W12X45	300	W12X30	1606.15	6.97	49.17
19	W14X211	120	W24X76	300	W12X45	300	W12X30	1619.66	6.65	45.17
18	W14X211	120	W24X76	300	W12X45	300	W12X30	1619.66	6.33	40.94
17	W14X211	120	W24X76	300	W12X45	300	W12X30	1619.66	6.00	36.91
16	W14X211	120	W24X76	300	W12X45	300	W12X30	1619.66	5.63	33.06
15	W40X277	120	W18X60	300	W12X45	300	W14X34	1617.73	5.21	29.37
14	W40X277	120	W18X60	300	W12X45	300	W14X34	1630.46	4.75	26.12
13	W40X277	120	W18X60	300	W12X45	300	W14X34	1630.46	4.29	22.85
12	W40X277	120	W18X60	300	W12X45	300	W14X34	1630.46	3.82	19.77
11	W40X277	120	W18X60	300	W12X45	300	W14X34	1630.46	3.34	16.89

Continued

Table 63 continued

Story (i)	Column Section	L_c (in)	Beam - Interior	L_g (in)	Beam - Perimeter	L_g (in)	Bracing Section	Weight (k)	δ (in)	Lateral Force (k)
10	W33X354	120	W18X50	300	W12X45	300	W14X34	1635.87	2.86	14.28
9	W33X354	120	W18X50	300	W12X45	300	W14X34	1648.22	2.39	11.90
8	W33X354	120	W18X50	300	W12X45	300	W14X34	1648.22	1.93	9.63
7	W33X354	120	W18X50	300	W12X45	300	W14X34	1648.22	1.51	7.59
6	W33X354	120	W18X50	300	W12X45	300	W14X34	1648.22	1.15	5.76
5	W14X398	120	W30X173	300	W21X68	300	W14X43	1761.32	0.87	4.46
4	W14X398	120	W30X173	300	W21X68	300	W14X43	1769.04	0.68	3.03
3	W14X398	120	W30X173	300	W21X68	300	W14X43	1769.04	0.54	1.84
2	W14X398	120	W30X173	300	W21X68	300	W14X43	1769.04	0.40	0.92
1	W14X398	144	W30X173	300	W21X68	300	W14X43	1781.78	0.26	0.31

APPENDIX D: MATLAB SCRIPT FILE

```
clc
clear all
close all

%=========================================================================
===%
%THIS PROGRAM MATCHES ANALYSIS/DESIGN SECTIONS WITH THEIR RESPECTIVE
AREA
%AND INERTIA DATA FROM THE AISC DATABASE SPREADSHEET.  THE PROPERTY
DATA IS
%THEN WRITEN INTO THE SPREADSHEET CONTAINING THE ADELI PERIOD FORMULAS
FOR
%FURTHER ANALYSIS.
%=========================================================================
===%


%---Importing File Containing Design/Analysis Sections---%
FILE1 = input('Input Data File Name:   ','s');


%---Separate Arrays for Columns, Girders, Bracings--%
[num,columns] = xlsread(FILE1,'Adeli Data','F5:F1084');  %CHANGE EACH
TIME
design_sections_columns = columns;

[num,girders] = xlsread(FILE1,'Adeli Data','P5:P1804');   %CHANGE EACH
TIME
design_sections_girders = girders;

[num,bracings] = xlsread(FILE1,'Adeli Data','X5:X244');   %CHANGE EACH
TIME
design_sections_bracings = bracings;

%---Importing File Containing All AISC Sections---%
[num1,str1] = xlsread('AISC_Shapes_Database','Sheet1');
all_sections = str1(:,1);
all_sections(1)=[];

%---Separating Area and Inertia Data for Each Section---%
A = num1(:,1);
I = num1(:,2);

%---Initializing Arrays---%
A_design_columns = [];
I_design_columns = [];
A_design_beams = [];
I_design_beams = [];
A_design_bracings = [];
I_design_bracings = [];
```

```
%---Matching Design/Analysis Columns with Column Properties---%
for j = 1:length(design_sections_columns)
    for i = 1:length(all_sections)
      TF = strcmp(design_sections_columns(j),all_sections(i));
      if TF == 1
          A_design_column(j,1) = A(i);
          I_design_column(j,1) = I(i);
          break
     else
     end
    end
end

%---Matching Design/Analysis Girders with Girder Properties---%
for j = 1:length(design_sections_girders)
    for i = 1:length(all_sections)
      TF = strcmp(design_sections_girders(j),all_sections(i));
      if TF == 1
          A_design_girders(j,1) = A(i);
          I_design_girders(j,1) = I(i);
          break
     else
     end
    end
end

%---Matching Design/Analysis Bracings with Bracings Properties---%
for j = 1:length(design_sections_bracings)
    for i = 1:length(all_sections)
      TF = strcmp(design_sections_bracings(j),all_sections(i));
      if TF == 1
          A_design_bracings(j,1) = A(i);
          I_design_bracings(j,1) = I(i);
          break
     else
     end
    end
end

%---Writing Property Data to Spreadsheet Containing Adeli Period
%Formula---%
xlswrite(FILE1,I_design_column,'Adeli Data','G5')
xlswrite(FILE1,A_design_column,'Adeli Data','H5')
xlswrite(FILE1,I_design_girders,'Adeli Data','Q5')
xlswrite(FILE1,A_design_girders,'Adeli Data','R5')
xlswrite(FILE1,I_design_bracings,'Adeli Data','Y5')
xlswrite(FILE1,A_design_bracings,'Adeli Data','Z5')

display(' ')
display('Property data has been written.')
```

APPENDIX E: VERIFICATION OF ADELI EQUATION FOR EBFS

Axial force in bracing: $F_b = \frac{V}{2cos\propto_b}$

Length of bracing: $l_b = \frac{L_b - e}{2cos\propto_b}$

Elongation of each bracing: $\delta_b = \frac{F_b l_b}{EA_b} = \frac{F_b\left(\frac{L_b-e}{2cos\propto_b}\right)}{EA_b} = \frac{V(L_b-e)}{4A_bEcos\propto_b^3}$

Story drift: $\Delta = \frac{\delta_b}{\cos(\propto_b)} = \frac{\frac{F_b\left(\frac{L_b-e}{2cos\propto_b}\right)}{EA_b}}{\cos(\propto_b)} = \frac{V(L_b-e)}{4A_bEcos\propto_b^3}$

Equivalent shear rigidity: $R = \frac{V}{(\Delta/h)} = \frac{4A_bEcos\propto_b^3}{Lb-e}$

Shear mode of vibration: $T_s = \sqrt{\frac{WH}{gR}} = \sqrt{\frac{WH}{g\frac{4A_bEcos\propto_b^3}{Lb-e}}}$

Let: $L_b = \frac{2h}{tan\propto_b} + e$

Therefore: $T_s = \frac{2.83}{\cos\propto_b}\sqrt{\frac{WH}{gA_bEsin\propto_b}}$